CalVal Jason
CLS.DOS/NT/06-302
Version : 1rev1, May 14, 2007
Nomenclature : SALP-RP-MA-EA-21377-CLS

Ramonville, May 14, 2007

Jason-1 validation and cross calibration activities

Contract No 03/CNES/1340/00-DSO310 - lot2.C

	AUTHORS	COMPANY	DATE	INITIALS
WRITTEN BY	M. Ablain	CLS		
	S. Philipps	CLS		
APPROVED BY	J. Dorandeu	CLS		
QUALITY VISA	AQM member	CLS		
APPLICATION AUTHORISED BY	N.Picot	CNES		
	P.Leloup	CNES		

CLS - 8-10 Rue Hermès - Parc Technologique du Canal - 31520 Ramonville St-Agne - FRANCE
Telephone 33 5 61 39 47 00 / Fax 33 5 61 75 10 14

DISTRIBUTION LIST

COMPANY	NAMES	COPIES
CLS/DOS	J.DORANDEU	1 electonic copy
	V.ROSMORDUC	1 electonic copy
	P.ESCUDIER	1 electonic copy
DOC/CLS	DOCUMENTATION	1 electonic copy
CNES	P.LELOUP	2 copy + 1 electonic copy
CNES	N.PICOT	1 electonic copy
CNES	D.SCHOLLER	1 electonic copy
CNES	J.LAMBIN	1 electonic copy

CHRONOLOGY ISSUE

Control Initials	ISSUE	DATE	REASON FOR CHANGE
	1.0		Creation
	1.1		Revision

LIST OF ACRONYMS

TBC	To Be Confirmed

List of Tables

List of Figures

Contents

APPLICABLE DOCUMENTS / REFERENCE DOCUMENTS

1 Introduction

This document presents the synthesis report concerning validation activities of Jason-1 GDRs under SALP contract (N° 03/CNES/1340/00-DSO310 Lot2.C) supported by CNES at the CLS Space Oceanography Division. It is divided into two parts: CAL/VAL Jason-1 activities(Lot2.C) - Jason-1 / T/P cross-calibration (Lot2.C).

Since the beginning of the mission, Jason-1 data have been analyzed and monitored in order to assess the quality of Jason-1 GDR products (AVISO and PODAAC User handbook, [47]) for oceanographic applications. This report is basically concerned with long-term monitoring of the Jason-1 altimeter system, from all GDR products available to date, that is for 5 years of data (cycles 1 to 175). This includes careful monitoring of all altimeter and radiometer parameters, performance assessment, geophysical evaluation and cross-calibration with T/P measurements. Moreover specific studies are presented in this document :

- the comparisons of the new GDRs release (version "b") with the former GDRs (version"a")
- the comparisons between the mean sea level and the sea surface temperature for all operational altimeter missions.

This work is routinely performed at CLS and in this frame, besides continuous analyzes in terms of altimeter data quality, Jason-1 GDR Quality Assessment Reports (e.g. Ablain et al. 2005 [4]) are produced and associated to data dissemination. Even if only low order statistics are mainly presented here, other analyzes including histograms, plots and maps are continuously produced and used in the quality assessment process. The work performed in terms of data quality assessment also includes cross-calibration analyzes mainly with the T/P mission until November 2005 (end of the T/P mission). Even if T/P mission is finished, cross-calibration analyzes are useful for the reprocessing activities in order to study the sea state bias or the SSH bias for instance.
Indeed, it is now well recognized that the usefulness of any altimeter data only makes sense in a multi-mission context, given the growing importance of scientific needs and applications, in particular for operational oceanography. One major objective of the Jason-1 mission is to continue the T/P high precision altimetry and to allow combination with other missions (ENVISAT, GFO). This kind of comparisons between different altimeter missions flying together provides a large number of estimations and consequently efficient long term monitoring of instrument measurements. Of course, other sources of comparisons are also needed, using independent datasets (e.g. Queffeulou et al. 2004 [50], Ray and Beckley 2003 [53], Arnault et al. 2004 [7], Provost et al. 2004 [48]).

2 Processing status

2.1 GDR and CAL/VAL Processing

Jason-1 GDRs from cycle 1 to 175(till 16/10/2006), are used in this report. They have been processed with two different versions of the CMA ground processing software (Jason-1 product versions "a" and "b"). New Jason-1 products (version "b") are available from cycle 136 onwards (see section 2.3). In order to have homogeneous time-series, cycles 1 to 135 will be reprocessed in GDR version "b". Cycles 1 to 21 and 128 to 135 were already reprocessed in version "b" early in 2006. Cycles 22 to 127 reprocessing is ongoing.
In this report the reprocessed cycles were not yet taken into account, therefore cycles 1 to 135 are in GDR version "a" and from cycle 136 onwards in GDR version "b". A report has been carried out for each cycle and is available for the GDR users. The purpose of this document is to report the major features of the data quality from the Jason-1 mission. Moreover, the document is associated with comparison results from T/P GDRs. All these cycle reports are available on AVISO website: http://www.jason.oceanobs.com.
In addition to these reports, several meeting (CAVE, OSTST) have been performed to inform the Jason-1 GDR's users about the main results and the studies in progress.

2.2 CAL/VAL status

2.2.1 Missing measurements

This section presents a summary of major satellite events that occurred from cycle 1 to 175. Table 1 gives a status about the number of missing passes (or partly missing) and the associated events for each cycle.
Gyro calibration, Star Tracker unavailability and ground processing issues were the main events which produced missing data from cycle 1 to 64 (2002 and 2003) recalling that ground processing issue will be resolved for the next GDR release.
During year 2004 (cycle 65 to 109), 2 safe hold mode incidents have produced 15 days of missing data due to a wheel anomaly. As result of this incident, only 3 wheels have been available but this has had no impact on scientific applications.
During year 2005 (110-146), most of incidents are due to SEU on C Band (see section 2.4. Few passes have only been impacted every time. Moreover some passes have been edited due to mispointing values out of the thresholds especially at the end of the period. This is mainly due to the star-tracker unavailability.
During year 2006 (cycles 147 - 175) Jason-1 worked almost without incidences, except for an altimeter SEU occurred on 19/09/2006 (cycle 173). It also happened that small data gaps occur (less than a minute duration).

Jason-1 Cycles	Number of Missing passes	Number of partly missing passes	Events
001	12	0	Science telemetry unavailability
002	16	0	On board Doris anomaly
			.../...

Jason-1 Cycles	Number of Missing passes	Number of partly missing passes	Events
003	0	1	Gyro-calibration
004	2	5	Gyro-calibration and Science telemetry unavailability
006	1	4	Altimeter echo data unavailability
008	5	0	Ground processing issue
009	9	3	Poseidon-2 altimeter SEU and Gyro-calibration
010	0	2	Gyro-calibration
014	2	1	Ground processing issue
015	2	1	Ground processing issue
016	1	1	Ground processing issue
019	2	1	Ground processing issue
021	0	1	Star tracker unavailability
023	0	1	Ground processing issue
026	0	2	Gyro-calibration
027	0	2	Gyro-calibration
029	4	2	Ground processing issue
031	1	1	Ground processing issue and Star tracker unavailability
032	38	1	DORIS data unavailability and ground processing issue
035	1	2	Ground processing issue
038	0	4	Ground processing issue
039	0	1	Gyro-calibration
042	8	2	Poseidon-2 altimeter SEU and ground processing issue
045	0	3	Gyro-calibration
046	0	1	Poseidon-2 altimeter SEU
048	0	1	Gyro-calibration
			.../...

Jason-1 Cycles	Number of Missing passes	Number of partly missing passes	Events
055	1	1	Ground processing issue
061	1	2	Ground processing issue
062	2	1	Ground processing issue
064	0	2	Exceptional calibrations
075	4	0	Poseidon-2 altimeter SEU
077	69	0	Safe hold mode (15/02/04 to 21/02/04)
078	82	0	Safe hold mode (15/02/04 to 21/02/04)
080	0	1	Calibration over ocean
082	54	0	Failure in module 3 of on board ...
087	0	1	Calibration over ocean
091	25	0	DORIS instrument switch to redundancy and altimeter incident (no C band information)
094	0	1	Under investigation : altimeter incident or star tracker unavailability
099	0	1	Under investigation : altimeter incident or star tracker unavailability
101	0	1	Under investigation : altimeter incident or star tracker unavailability
102	2	0	Altimeter SEU (no C band information)
103	4	1	Altimeter SEU (no C band information)
104	0	1	No data between 21:29:18 and 21:30:07 on November 8th pass 189
106	3	2	Altimeter SEU (no C band information)
108	5	0	Altimeter SEU (no C band information)
114	3	1	Altimeter SEU (no C band information)
			.../...

Jason-1 Cycles	Number of Missing passes	Number of partly missing passes	Events
115	6	2	2 altimeter SEU incidents (C band) and altimeter initialization procedure.
118	6	2	Altimeter SEU (no C band information)
131	0	7	TRSR2 "elephant packets" anomaly
132	0	1	Altimeter SEU (no C band information)
136	104	2	Altimeter SEU (no C band information), Platform incident (20/09/05 to 28/09/05)
137	91	2	Platform incident (20/09/05 to 28/09/05)
161	0	5	TRSR elephant packets
165	0	1	(planned) Poseidon calibration (board filter)
173	0	3	Altimeter SEU (no C band information)

Table 1: *M*issing pass status

2.2.2 Edited measurements

Table 2 indicates the cycles which have a larger amount of removed data due to editing criteria (see section 3.2.1). Most of the occurrences correspond to Star Tracker unavailability.
Notice that since cycle 78, the satellite operates with only 3 wheels: the maneuver impact (burn maneuver, yaw transition) is greater than before on the attitude control. Consequently, some measurements can be edited due to higher mispointing values when a maneuver occurs. Improvements in ground retracking algorithm have been set up in place and are resolved in the GDR "b" release, and improvements on Star Tracker behavior are performed in 2006. Therefore only few measurements were edited by mispointing criterion.

Jason-1 Cycles	Comments
003	Pass 1 is removed due to bad orbit quality. The burn maneuver is not correctly taken into accounts on this pass.
006	Pass 56 (in the Pacific ocean) is partly edited due to the bad quality of data. Indeed, the altimetric parameters values are out of the thresholds.
	.../...

Jason-1 Cycles	Comments
008	All the altimetric parameters are edited for 10% of pass 210 due to the bad quality of all the altimetric parameters as a result of a Star Tracker incident leading to a quite high off nadir angle. A part of pass 087 is edited by the square of the mispointing angle criterion due to a Star Tracker incident.
010	All the altimetric parameters are edited for 15% of pass 210. This is due to the Star Tracker unavailability as for cycle 6.
021	Small part of pass 254 is edited after checking the square of the mispointing angle criterion.
053	Some mispointing angle values are out of threshold. This is due to a satellite maneuver on this pass.
069	Passes 209 to 211 are edited due to the JMR set to default value. This is linked to the safe hold mode on cycle 69 : the JMR has been set on 2 hours after the altimeter.
078	Passes 83 to 85 are edited due to the JMR set to default value. This is linked to the safe hold mode on cycle 88 : the JMR has been set on 2 hours after the altimeter.
084	Pass 84 is partly edited (great mispointing values) due to a yaw flip.
089	Pass 167 is partly edited (great mispointing values) due to a yaw flip.
096	Pass 36 is partly edited (great mispointing values) due to a yaw flip.
098	Pass 98 is partly edited (great mispointing values) due to the star-tarcker unavailability.
098	Pass 115 is partly edited (great mispointing values) due to the star-tarcker unavailability.
101	Pass 254 is partly edited (great mispointing values) due to a burn maneuver
102	Pass 37 is partly edited (great mispointing values) due to a yaw flip maneuver
107	Pass 138 is partly edited (great mispointing values) due to a yaw flip maneuver
109	Pass 219 and 220 are partly edited (great mispointing values). Star-tracker is out of the SCAO loop during 2 hours (dark current monitoring).
113	Pass 213 is partly edited (great mispointing values) due to a yaw flip maneuver
119	Pass 190 is partly edited (great mispointing values) due to the star-tarcker unavailability.
122	Passes 142 to 143 were partially edited (great mispointing values). Star-tracker is out of the SCAO loop.
	.../...

Jason-1 Cycles	Comments
124	Passes 3 and 4 were partially edited (great mispointing values) due to a burn maneuver.
125	Pass 89 is partly edited (great mispointing values) due to a yaw flip maneuver.
131	Pass 190 is partly edited (great mispointing values) due to a yaw flip maneuver.
133	Pass 21 is partly edited (great mispointing values) due to the star-tracker unavailability.
134	Passes 83, 153, 177, 233 and 235 are partly edited (great mispointing values) due to the star-tracker unavailability.
135	Many passes are partly edited (great mispointing values) due to the star-tracker unavailability.
137	Passes 92, 93 and partly 94 are edited by radiometer wet tropospheric correction, since the radiometer was later switched on than the other instruments.
173	As the altimeter is only restarted during pass 68, the dual-frequency ionospheric correction is partially missing for passes 65 and 68 and fully for passes 66 and 67.
175	Pass 9 is partly edited by mispointing criterion out of threshold (probably aberrant quaternion).

Table 2: *E*dited measurement status

2.3 Jason-1 product version "b"

2.3.1 Models and Standards History

Two versions of the Jason-1 Interim Geophysical Data Records (IGDRs) and Geophysical Data Records (GDRs) have been generated to date. These two versions are identified by the version numbers "a" and "b" in the name of the data products. For example, version "a" GDRs are named "JA1_GDR_2Pa" and version "b" GDRs are named "JA1_GDR_2Pb". Both versions adopt an identical data record format as described in Jason-1 User Handbook and differ only in the models and standards that they adopt. Version "a" I/GDRs were the first version released soon after launch. Version "b" I/GDRs were first implemented operationally from the start of cycle 140 for the IGDRs and cycle 136 for the GDRs. Reprocessing to generate version "b" GDRs for cycles 1-135 will be performed to generated a consistent data set early in 2007. The table 3 below summarizes the models and standards that are adopted in these two versions of the Jason I/GDRs. More details on some of these models are provided in Jason-1 User Handbook document.

Model	Product Version "a"	Product Version "b"
Orbit	JGM3 Gravity Field DORIS tracking data for IGDRs DORIS+SLR tracking data for GDRs	EIGEN-CG03C Gravity Field DORIS tracking data for IGDRs DORIS+SLR+GPS tracking data for GDRs
Altimeter Retracking	MLE3 + 1st order Brown model (mis pointed estimated separately)	MLE4 + 2nd order Brown model : MLE4 simultaneously retrieves the 4 parameters that can be inverted from the altimeter waveforms: epoch, SWH, Sigma0 and mispointing angle. This algorithm is more robust for large off-nadir angles (up to 0.8°).
Altimeter Instrument Corrections	Consistent with MLE3 retracking algorithm.	Consistent with MLE4 retracking algorithm.
Jason Microwave Radiometer Parameters	Using calibration parameters derived from cycles 1-30.	Using calibration parameters derived from cycles 1-115.
Dry Troposphere Range Correction	From ECMWF atmospheric pressures.	From ECMWF atmospheric pressures and model for S1 and S2 atmospheric tides.
Wet Troposphere Range Correction from Model	From ECMWF model	From ECMWF model.
		.../...

Model	Product Version "a"	Product Version "b"
Back up model for Ku-band ionospheric range correction.	Derived from DORIS measurements.	Derived from DORIS measurements.
Sea State Bias Model	Empirical model derived from cycles 19-30 of version "a" data.	Empirical model derived from cycles 11-100 of MLE3 altimeter data with version "b" geophysical models.
Mean Sea Surface Model	GSFC00.1	CLS01
Along Track Mean Sea Surface Model	None (set to default)	None (set to default)
Geoid	EGM96	EGM96
Bathymetry Model	DTM2000.1	DTM2000.1
Inverse Barometer Correction	Computed from ECMWF atmospheric pressures	Computed from ECMWF atmospheric pressures after removing model for S1 and S2 atmospheric tides.
Non-tidal High-frequency Dealiasing Correction	None (set to default)	Mog2D ocean model on GDRs, none (set to default) on IGDRs. Ocean model forced by ECMWF atmospheric pressures after removing model for S1 and S2 atmospheric tides.
Tide Solution 1	GOT99	GOT00.2 + S1 ocean tide . S1 load tide ignored.
Tide Solution 2	FES99	FES2004 + S1 and M4 ocean tides. S1 and M4 load tides ignored.
Equilibrium long-period ocean tide model.	From Cartwright and Taylor tidal potential.	From Cartwright and Taylor tidal potential.
Non-equilibrium long-period ocean tide model.	None (set to default)	Mm, Mf, Mtm, and Msqm from FES2004.
Solid Earth Tide Model	From Cartwright and Taylor tidal potential.	From Cartwright and Taylor tidal potential.
Pole Tide Model	Equilibrium model	Equilibrium model.
Wind Speed from Model	ECMWF model	ECMWF model
Altimeter Wind Speed	Table derived from TOPEX/POSEIDON data.	Table derived from version "a" Jason-1 GDR data.
		.../...

Model	Product Version "a"	Product Version "b"
Rain Flag	Derived from TOPEX/POSEIDON data.	Derived from version "a" Jason-1 GDRs.
Ice Flag	Climatology table	Climatology table

Table 3: *M*odels and standards adopted for the Jason-1 product version "a" and product version "b"

2.3.2 Impact of product version ”b” for the SSH calculation

2.3.2.1 Editing procedure

The new MLE4 retracking algorithm based on a second-order altimeter echo model is more robust for large off-nadir angles (up to 0.8 degrees). For product version "a" (previous CMA version 6.3), the maximum threshold on square off-nadir angle proposed in Jason-1 User Handbook document was set to 0.16 deg^2. Henceforth, this threshold is too restrictive and has to be set to 0.64 deg^2.

However, this editing criteria had the side effect of removing some bad measurements impacted by rain cells, sigma0 blooms or ice. With the new threshold (0.64 deg^2), these measurements are not rejected any more even though the estimated SSH is not accurate for such waveforms.
Therefore 2 new criteria have to be added to check for data quality:

- Standard deviation on Ku sigma0 $\leq$ 1 dB
- Number measurements of Ku sigma0 $\geq$ 10

The Jason-1 User Handbook suggests the following editing criteria for the version "a" GDRs:

- -0.2 $deg^2 \leq$ square of off-nadir angle from waveforms (off_nadir_angle_ku_wvf) $\leq$ 0.16 deg^2
- sigma0_rms_ku $<$ 0.22 dB (optional criterion)

For the version "b" GDRs these two edit criteria should be replaced by:

- -0.2 $deg^2 \leq$ square of off-nadir angle from waveforms (off_nadir_angle_ku_wvf) $\leq$ 0.64 deg^2
- and sigma0_rms_ku $\leq$ 1.0 dB
- and sig0_numval_ku $\geq$ 10

With these new criteria, the editing gives similar results for both product versions. Most of anomalous SSH measurements are rejected. Please note that some of them are still not detected, in particular close to sea ice. This is due to the ice flag which is not perfect.

2.3.2.2 Impact on mean SSH

Some evolutions have a direct impact on the SSH estimation. The global bias between version "a" and "b" of the products is 1.9 cm :

$$\overline{SSH_{CMA_{7.1}}} = \overline{SSH_{CMA_{6.3}}} - 1.9cm$$

This comes from two main components:

- A very slight effect of the MLE4 retracking and of the new instrumental tables (0.1 cm).
- The improved SSB correction is shifted in average by 2.0 cm in comparison with the previous one

$$\overline{SSB_{CMA_{7.1}}} = \overline{SSB_{CMA_{6.3}}} + 2.0cm$$

For several scientific applications (mean sea level trend, ...), it is important to take this difference in mean SSH into account until all the GDRs cycles are provided with the new ground processing version.

2.3.2.3 Impact on mean SWH and sigma0

MLE4 retracking algorithms has no impact on SWH mean value.
Impact of MLE4 retracking algorithms on sigma0_ku mean value is 0.1 dB (sigma0_ku becoming higher).
Please note that the rms on 20 Hz Ku sigma0 has increased as a consequence of the MLE4 inversion scheme.

2.3.2.4 Jason-1 Radiometer wet troposphere correction

The Jason-1 Microwave Radiometer (JMR) has been re-calibrated using data from repeat cycles 1-115. Version "b" GDRs contain the re-calibrated JMR data and some improved algorithms to derive JMR brightness temperatures. The re-calibrated JMR data remove the anomalous jumps observed in the JMR path delays on the version "a" GDRs. As a result of this recalibration a bias of approximately 0.9 cm in the JMR wet path delays exists between the version "a" GDRs from cycle 135 and the version "b" GDRs from cycle 136. This bias will then also affect mean SSH at this transition when JMR wet path delays are used to compute SSH.

A JMR replacement product that contains re-calibrated JMR wet path delay measurements for cycles that are still in version "a" GDRs (e.g. cycles < 136) has been released. This replacement product can be used to correct JMR behavior for early cycles. Nevertheless to ensure a stable sea surface height time series for precision applications such as mean sea level monitoring, it is preferable to use the ECMWF model wet troposphere correction.

2.4 Data quality during C band SEU

2.4.1 Presentation

During an SEU (Single Event Upset), radiation of particles changes the configuration of the onboard computer causing loss of the altimeter measurements in C band. Therefore the ionospheric correction based on dual frequency measurements is impossible. Generally the corresponding GDRs wont be delivered.
The aim of this work is to study the quality of the data in the Ku band in order to be able to diffuse the GDRs even if no ionospheric correction is possible.
For this study we used 22 SEU passes coming from cycles 091 (passes 127 to 129), 102 (passes 187 to 189), 103 (passes 28 to 31), 108 (passes 14 to 18), and 115 (passes 19 to 21 and 28 to 31).

The cycles containing GDRs with SEU were reprocessed in the frame of a study by a Calval type chain. A flag containing the information of SEU was updated in the database and for the case of SEU the ionospheric correction based on dual frequency measurements was replaced by the model ionospheric correction GIM.

2.4.2 Quality of altimeter parameters during SEU

We first verified that the measured altimetric parameters during SEU were fine. The Figure 1 shows the histogram of the square of the off nadir angle from waveforms for the SEU incidences (left). In the right the histogram of passes from cycle 115 without SEU are shown. The histograms are very similar.

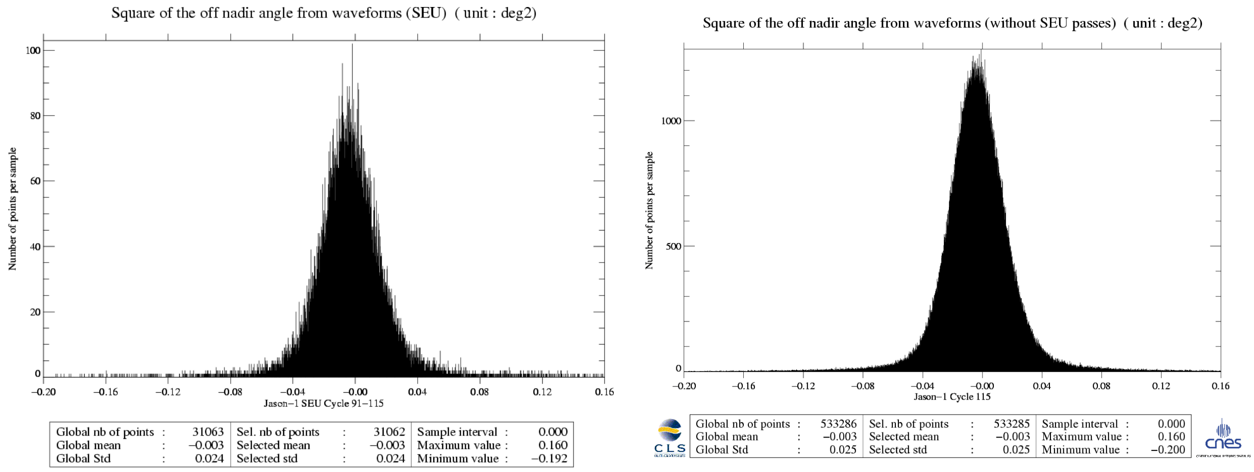

Figure 1: *Square of the off nadir angle from waveforms for the SEU incidences (cycles 091,102,103,108,115) (left) and for the passes without SEU of cycle 115 (right).*

The table 4 shows some statistical values for several altimetric parameters both for the SEU passes and (for comparison) passes from cycle 117 (which had no SEU incidences).
The values are quite similar, so we can conclude that the altimetric parameters during an SEU incident are good.

Parameter	Mean SEU/Cycle117	Rms SEU/Cycle117	Max SEU/Cycle117	Min SEU/Cycle117
ATT_FO_CARRE	-0.0 / -0.0	0.0 / 0.0	0.1 / 0.1	-0.1 / -0.2
SIG0	13.6 / 13.7	1.3 / 1.6	23.3 / 23.4	9.5 / 9.3
SWH	262.1 / 270.2	122.4 / 125.8	957.9 / 1099.1	0.8 / 0.0
ECT_SWH	52.7 / 52.9	11.2 / 11.3	520.1 / 765.0	0.0 / 0.0
DALT	1346.5 / 1347.0	5.3 / 5.4	1356.3 / 1355.9	1339.1 / 1338.8
NB_DALT	19.6 / 19.5	0.7 / 0.8	20.0 / 20.0	10.0 / 0.0
ECT_DALT	7.3 / 7.4	1.9 / 1.9	19.8 / 20.0	1.4 / 0.8
TRO_HUM_RAD	-14.3 / -13.6	9.7 / 9.2	-0.1 / -0.0	-47.5 / 49.3

Table 4: Statistical values (Mean, Rms, Max, Min) of several altimetric parameters during passes with SEU and a cycle (117) without SEU.

2.4.3 Quality of SSH during SEU

Since cycle 115 was the cycle with the most SEU passes, table 5 shows the crossover differences for the 7 passes with SEU incident of cycle 115, for the 247 passes without SEU, and for all (254) passes. The crossover differences computed with the SEU values are slightly worse (are more biased) than crossover differences computed without SEU values. Nevertheless these values are still useful. Figure 2 shows a zoom of the evolution of SSH computed for passes with and without SEU. The SSH of the SEU pass is not noisier than the SSH of the other passes.

Selection	Number of Points (SEU/withoutSEU/Total)	Mean (SEU/withoutSEU/Total)	Rms (SEU/withoutSEU/Total)
No selection	335 / 7891 / 8223	1.02 / -0.26 / -0.26	8.01 / 6.92 / 6.98
Geographical Selection	117 / 2766 / 2880	-1.12 / -0.05 / -0.10	4.76 / 6.00 / 5.89

Table 5: Statistical values of crossover differences for cycle 115 for no selection and geographical selection. 3 cases: SEU passes, passes without SEU, all passes.

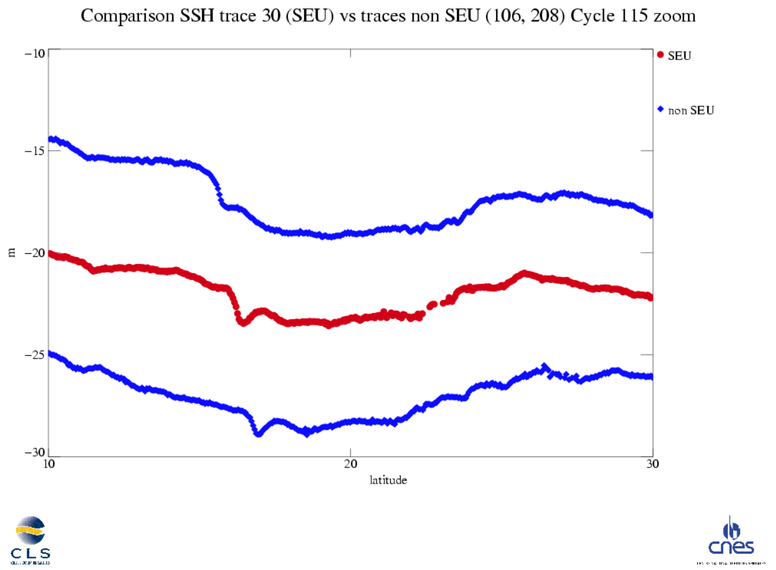

Figure 2: *Comparison of SSH of pass with SEU incidences (in red, pass 30 cycle 115) vs SSH of passes without SEU incidences (in blue, passes 106 and 208, cycle 115).*

3 Data coverage and edited measurements

3.1 Missing measurements

3.1.1 Over ocean

Determination of missing measurements relative to the theoretically expected orbit ground pattern is used to detect missing telemetry in Jason-1 datasets due to altimetry events for instance. This procedure is applied cycle per cycle and leads to results plotted on the left figure 3. It represents the percentage of missing measurements relative to the theory, when limited to ocean surfaces. The mean value is about 3.8% but this figure is not significant due to several events where the measurements are missing. All these events are described on table 1.
On figure 3 on the right, the percentage of missing measurements is plotted without taking into account the cycles where instrumental events or other anomalies occurred. Moreover shallow waters and high latitudes have been removed. This allows us to detect small data gaps in open ocean. The mean value is about 0.02%. This weak percentage of missing measurements is mainly explained by the rain cells, ice sea or sigma0 blooms. These sea states can disturb significantly the Ku band waveform shape leading to a non significant measure.

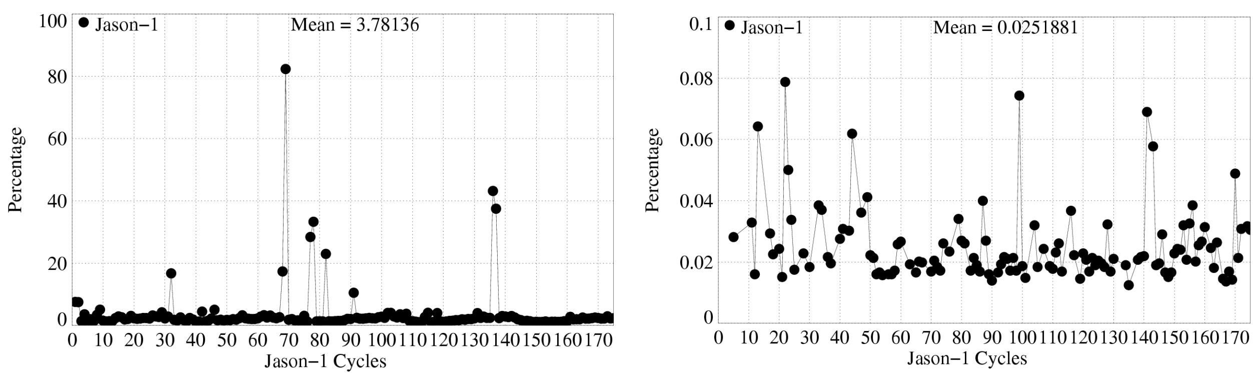

Figure 3: *Cycle per cycle percentage of missing measurements over ocean*

3.1.2 Over land and ocean

Figure 4 shows the percentage of missing measurements for Jason-1 and T/P (all surfaces) computed with respect to a theoretical possible number of measurements. Due to differences between tracker algorithms, the number of data is greater for T/P (excepted when T/P experienced problems, especially since the tape recorders were no longer in service (T/P cycle 444, Jason-1 cycle 101)) than for Jason-1. Differences appear on land surfaces as is shown in figure 5.

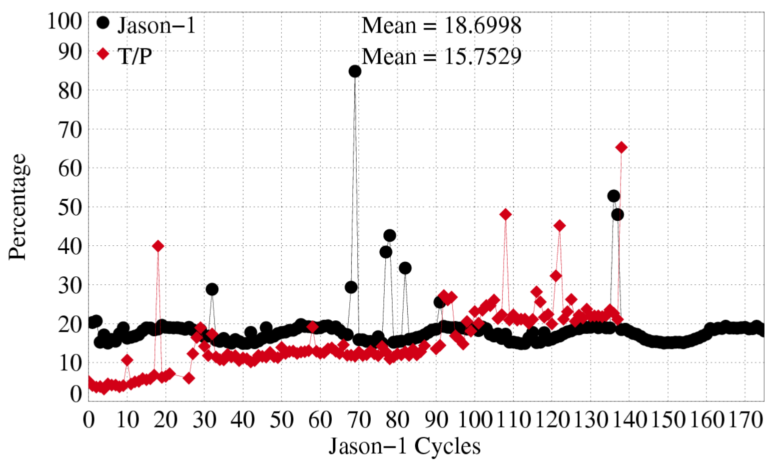

Figure 4: *Percentage of missing measurements over ocean and land for J1 and T/P*

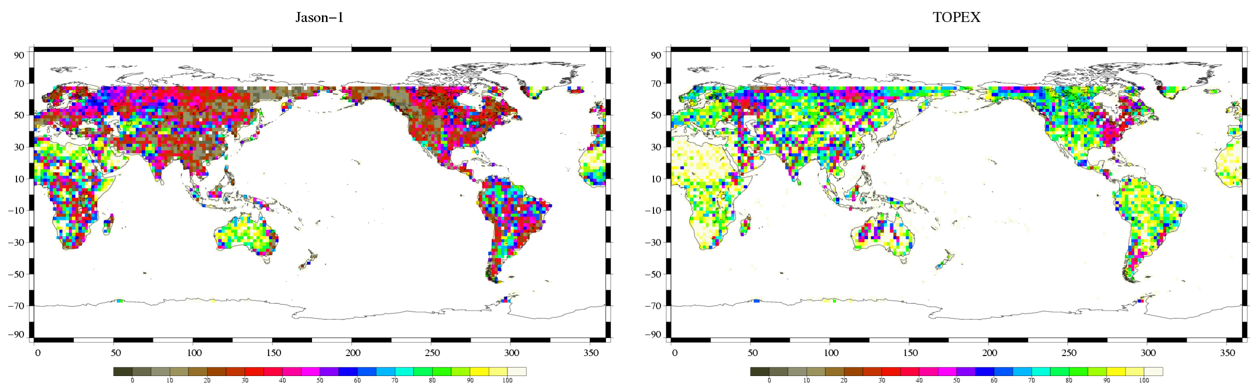

Figure 5: *Map of percentage of available measurements over land for Jason-1 on cycle 61 (left) and for TOPEX on cycle 404 (right)*

3.2 Edited measurements

3.2.1 Editing criteria definition

Editing criteria are used to select valid measurements over ocean. The editing criteria are divided into 4 parts. First, only measurements over ocean and lake are kept (see section 3.2.2). Second, the quality criteria concern the flags which are described in section 3.2.3 and 3.2.5. Then, threshold criteria are applied on altimeter, radiometer and geophysical parameters and are described in the table 6. Moreover, a spline criterion is applied to remove the remaining spurious data. These criteria defined for the GDR products "a" are also defined in AVISO and PODAAC User handbook. They will be modified for the GDR products "b" (see section 2.3). For each criterion, the cycle per cycle percentage of edited measurements has been monitored. This allows detection of anomalies in the number of removed data, which could come from instrumental, geophysical or algorithmic changes.

Parameter	Min thresholds	Max thresholds	mean edited
Sea surface height	$-130\ m$	$100\ m$	1.71%
Sea level anomaly	$-10\ m$	$10.0\ m$	2.63%
Number measurements of range	10	*Not applicable*	2.11%
Standard deviation of range	0	$0.2\ m$	2.16%
Square off-nadir angle	$-0.2\ deg^2$	$0.64\ deg^2$	1.66%
Dry troposphere correction	$-2.5\ m$	$-1.9\ m$	0.00%
Inverted barometer correction	$-2.0\ m$	$2.0\ m$	0.00%
JMR wet troposphere correction	$-0.5m$	$-0.001\ m$	0.21%
Ionosphere correction	$-0.4\ m$	$0.04\ m$	1.96%
Significant waveheight	$0.0\ m$	$11.0\ m$	1.30%
Sea State Bias	$-0.5\ m$	$0.0\ m$	1.59%
Number measurements of Ku-band Sigma0	10	*Not applicable*	2.09%
Standard deviation of Ku-band Sigma0	0	$1.0\ dB$	2.21%
Ku-band Sigma0 [1]	$4.6\ dB$	$27.6\ dB$	1.21%
Ocean tide	$-5.0\ m$	$5.0\ m$	0.86%
Equilibrium tide	$-0.5\ m$	$0.5\ m$	0.00%
Earth tide	$-1.0\ m$	$1.0\ m$	0.00%
Pole tide	$-15.0\ m$	$15.0\ m$	0.00%
			.../...

Parameter	Min thresholds	Max thresholds	mean edited
Altimeter wind speed	$0\,m.s^{-1}$	$30.0\,m.s^{-1}$	1.60%
All together	-	-	3.84%

Table 6: *E*diting criteria

[1] The thresholds used for the Ku-band Sigma0 are the same than for T/P, but the sigma0 bias between Jason-1 and T/P (about 2.4 dB) is applied.

3.2.2 Selection of measurements over ocean and lakes

In order to remove data over land, a land-water mask is used. Only measurements over ocean or lakes are kept. Indeed, this allows us to keep more data near the coasts and then detecting potential anomalies in these areas. Furthermore, there is no impact on global performance estimations since the most significant results are derived from analyzes in deep ocean areas. Figure 6 shows the cycle per cycle percentage of measurements eliminated by this selection. It shows a seasonal signal. This is due to the varying number of measurements available in the GDRs, which varies not only over ocean, but also over land.

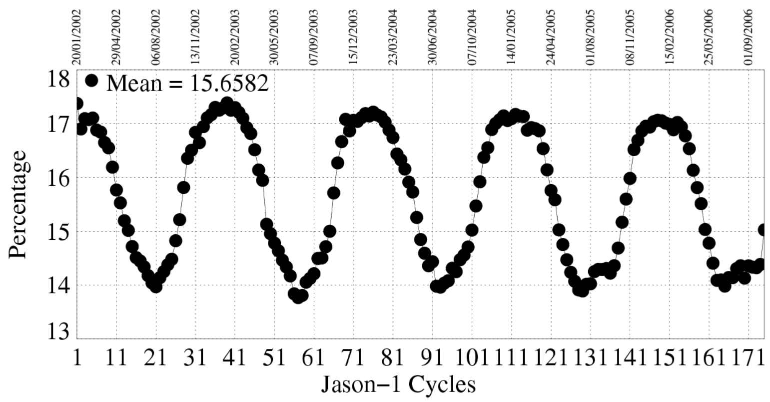

Figure 6: *Cycle per cycle percentage of eliminated measurements during selection of ocean/lake measurements*

3.2.3 Flagging quality criteria: Ice flag

The ice flag is used to remove the sea ice data. Figure 7 shows the cycle per cycle percentage of measurements edited by this criterion. No anomalous trend is detected but an annual cycle is visible. Indeed, the maximum number of points over ice is reached during the northern fall. The ice flag edited measurements are plotted in Figure 8 for one cycle. It shows that the ice flag is not perfectly tuned especially in the northern hemisphere, for instance the Hudson Bay is divided into 2 parts (figure 8, left). By using an empirical ice flag similar to the one used for ERS satellite (which involves the difference between bifrequency radiometer wet troposphere and model wet troposphere), the detection of ice is improved (see section 3.2.4).

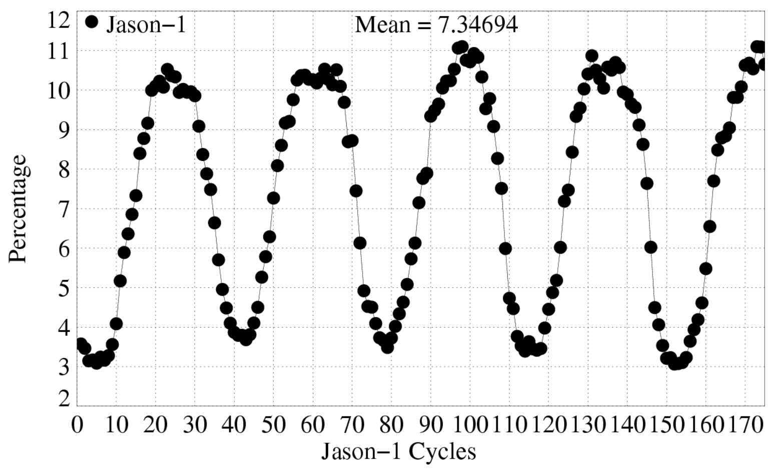

Figure 7: *Cycle per cycle percentage of edited measurements by ice flag criterion*

3.2.4 Flagging quality criteria: Ice flag with ERS method

The ice flag of ERS uses the difference between the dual-frequency radiometer wet troposphere and the ECMWF model wet troposphere. This difference is small over ocean, but important over ice. In [25] this method was adapted for Jason-1. The dual-frequency wet troposphere is calculated by

- Tropo_bifr = -0.01*(142.932-56.2442*LOG(280-TEMP_BRI_C2)+28.5724*LOG(280-TEMP_BRI_C3))

Ice is detected when for latitudes higher than 50° the following 2 conditions are fullfilled:

- Number of elementary measurements < 10
- |dual-frequency wet troposphere - ECMWF model wet troposphere| > 10 cm

This criteria works fine, and detects ice in the entire Hudson Bay. Nevertheless ice cover can also be found south of 50°N as for example in the northern part of Caspian sea, in the Aral Sea or in the La Perouse strait (north of Japon). Therefore the ERS ice flag should be extended to a latitude of 40°N within a coast distance of 500 km (to avoid erroneous ice detection in open sea). Figure 8 (right) shows ice detected on cycle 150 using the extended ERS ice flag. It shows that, ice is detected in the entire Hudson Bay, as well as in the Aral sea and in the northern part of the Caspian Sea.
This ice flag is an empirical method, which certainly does also have erroneous ice detection or ice which is not detected, but statistically is works fine and better than the current ice flag present in the GDRs.

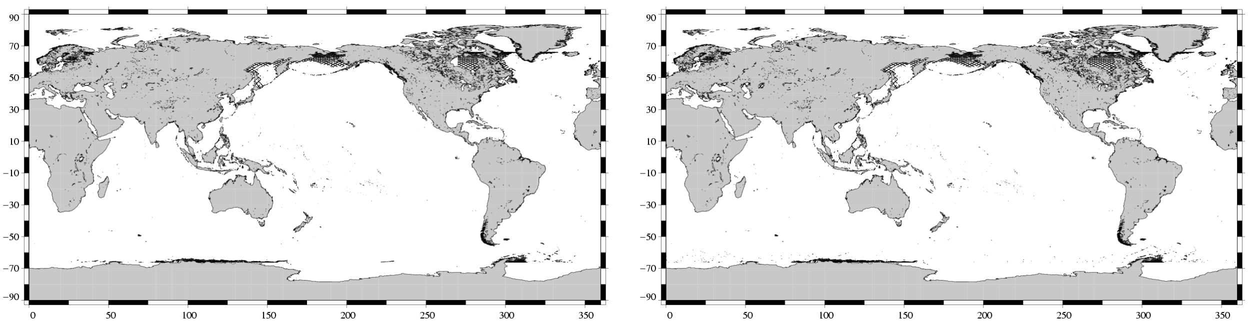

Figure 8: *Map of edited measurements by ice flag criterion on cycle 150 (left) and map of measurements, which would be edited when using ice flag criterion of type ERS on cycle 150 (right).*

3.2.5 Flagging quality criteria: Rain flag

The rain flag is not used for data selection since it is not yet tuned. It is thus recommended not to be used by users. The rain edited measurements are plotted in figure 9 for one cycle. It shows that too many measurements are edited by this flag.

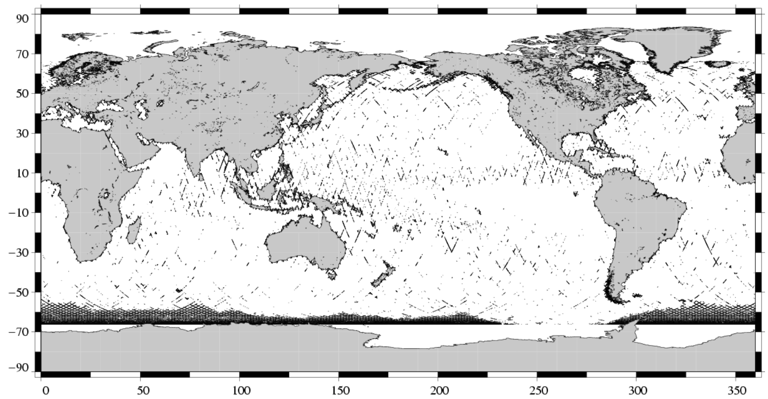

Figure 9: *Map of edited measurements by rain flag criterion (cycle 171)*

3.2.6 Threshold criteria: Global

Instrumental parameters have also been analyzed from comparison with thresholds, after having selected only ocean/lake measurements and applied flagging quality criteria (product ice flag). Notice that no measurements are edited by the following corrections : dry troposphere correction, inverted barometer correction, equilibrium tide, earth and pole tide pole.

The percentage of measurements edited using each criterion has been monitored on a cycle per cycle basis (figure 10). The mean percentage of edited measurements is about 3.8%. An annual cycle is visible due to the seasonal sea ice coverage in the northern hemisphere. Indeed most of northern hemisphere coasts are without ice during northern hemisphere summer. Consequently some of these coastal measurements are edited by the thresholds criteria in summer instead of the ice flag in winter. This seasonal effect visible in the statistics is not balanced by the southern hemisphere coasts due to the shore distribution between both hemispheres.
Notice that for cycle 69, 78 and 137, the percentage of edited measurements is higher than usual. This is due to the radiometer wet troposphere correction, see section 3.2.11.

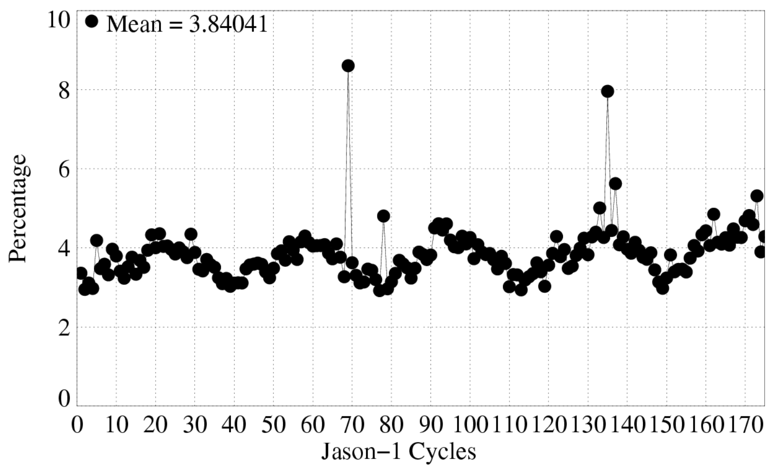

Figure 10: *Cycle per cycle percentage of edited measurements by threshold criteria*

3.2.7 Threshold criteria: 20-Hz measurements number

The percentage of edited measurements because of a too low number of 20-Hz measurements is represented in figure 11. No trend neither any anomaly has been detected.

The map of measurements edited by 20-Hz measurements number criterion is plotted in figure 12 for cycle 171 and shows correlation with heavy rain, wet areas and probably sea ice (near Antarctica) which has not been detected by the ice flag.

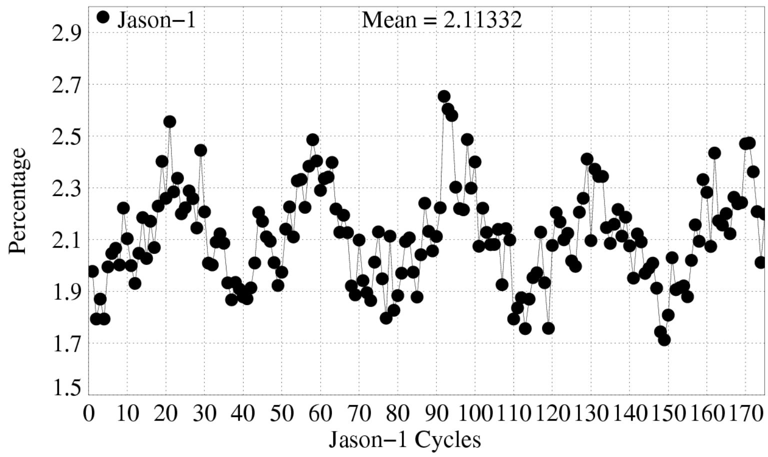

Figure 11: *Cycle per cycle percentage of edited measurements by 20-Hz measurements number criterion*

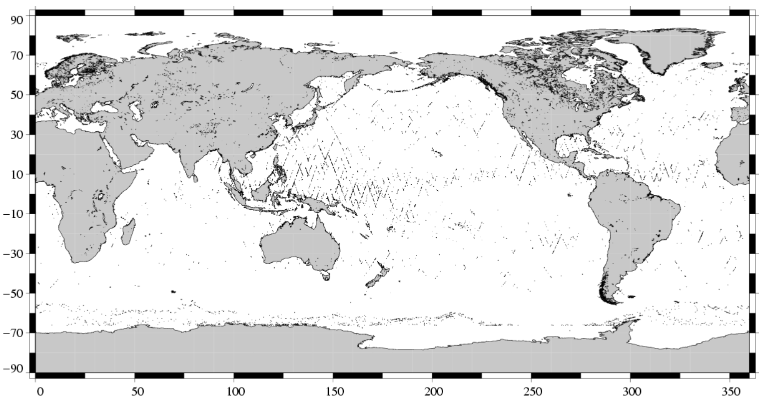

Figure 12: *Map of edited measurements by 20-Hz measurements number criterion for cycle 171*

3.2.8 Threshold criteria: 20-Hz measurements standard deviation

Same comment as in section 3.2.7 for the percentage of edited measurements due to the 20-Hz measurements standard deviation criterion (Figure 13 and 14).

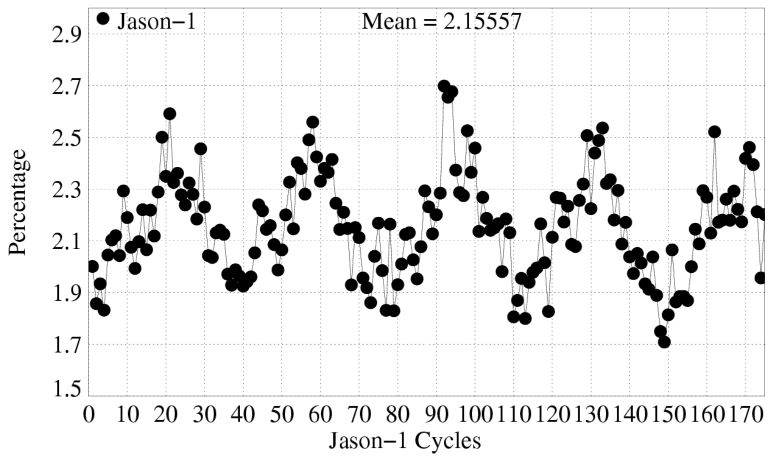

Figure 13: *Cycle per cycle percentage of edited measurements by 20-Hz measurements standard deviation criterion*

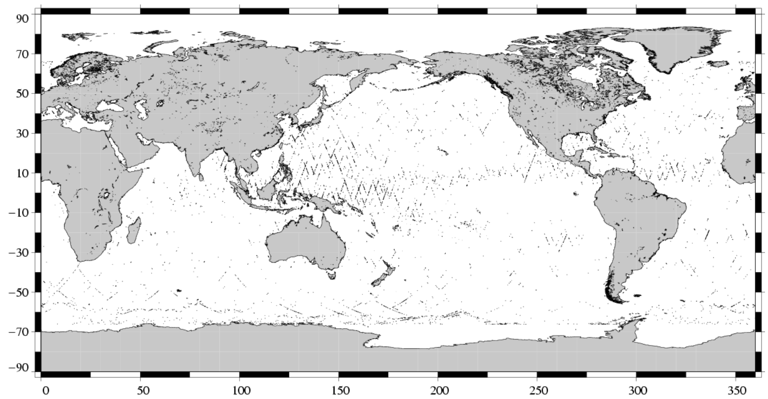

Figure 14: *Map of edited measurements by 20-Hz measurements standard deviation criterion for cycle 171*

3.2.9 Threshold criteria: Significant wave height

The percentage of edited measurements because of significant wave height out of threshold is represented in figure 15 and 16. A significant drop of edited measurements is observable at cycle 136. This is due to the new GDR "b" version with a new retracking algorithm. After reprocessing of cycle 1 to 135 in GDR version "b" this jump will probably disappear.

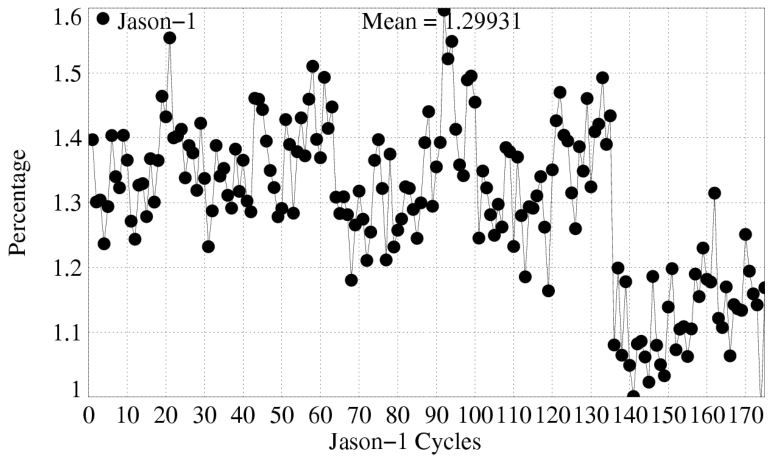

Figure 15: *Cycle per cycle percentage of edited measurements by SWH criterion*

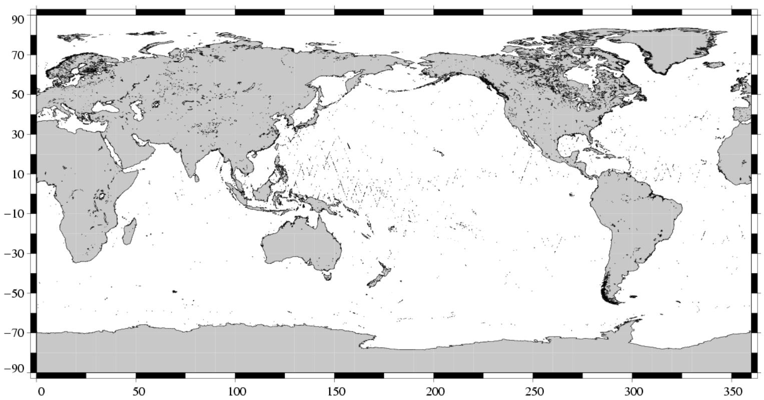

Figure 16: *Map of edited measurements by SWH criterion for cycle 171*

3.2.10 Backscatter coefficient

Same comment as in section 3.2.7 for the percentage of edited measurements due to the backscatter coefficient criterion (Figure 17 and 18).

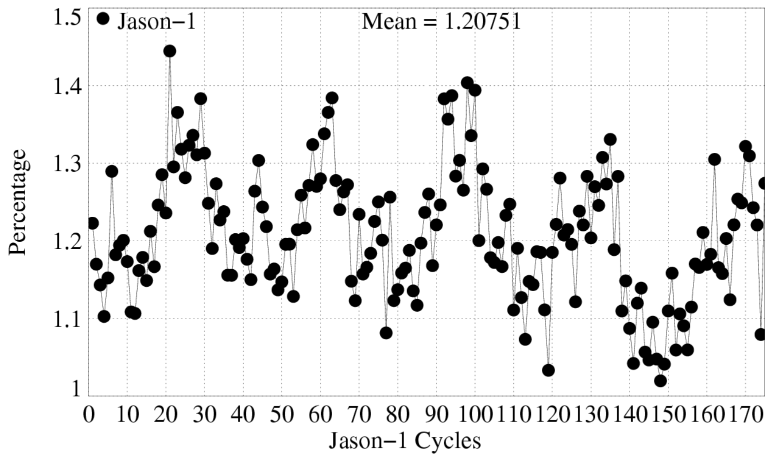

Figure 17: *Cycle per cycle percentage of edited measurements by Sigma0 criterion*

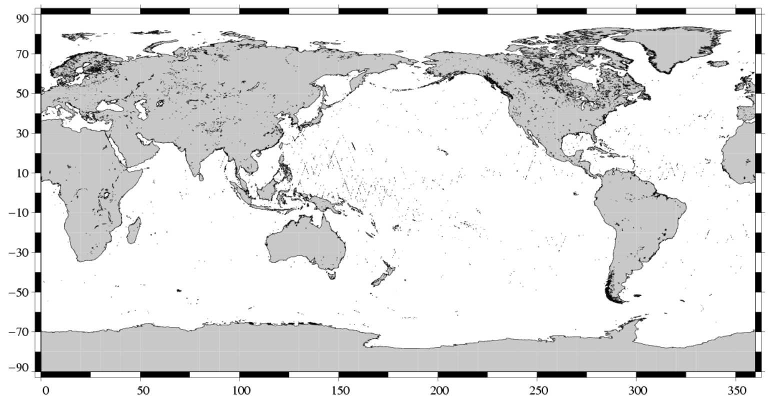

Figure 18: *Map of edited measurements by Sigma0 criterion for cycle 171*

3.2.11 Radiometer wet troposphere correction

Same comment as in section 3.2.7 for the percentage of edited measurements due to the radiometer wet troposphere criterion (Figure 19 and 20).
Notice that for cycle 69, 78 and 137, the percentage of edited measurements is higher than usual. This is linked to the Jason hold safe mode on these cycles: the radiometer has been set 2 hours later than the altimeter. As a result, the radiometer wet troposphere correction has been set to default value during this period and these measurements have been edited.

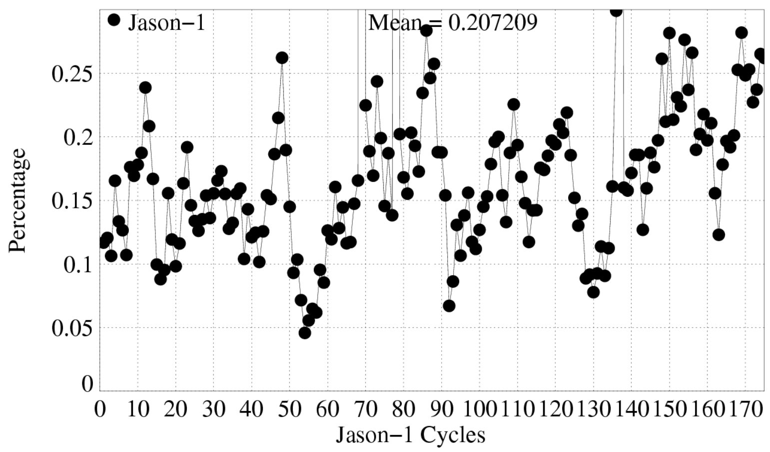

Figure 19: *Cycle per cycle percentage of edited measurements by radiometer wet troposphere criterion*

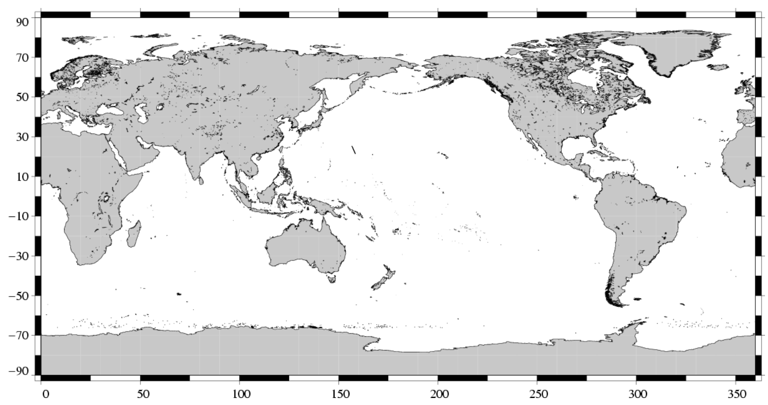

Figure 20: *Map of edited measurements by radiometer wet troposphere criterion for cycle 171*

3.2.12 Dual frequency ionosphere correction

Same comment as in section 3.2.7 for the percentage of edited measurements due to the dual frequency ionosphere criterion (Figure 21 and 22). Notice that for cycles 91, 133 and 173, the percentage of edited measurements is higher than usual. This is linked to the altimeter SEU (C band) on these cycles. The dual frequency ionosphere correction has been set to default value during this period and these measurements have been edited.

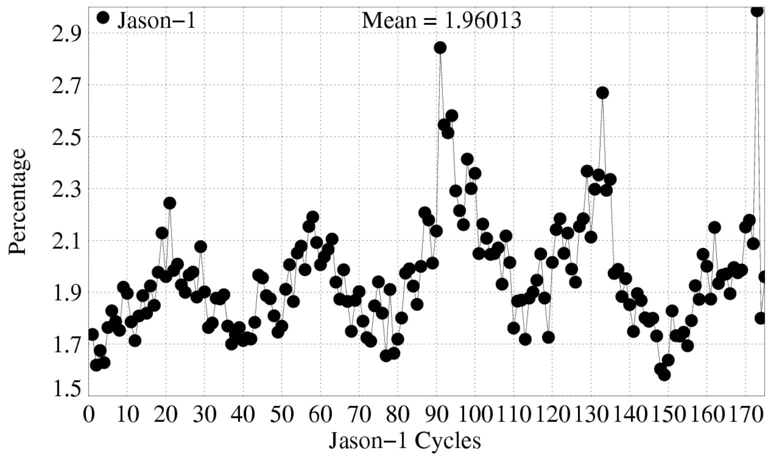

Figure 21: *Cycle per cycle percentage of edited measurements by dual frequency ionosphere criterion*

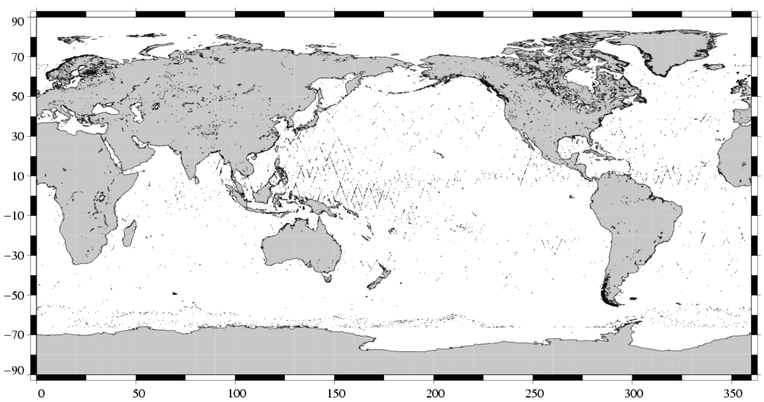

Figure 22: *Map of edited measurements by dual frequency ionosphere criterion for cycle 171*

3.2.13 Square off-nadir angle

The percentage of edited measurements because of square off-nadir angle out of threshold is represented in figure 23 and 24. From cycle 120 onward, a rise in edited measurements is observable with a maximum for cycle 135. This is due to problems with star-tracker data availability. Since introduction of GDR version "b" (cycle 136), the use of the new retracking algorithm lead to a significant drop of edited measurements (for more details see section 2.3). After reprocessing of cycle 1 to 135 in GDR version "b" this jump will probably disappear.

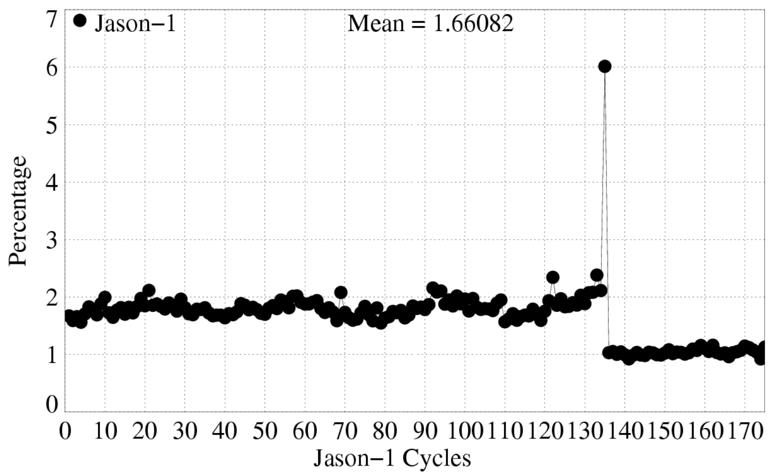

Figure 23: *Cycle per cycle percentage of edited measurements by square off-nadir angle criterion*

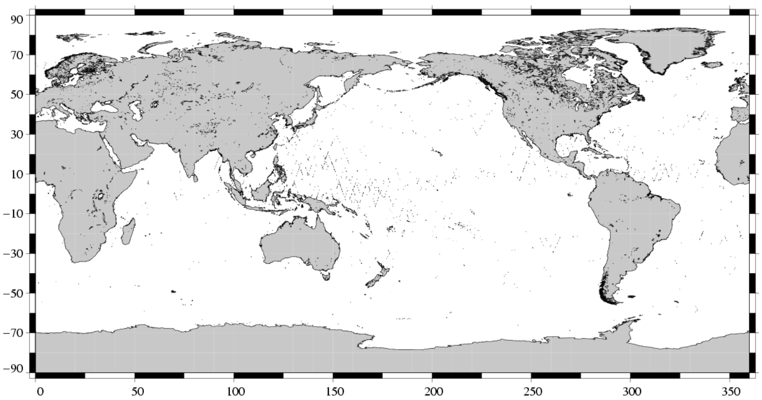

Figure 24: *Map of edited measurements by square off-nadir angle criterion for cycle 171*

3.2.14 Sea state bias correction

Same comment as in section 3.2.7 for the percentage of edited measurements due to the sea state bias criterion (Figure 25 and 26).

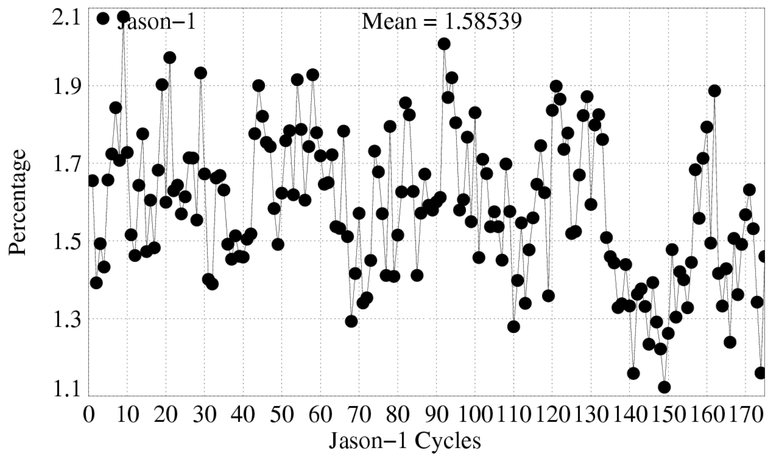

Figure 25: *Cycle per cycle percentage of edited measurements by sea state bias criterion*

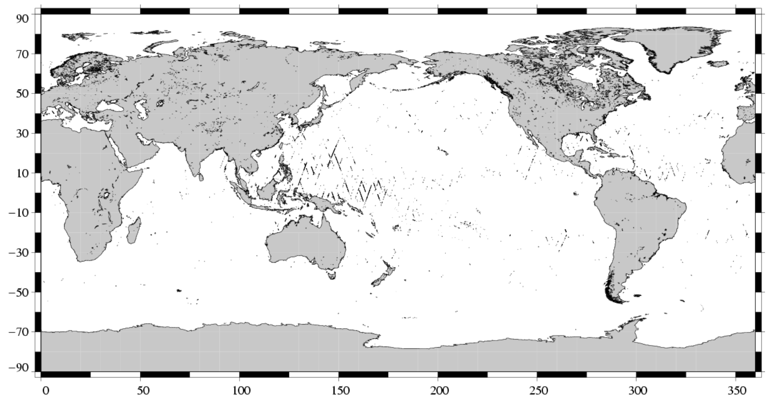

Figure 26: *Map of edited measurements by sea state bias criterion for cycle 171*

3.2.15 Altimeter wind speed

Same comment as in section 3.2.7 for the percentage of edited measurements due to the altimeter wind speed criterion (Figure 27 and 28).

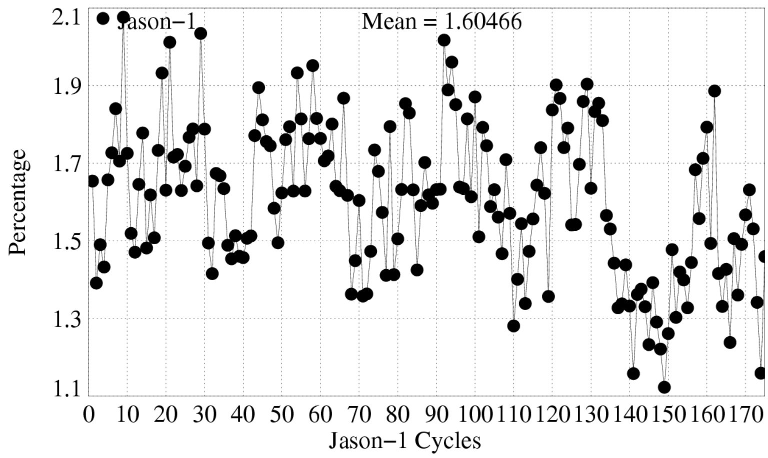

Figure 27: *Cycle per cycle percentage of edited measurements by altimeter wind speed criterion*

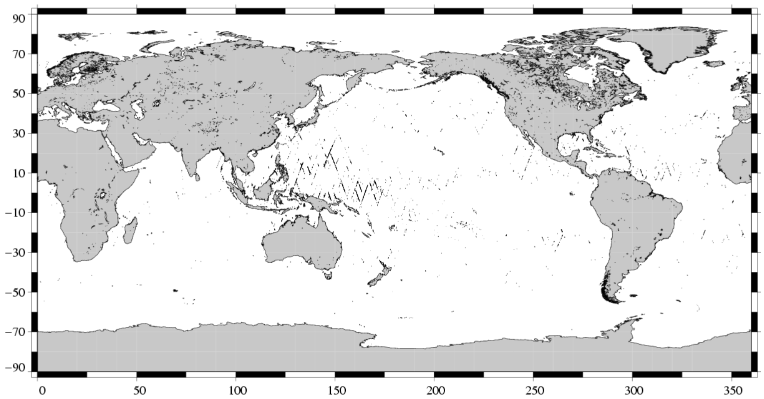

Figure 28: *Map of edited measurements by altimeter wind speed criterion for cycle 171*

3.2.16 Ocean tide correction

Same comment as in section 3.2.7 for the percentage of edited measurements due to the ocean tide criterion (Figure 29 and 30). The observed jump at cycle 136 is due to use of the GDR version "b". After reprocessing of cycles 1 to 135, the graph will be homogeneous.

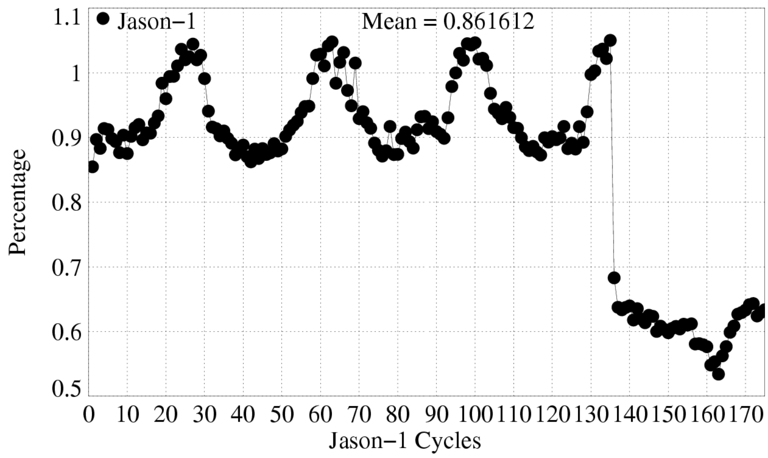

Figure 29: *Cycle per cycle percentage of edited measurements by ocean tide criterion*

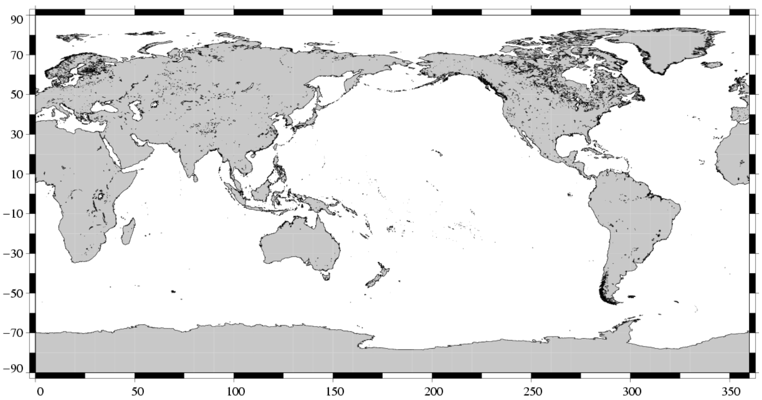

Figure 30: *Map of edited measurements by ocean tide criterion for cycle 171*

3.2.17 Sea surface height

Same comment as in section 3.2.7 for the percentage of edited measurements due to the sea surface height criterion (Figure 31 and 32).

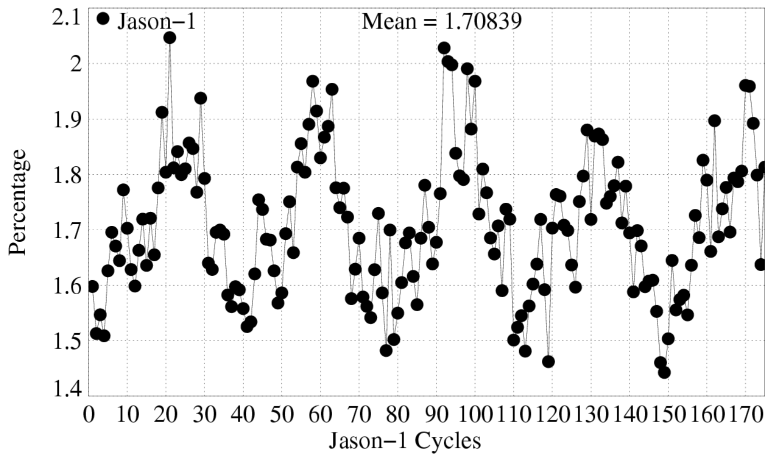

Figure 31: *Cycle per cycle percentage of edited measurements by sea surface height criterion*

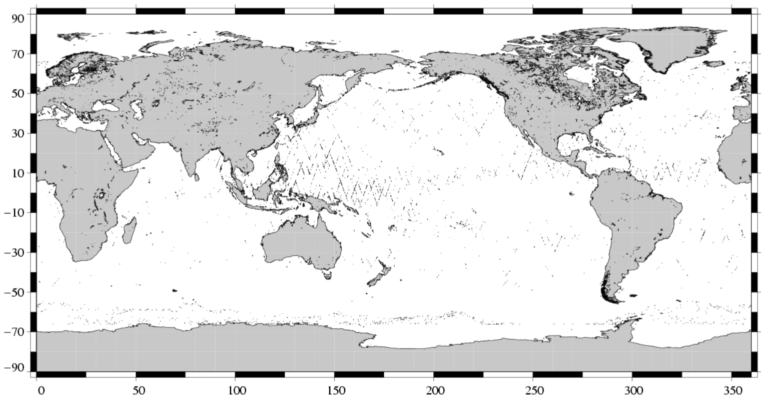

Figure 32: *Map of edited measurements by sea surface height criterion for cycle 171*

3.2.18 Sea level anomaly

Same comment as in section 3.2.7 for the percentage of edited measurements due to the sea level anomaly criterion (Figure 33). The map in figure 34 allows us to plot the measurements edited by the sea level anomaly criterion after applying all other threshold criteria.

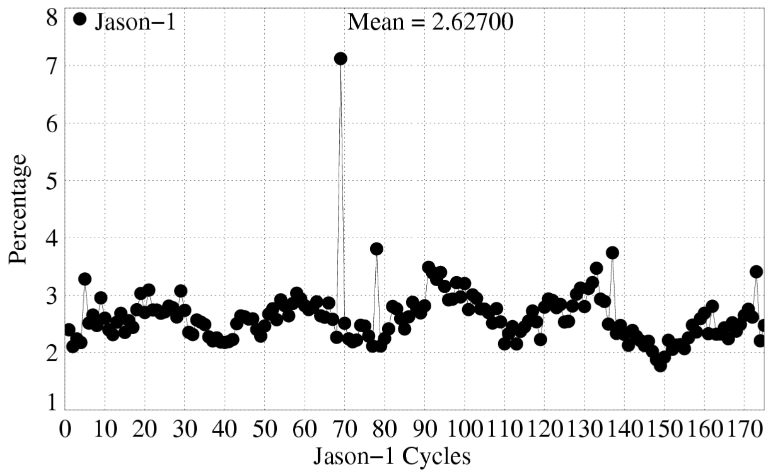

Figure 33: *Cycle per cycle percentage of edited measurements by sea level anomaly criterion*

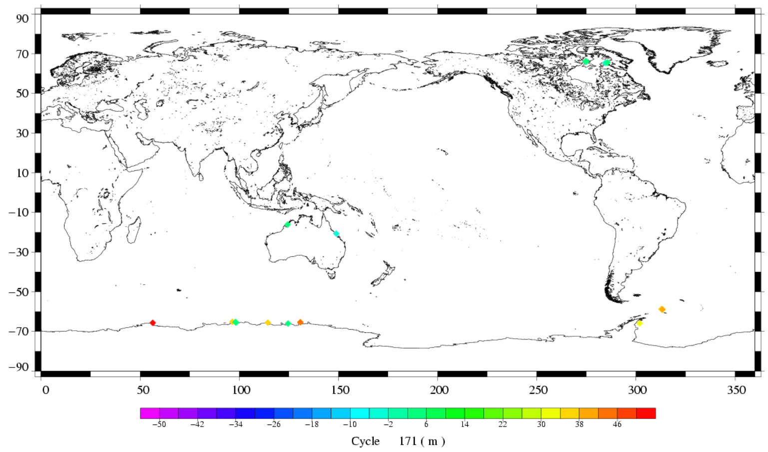

Figure 34: *Map of edited measurements by sea level anomaly criterion for cycle 171*

4 Monitoring of altimeter and radiometer parameters

4.1 Methodology

Both mean and standard deviation of the main parameters of Jason-1 have been monitored since the beginning of the mission. Moreover, a comparison with T/P parameters has been performed: it allows us to monitor the bias between the parameters of the 2 missions. The comparison is done till the end of scientific mission of T/P, which occurred during Jason-1 cycle 139. Two different methods have been used to compute the bias:

- During the verification phase, Jason-1 and T/P ground tracks are on the same ground track and are spaced out about 1 minute apart. The mean of the T/P Jason-1 differences can be computed using a point by point repeat track analysis.
- From cycle Jason-1 22 (Cycle T/P 365), the 15th of August 2002, a maneuver sequence was conducted over 30 days to move T/P to the new Tandem Mission orbit : T/P is now located one half the TP/Jason-1 track spacing to the West of Jason-1. Geographical variations are then too strong to directly compare Jason-1 and T/P parameters on a point by point basis. Therefore cycle per cycle differences have been carried out to monitor Jason-1 and T/P differences, but data gaps on both satellites have been taken into account.

4.2 20 Hz Measurements

The monitoring of the number and the standard deviation of 20 Hz elementary range measurements used to derive 1 Hz data is presented here. These two parameters are computed during the altimeter ground processing. Before a regression is performed to derive the 1 Hz range from 20 Hz data, a MQE criterion is used to select valid 20 Hz measurements. This first step of selection thus consists in verifying that the 20 Hz waveforms can be effectively approximated by a Brown echo model (Brown, 1977 [8]) (Thibaut et al. 2002 [60]). Through an iterative regression process, elementary ranges too far from the regression line are discarded until convergence is reached. Thus, monitoring the number of 20 Hz range measurements and the standard deviation computed among them is likely to reveal changes at instrumental level.

4.2.1 20 Hz measurements number in Ku-Band and C-Band

Figure 35 shows the cycle per cycle mean of 20-Hz measurements number in Ku-Band (on the left) and C-Band (on the right). Apart from a weak seasonal signal and a jump due to the use of GDR version "b", no trend neither any anomaly has been detected.

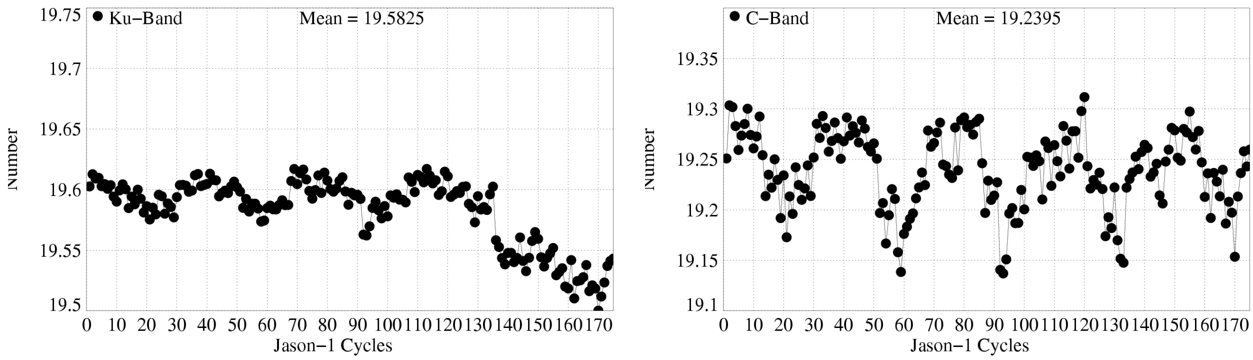

Figure 35: *Cycle per cycle mean of 20-Hz measurements number in Ku-Band (left) and C-Band (right)*

4.2.2 20 Hz measurements standard deviation in Ku-Band and C-Band

Same comment as in section 4.2.1 for the 20 Hz measurements standard deviation parameter (figure 36). Since cycle 136 (GDR version "b") 20 Hz measurements standard deviation of Ku-band range is increased. This is due to the new retracking algorithm MLE4, which estimates 4 instead of only 3 parameters, in consequence noise on the estimated parameters (like 20 Hz range) increases (see section 7.2.3 on noise of 20 Hz and 1 Hz measurements for GDR "a" and "b").

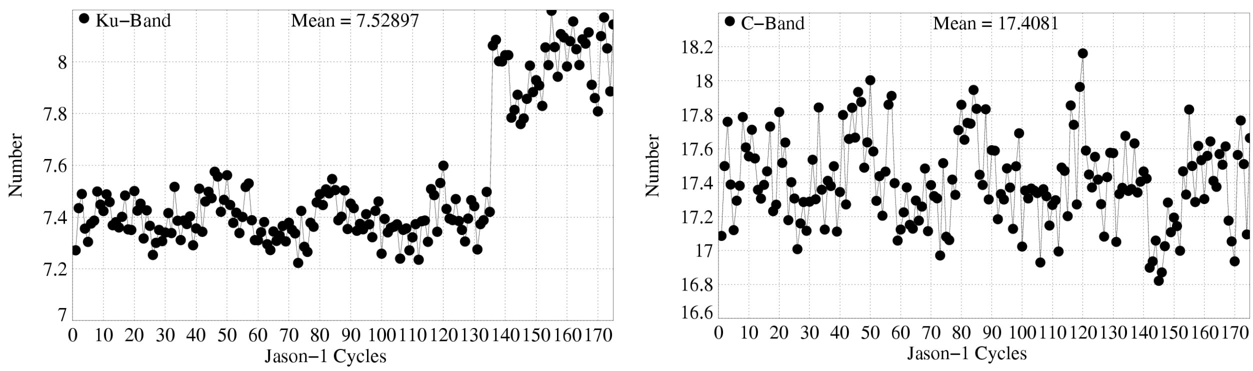

Figure 36: *Cycle per cycle mean of 20-Hz measurements standard deviation in Ku-Band (left) and C-Band (right)*

4.3 Off-Nadir Angle from waveforms

The off-nadir angle is estimated from the waveform shape during the altimeter processing. The square of the off-nadir angle, averaged in a one-cycle basis, has been plotted in figure 37. The mean value is slightly negative for GDR "a" and slightly positive for the GDR "b". This mean value is not significant in terms of actual platform mispointing. The negative figure is only representative of a bias in the on-ground algorithm. In fact squared attitude is what is retrieved from waveforms, not attitude, and noise in the retrieval can cause this otherwise positive quantity to measure negative. A peak is evidenced for cycle 69: it is linked with the platform safe hold mode that occurred during this cycle. Mispointing seems to be larger between cycles 30 and 42: this correlated with short periods of unavailability of the Jason-1 star trackers. The same reason explains the strong mispointing values at the end of the period (from cycle 132 onward). As noticed by several investigators (Tournadre et al., 2002 [62]), there are some periods when the off-nadir angle is larger than the 0.2 degree specification, which can introduce errors in the altimeter parameters if not taken into account in the ground processing (Vincent et al., 2003). One improvement of the science processing with respect to the verification phase was that, in the GDR version "a", real time estimates of the mispointing angle are used in input of the ground retracking algorithm. This allows correcting re-tracked geophysical parameters for mispointing effects up to 0.3 deg. (Vincent et al. 2003c [66]). Further improvements available in the GDR version "b" (section 2.3) of the ground retracking algorithm lead to correct estimations of altimeter parameters for mispointing angle errors up to 0.8 deg. (Amarouche et al. 2004 [6]). For more details see section 2.3.

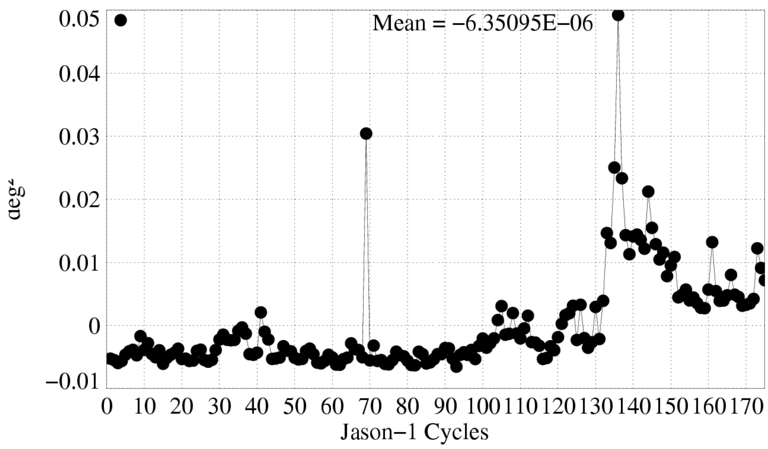

Figure 37: *Cycle mean of the square of the off-nadir angle deduced from waveforms (deg^2)*

4.4 Significant wave height

4.4.1 Ku-band SWH

Jason-1 and T/P Ku SWH are compared in terms of global statistics in figure 38: cycle means and standard deviations of both missions are presented in a cycle basis, as well as mean differences between T/P and Jason-1. Global variations of the SWH statistics are the same on the two missions. The (TOPEX - Jason-1) SWH bias is about 8.8 cm. This value remains steady at the 1 cm level throughout the Jason-1 mission, even if some variability is observed for particular cycles. It should be noticed that the global comparison method and the repeat-track analysis method agree very well, as shown in the first part of the mission (cycles 1 to 21). The estimation of the (Poseidon-1 - Poseidon-2) SWH difference is about 15.5 cm for Poseidon cycle 18 not plotted here. The same comparison with the C-band SWH (figure 39) leads to a mean bias between TOPEX and Jason-1 of about 11 cm.
The coherence between the Jason-1 and T/P Ku SWH is good. However, it has been shown (Dorandeu et al. 2002b [20], Ray and Beckley 2003 [52]) that the Jason-1 (Poseidon-2 altimeter) SWH were slightly underestimated for high values of SWH, when compared to both TOPEX and Poseidon-1 altimeters. Studies about corrections tables to be applied to the altimeter parameters (Thibaut et al., 2004 [61]) have shown that updating these tables would cancel a large part of this difference between Jason-1 and T/P for high waves. This was into account in the GDR version "b" release (section 2.3).

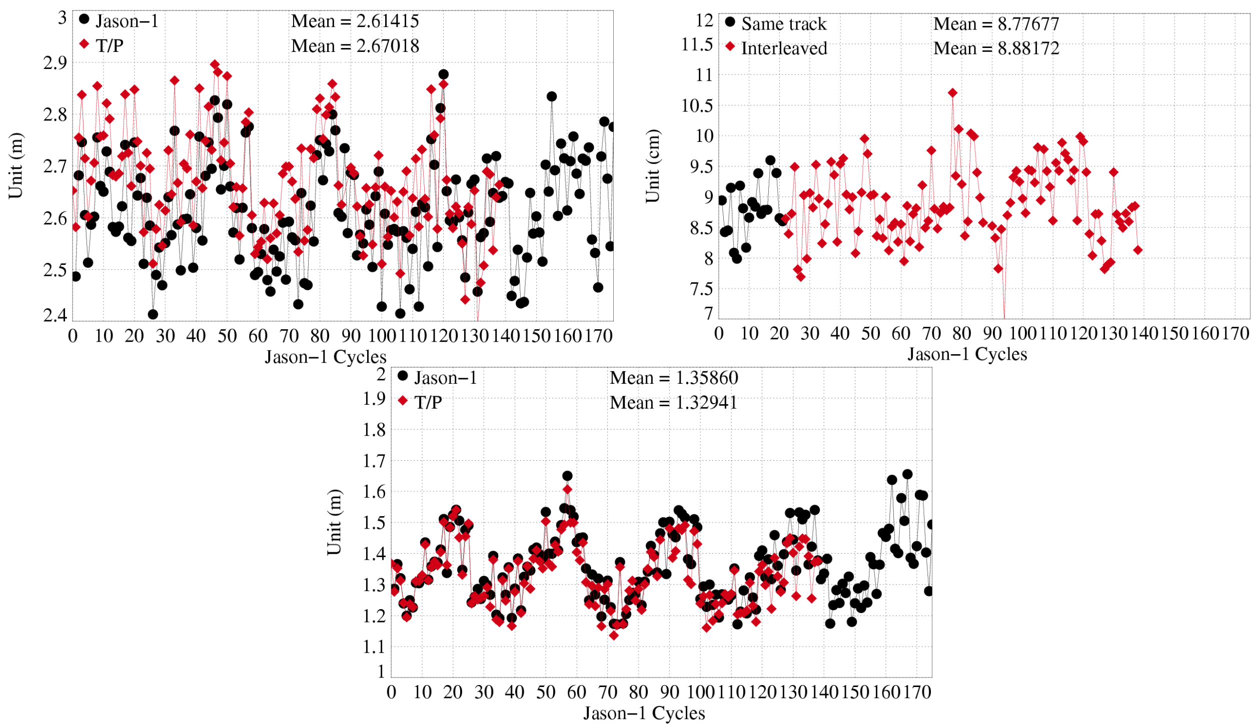

Figure 38: *Cycle per cycle mean (left), T/P−Jason mean differences (right), and standard deviation (bottom) of Ku-band SWH*

4.4.2 C-band SWH

Same comment as in section 4.4.1 for the C-band SWH parameter (figure 39).

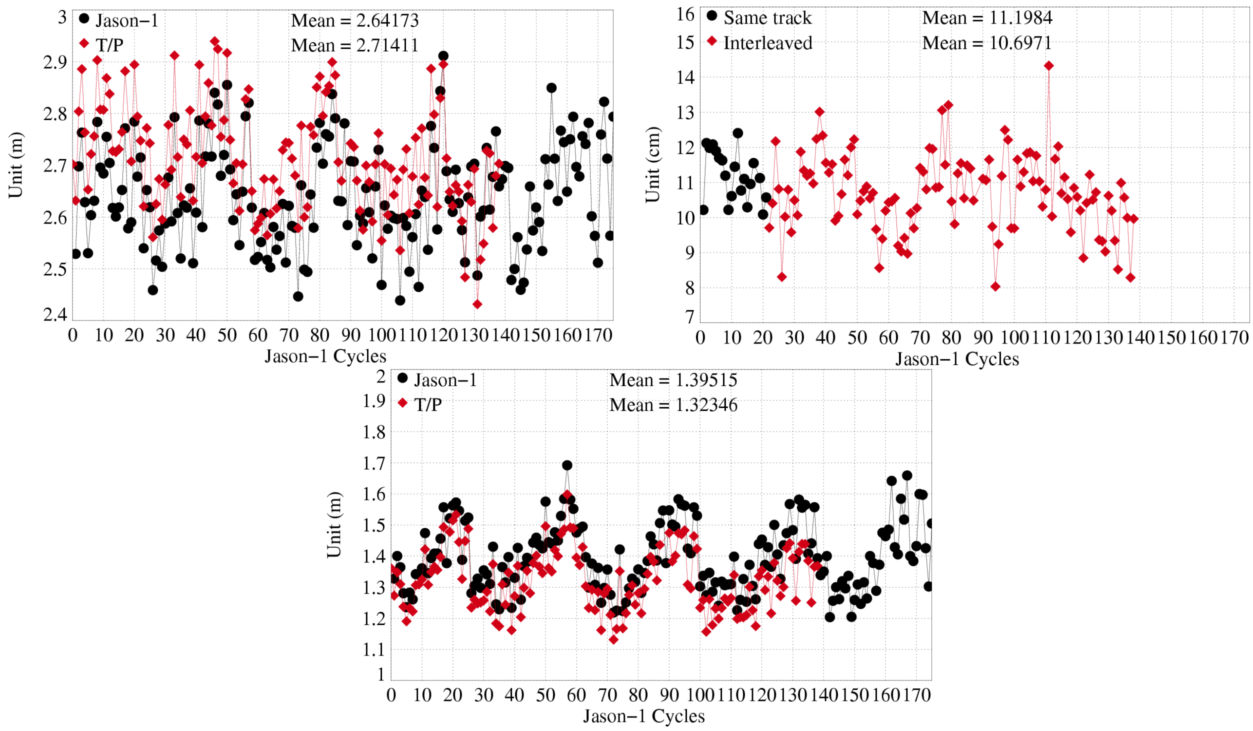

Figure 39: *Cycle per cycle mean (left), T/P−Jason mean differences (right), and standard deviation (bottom) of C-band SWH*

4.5 Backscatter coefficient

4.5.1 Ku-band Sigma0

The cycle per cycle mean (figure 40: top panel on the left) for Jason-1 (black curve) is coherent with the TOPEX mean (red curve). In order to compare both parameters and keep a significant dynamic scale, TOPEX Ku-Sigma0 is biased by a 2.26 dB value to align TOPEX with the Jason-1 uncalibrated Sigma0. The bias between the two corrections (figure 40: top panel on the right) is quite stable about -2.4 dB: this value is near from the -2.26 dB bias which is applied in the ground processing and that was anticipated to represent the TOPEX to Jason-1 bias when computed on a small volume of data.
Notice that the absolute bias is higher than usual from T/P cycle 433 to 437 (J1 cycles 90 to 94) by 0.1 dB : this is due to the TOPEX Sigma0. Indeed, the satellite attitude was impacted by a pitch wheel event linked to the T/P safe-hold mode occurred on cycle T/P 430 (see electronic communication : T/P Daily Status (26/07/2004)). This anomaly has probably biased the TOPEX sigma0 during this period.
The strong Jason-1 mispointing values from cycle 132 to 138 have a very weak impact on the Sigma0 bias by 0.05 dB. Since J1 cycle 136, Ku-band Sigma0 bias between T/P and Jason-1 increases by about 0.1 dB. This is due to the MLE4 retracking algorithm used for the GDR version "b" (see section 7.2.2.5)
Jason-1 and T/P curves on bottom panel, showing the standard deviation differences, are very similar .

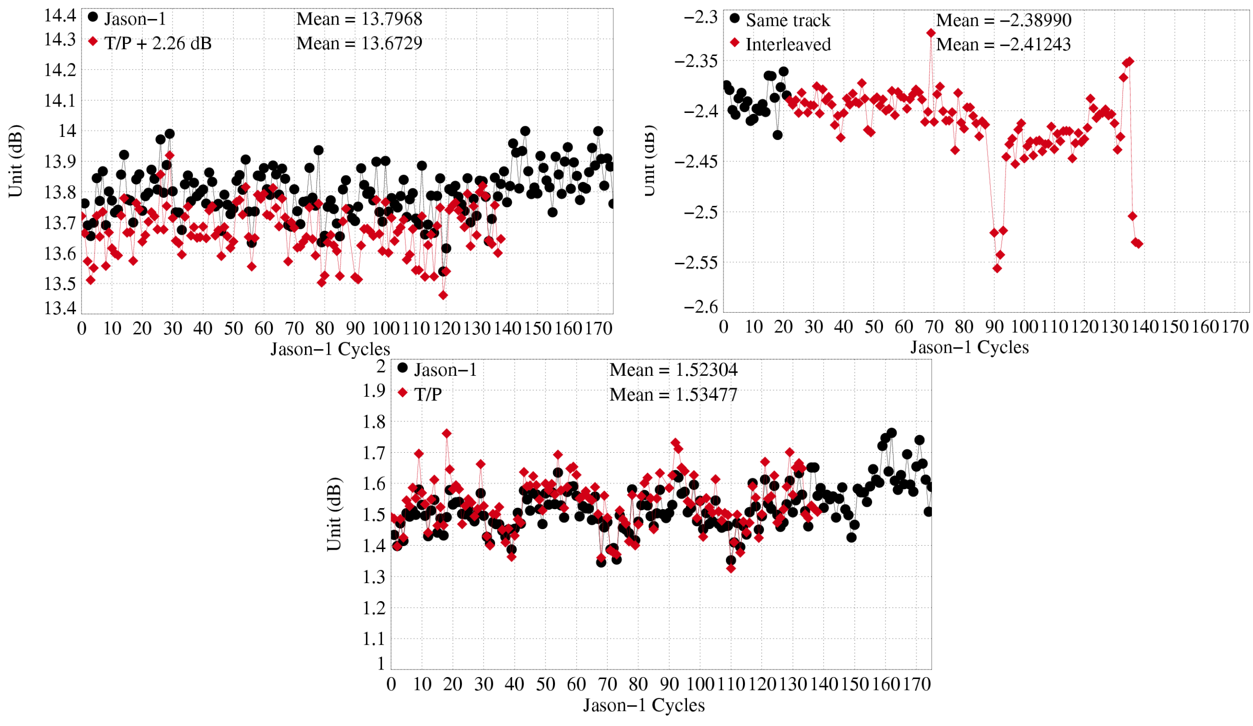

Figure 40: *Cycle per cycle mean (left), T/P−Jason mean differences (right), and standard deviation (bottom) of Ku-band SIGMA0*

4.5.2 C-band Sigma0

Same comment as in section 4.5.1 for the C-band Sigma0 parameter (figure 41). The bias between TOPEX and Jason-1 decreases from -0.6 dB to -0.7 dB. This is due to the T/P C-band Sigma0 (Ablain et al. 2004 [3]).
Notice that, the Jason C-Sigma0 is biased by a -0.26 dB value to align it on TOPEX in the science processing software.

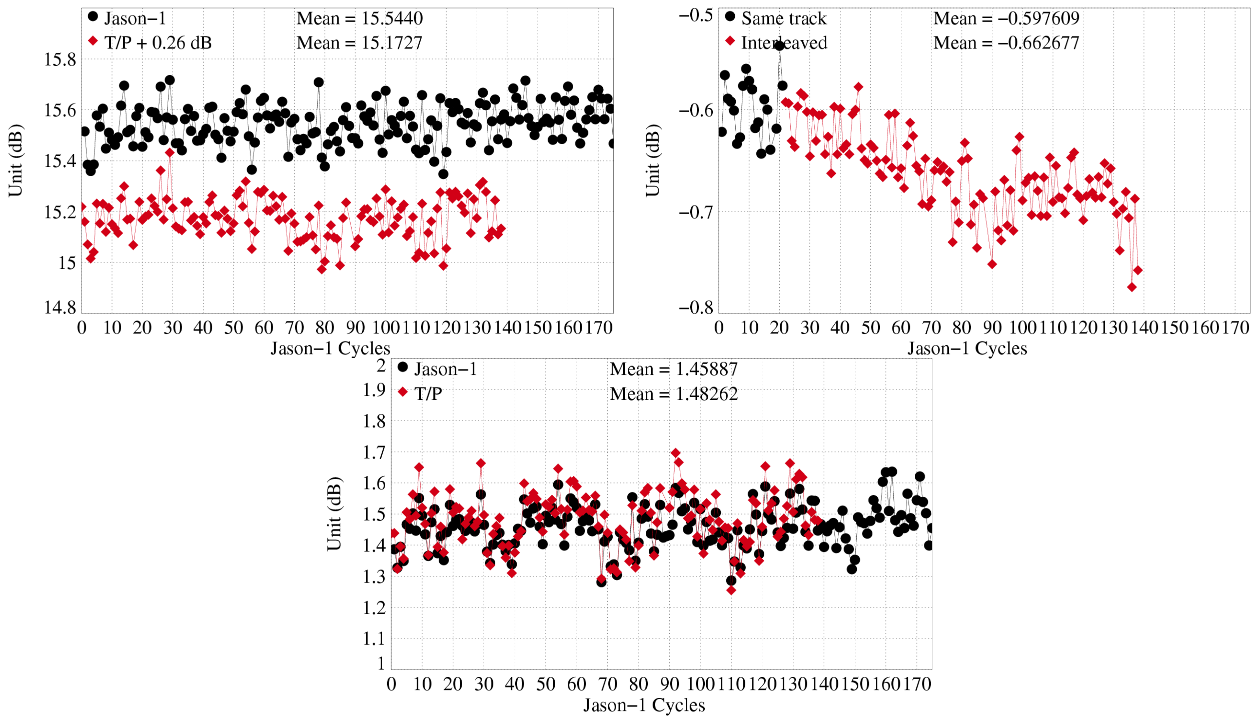

Figure 41: *Cycle per cycle mean (left), T/P−Jason mean differences (right), and standard deviation (bottom) of C-band SIGMA0*

4.6 Dual-frequency ionosphere correction

The dual frequency ionosphere corrections derived from the TOPEX and Jason-1 altimeters have been monitored and compared in the same way (figure 42). The mean difference between TOPEX and Jason-1 estimates is about -2.8 mm for the GDR "a" and 0 mm for the GDR "b", with cycle to cycle variations lower than 2 mm. This small difference with the GDR "a" shows that the C-band calibration was not exactly the same for the two altimeters. Differences in the ionosphere correction may depend on the Sea State Bias (SSB) model used to correct the Ku-band and C-Band ranges. Apart from this bias, the two corrections are very similar and vary according to the solar activity. Notice that, as for TOPEX (Le Traon et al. 1994 [39]), it is recommended to filter the Jason-1 dual frequency ionosphere correction before using it as a SSH geophysical correction (Chambers et al. 2002 [13]). A low-pass filter has thus been used to remove the noise of the correction in all SSH results presented in the following sections.

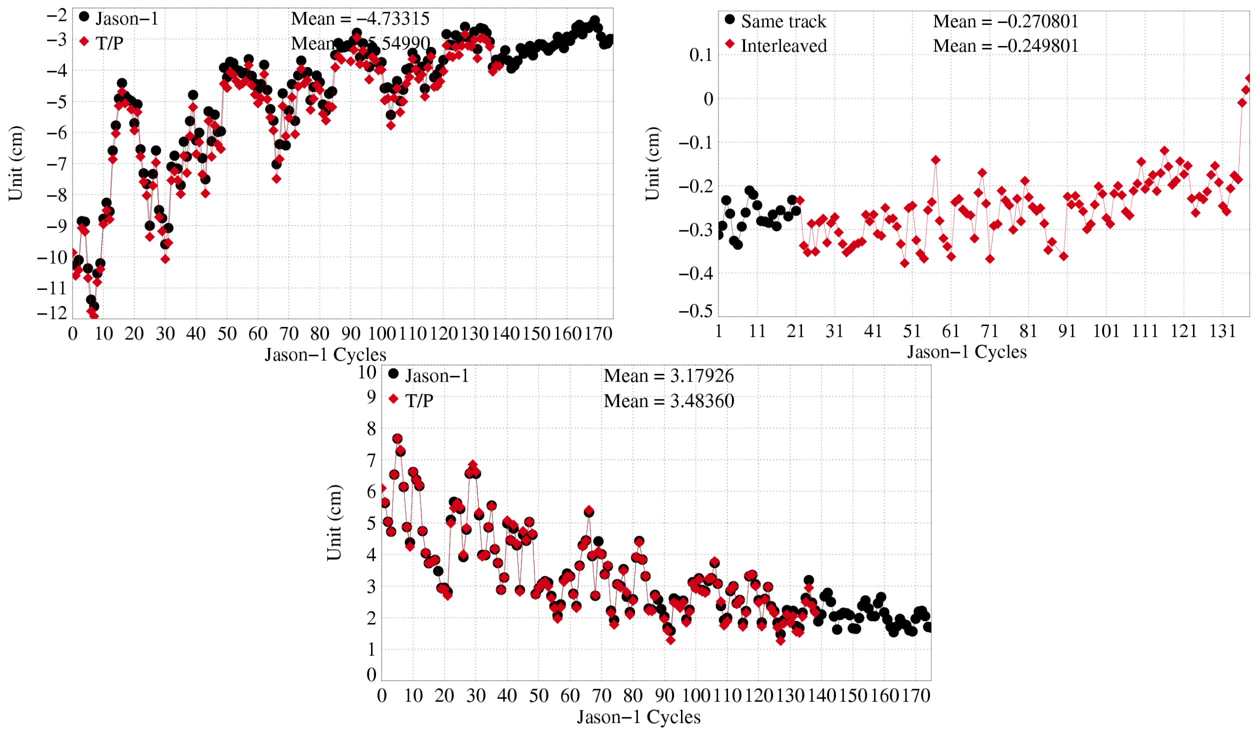

Figure 42: *Cycle per cycle mean (left), T/P−Jason mean differences (right), and standard deviation (bottom) of dual frequency ionosphere correction*

4.7 JMR Wet troposphere correction

4.7.1 Comparison with the ECMWF model

The JMR correction provided in the GDR "a" contains several anomalies already described in the previous Jason-1 annual report. These anomalies were brought out using a comparison with the ECMWF model which is stable in term of bias through the Jason-1 mission (except for the first cycle : (see http://www.ecmwf.int/products/data/operational_system/evolution/evolution_2003.html). The daily mean of radiometer and ECMWF model wet troposphere correction differences using GDR "a" have been plotted on the left figure 43 (red curve) which highlighted these following anomalies :

- A drift of about 5 mm from cycle 27 to cycle 32 due to instrumental changes (see Obligis et al.,2004 [45])
- A jump of 9 mm at cycle 69 linked to a platform incident
- 60-day signals of an amplitude of almost 5 mm due to yaw mode transistions

The JMR correction provided in the GDR "b" is also available in a podaac's product for Jason-1 cycles not yet reprocessed in version "b". The JMR correction has been updated from this product in the CALVAL database in order to make an homogeneous JMR correction since the beginning of the mission. As for the GDR "a" correction, the radiometer and ECMWF model wet troposphere correction differences using this new correction have been plotted in the same figure 43 (black curve). This figure show that the new JMR correction allows us to correct partially the previous anomalies:

- The first anomaly between cycle 27 and 32 is softened, but still visible.
- The jump of 9 mm observed at cycle 69 is very well corrected.
- The 60 day signals are only partially corrected. Several of them are still present.

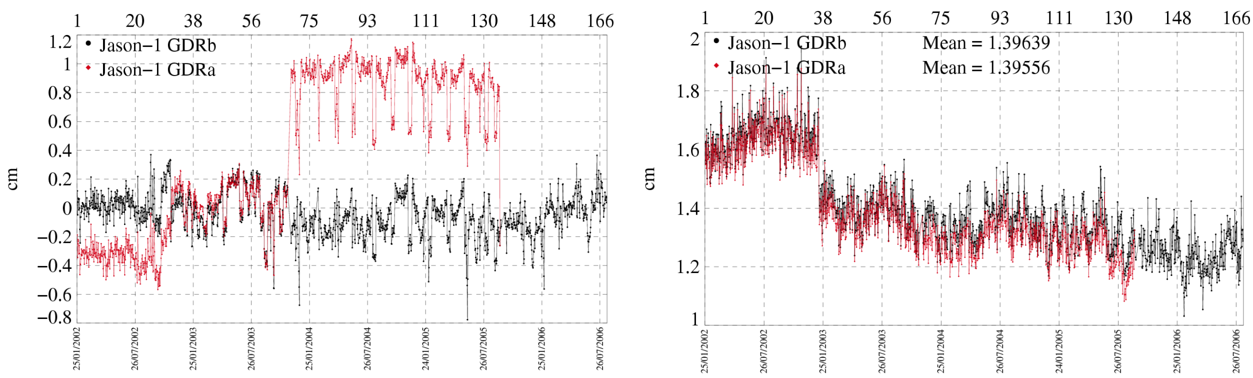

Figure 43: *Daily mean (left) and standard deviation (right) of radiometer and ECMWF model wet troposphere correction differences for Jason-1 using radiometer correction of GDR version "a" (red) and GDR version "b" (black).*

4.7.2 Comparison with others missions using the ECMWF model

Figure 44 shows the difference of radiometer and ECMWF model wet troposphere correction for different missions. For Jason-1, the monitoring of the mean of the wet troposphere difference shows, that it is noisier than for the other missions. This is probably due to the signals generated by the yaw mode transitions. Furthermore, the difference seems to increase to the end of the period (2 mm within about 6 months). The standard deviation of the wet troposphere correction difference (figure 44, left) is for Jason-1 the smallest among the different missions. But this does not mean that the JMR is better than the other radiometers. Indeed, if the JMR correction is too smooth, it will be more consistent with the model (which is itself quite smooth).

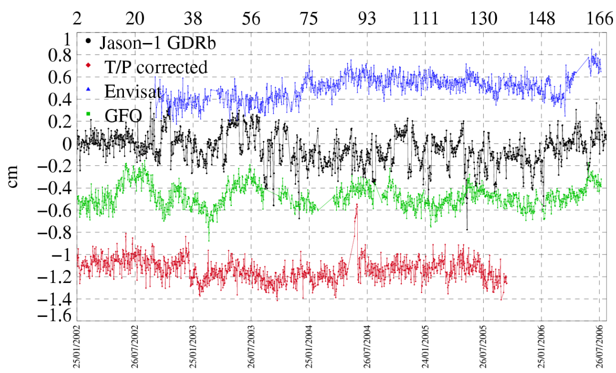

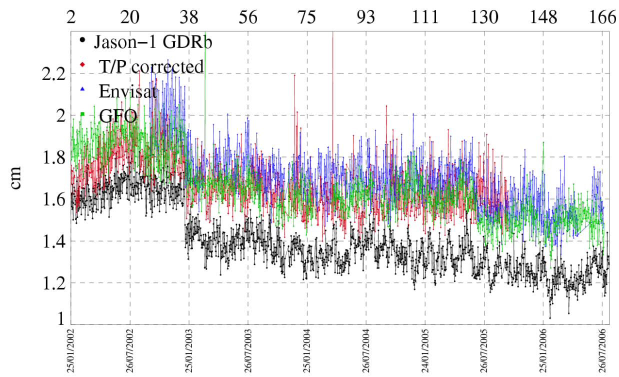

Figure 44: *Comparison of daily mean (left) and standard deviation (right) of radiometer and ECMWF model wet troposphere correction differences between several altimeter missions: Jason-1 (black), Envisat (blue), Topex/Poseidon (red) and GFO (green).*

4.7.3 Impact for the Mean Sea Level

It should now be possible to use the new radiometer wet troposphere correction available in GDR version "b" to compute the mean sea level, instead of the model correction, which might change (jump of several mm in January 2002). The local and global slopes of the radiometer and model (wet troposphere) differences are shown on figure 45, in order to show which error will be committed when using either one or the other wet tropospheric correction. Using the radiometer correction to estimate the global slope of the mean sea level, comes to increase the slope of the MSL by 0.25 mm/year (it was 2.9 mm/year with the model corrections). The cartography of the local slopes shows differences reaching locally 5 mm/year. This is quite high, since the observed maximum of the local slopes of the Jason-1 MSL are 10 mm/year. This shows that the wet troposphere correction remains a big budget error to compute the global and local MSL trends.

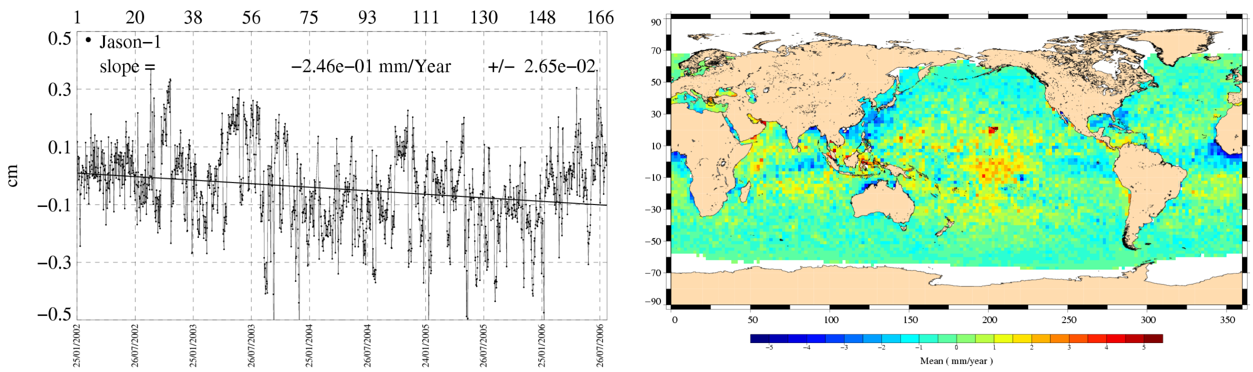

Figure 45: *Local and global slopes of the difference between radiometer and model wet troposphere for Jason-1.*

5 Crossover analysis

Crossover differences are systematically analyzed to estimate data quality and the Sea Surface Height (SSH) performances. Furthermore, T/P crossover performances (as long as they were available) have been monitored in order to compare both performances. SSH crossover differences are computed on a one cycle basis, with a maximum time lag of 10 days, in order to reduce the impact of ocean variability which is a source of error in the performance estimation. The main SSH calculation for Jason-1 and T/P are defined below. For Jason-1 and TOPEX, new standards have been used for the tidal and atmospheric corrections. These corrections are present in the Jason-1 GDR version "b" release (see section 2.3).

$$SSH = Orbit - Altimeter\ Range - \sum_{i=1}^{n} Correction_i$$

with $Jason-1\, Orbit = POE\, CNES\, orbit$ and

$$\begin{aligned}
\sum_{i=1}^{n} Correction_i &= Dry\ troposphere\ correction : new\ S1\ and S2\ atmospheric\ tides\ applied \\
&+ Combined\ atmospheric\ correction :\ MOG2D\ and\ inverse\ barometer \\
&+ Radiometer\ wet\ troposphere\ correction \\
&+ Filtered\ dual\ frequency\ ionospheric\ correction \\
&+ Non\ parametric\ sea\ state\ bias\ correction \\
&+ Geocentric\ ocean\ tide\ height,\ GOT\ 2000 :\ S1\ atmospheric\ tide\ is\ applied \\
&+ Solid\ earth\ tide\ height \\
&+ Geocentric\ pole\ tide\ height
\end{aligned}$$

Note that for TOPEX data, a non-parametric sea state bias has been updated over TOPEX B period according to the collinear method (Gaspard et al., October 2002, [29]). For Poseidon-1 data, non-parametric SSB is not yet available.

5.1 Mean crossover differences

The mean of crossover differences represents the average of SSH differences between ascending and descending passes. It should not be significantly different from zero. The cycle mean of Jason-1 and T/P SSH crossover differences is plotted for the whole Jason-1 period in figure 46 (bottom). Slightly larger variations are observed for Jason-1 than for TOPEX in the first cycles. However, some correlation between the two curves can be deduced from this figure. That shows that consistent signals impact the two systems. The map of the Jason-1 crossover differences averaged over the whole period of GDR version "a" (cycle 1 to 135) has been plotted in figure 46 (on the left). Systematic differences between ascending and descending passes, as large as 4 cm, are observed depending on geographical areas. This kind of signals is due to geographically correlated orbit errors, in particular gravity model errors (e.g. Luthcke et al. 2003 [41]). Notice that the JGM3 gravity model was used for both Jason-1 and T/P precise orbit calculations. Substantial improvements in orbit calculation are made by the use of new gravity models (based on GRACE) in GDR version "b", see section 7.2.4.1. On the right of figure 46 the Jason-1 crossover differences averaged over the period of cycle 136 to 175(GDR version "b"), is more homogeneous. A bias between northern and southern hemisphere is observable. For more details see section 7.2.4.1.

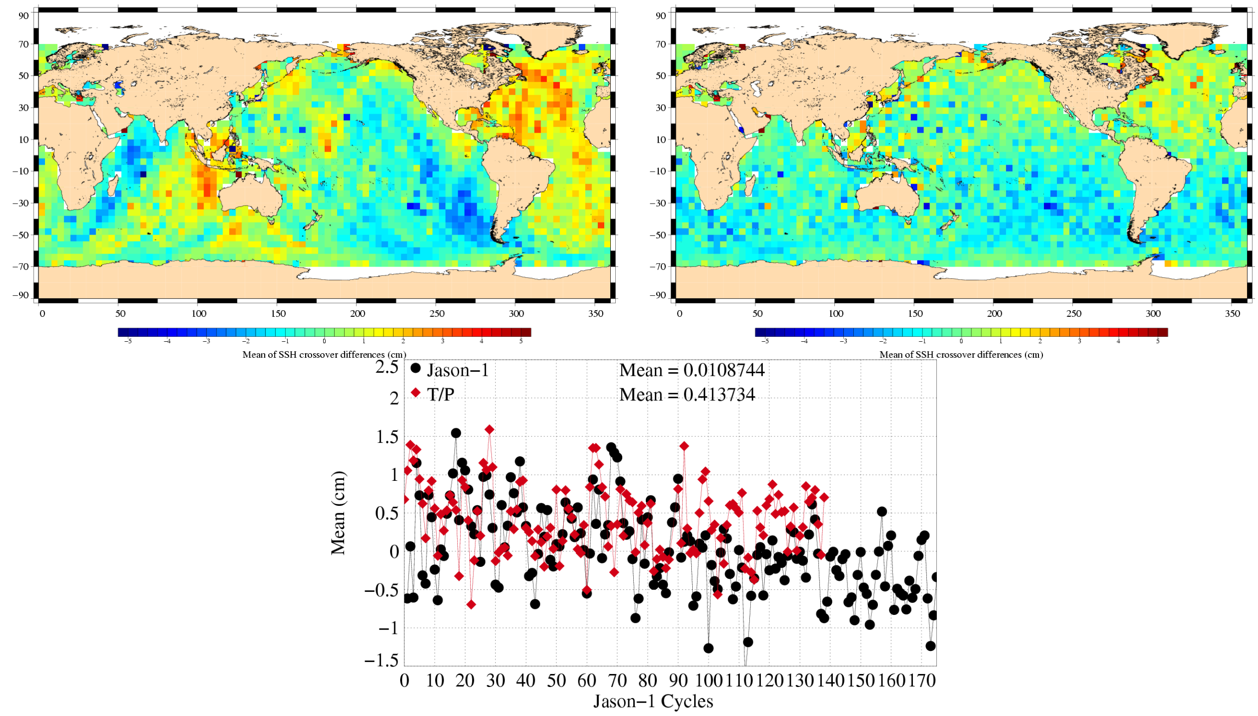

Figure 46: *Map of mean crossovers for Jason cycle 1 to 135 (GDR version "a", left) and cycle 136 to 175(GDR version "b", right), and cycle per cycle mean crossovers (bottom)*

5.2 Standard deviation of crossover differences

The cycle per cycle standard deviation of crossover differences are plotted in figure 47 (on the left) according to different crossover selection. 3 selections are applied:

- Black curve: no selection is applied. The mean value is 6.93 cm. It shows an annual signal linked to the sea ice variations in the Northern Hemisphere.
- Red curve: shallow waters have been removed (bathy<-1000m). The previous annual signal has been removed by this selection even though it remains a signal probably due to seasonal ocean variations.
- Blue curve: the last selection allows monitoring the Jason-1 system performance. Indeed, areas with shallow waters (1000 m), of high ocean variability (> 20 cm) and of high latitudes (> |50| degrees) have been removed. The standard deviation then provides reliable estimates of the altimeter system performances. In that case, no trend is observed in the standard deviation of Jason-1 SSH crossovers: good performances are obtained, with a standard deviation value of about 5.7 cm all along the mission.

The map of standard deviation of crossover differences over cycle 1 to 175, in figure 47 (on the right) shows usual results with high variability areas linked to ocean variability.

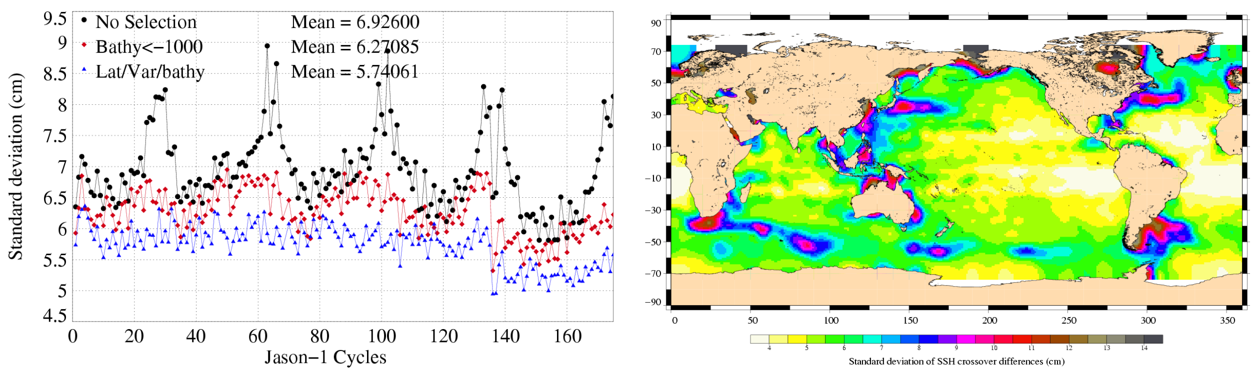

Figure 47: *Cycle per cycle standard deviation crossovers with different selections and map of Jason-1 standard deviation crossovers*

5.3 Comparison of Jason-1 and T/P at crossovers

When comparing performances relative to another mission, much care has to be taken in order to cancel out the contributions of ocean variability and geophysical corrections. Such a comparison between Jason-1 and T/P results has been performed. Apart from homogeneity in geophysical corrections for the two missions, additional processing care has been taken in order to get the most meaningful comparison figures as possible: only open ocean data are selected, away from areas with large ocean variability or with seasonal coverage by sea ice. Furthermore, to account for missing measurements on both missions - in particular due to tape recorder problems on T/P - data are only considered from common datasets. Finally, the SSH computation at crossovers is performed with exactly the same interpolation procedure using cubic spline functions. In order to keep the full 1 Hz high frequency content of the two missions, the spline functions are forced to go through the exact values of the points used in the interpolation, without any smoothing.

In order to distinguish between the effects of long wavelength signals such as orbit errors and the effects of short wavelengths such as instrumental noise, an along-track filtering procedure is used before crossovers are computed. A low-pass filter (Hamming, 1977 [31]) with a cut-off wavelength of 50 km is applied to both Jason-1 and T/P (SSH - MSS) differences. In this case, the CLS01 MSS global model is used. The low frequency signal is directly the output of the filtering routine, while the high frequency signal is derived from the difference between the original signal and the low frequency signal. Then the standard deviation of crossover differences is computed for both satellites on three different datasets: for all wavelengths, for wavelengths larger than 50 km and for wavelengths shorter than 50 km.

The results are presented in figure 48 (bottom). The overall standard deviation is higher for Jason-1 than for TOPEX. However, the 1 Hz high frequency content is not the same, due to different altimeter ground processing. At the opposite of TOPEX, Jason-1 data are processed by a ground retracking algorithm which makes altimeter measurements more decorrelated (Zanife et al. 2003 [67]). Therefore, TOPEX data are then smoother than Jason-1 data: the 1 Hz high frequency content is lower for TOPEX. The respective contribution of low and high frequencies in Jason-1 and TOPEX crossover residuals is displayed in figure 48.

Figure 48 on the top right shows that short wavelengths contribute a lot in the difference between Jason-1 and TOPEX. While a value of 3 cm is obtained for Jason-1, less than 2.5 cm is observed on TOPEX when wavelengths shorter than 50 km are only considered. Note that for T/P cycle 361 (Jason-1 cycle 18), the Poseidon-1 altimeter was switched on and leads to comparable results relative to Jason-1. Still in figure 48 on the right, another interesting feature is observed from T/P cycles 366 to 369 (Jason-1 cycles 22 to 25): the T/P standard deviation increases and then remains higher than at the beginning of the series. During this period, the T/P satellite was moved away from its original ground track (presently the Jason-1 ground track). Since the along-track filtering is performed on (SSH - MSS) differences, (SSH - MSS) differences between ascending and descending passes are computed instead of SSH differences. Thus errors of the global MSS model away from the initial nominal T/P ground track impact the T/P results after the orbit is moved. Since the crossover location is the same on the two passes - ascending and descending -, higher variance reveals the signature of MSS slope errors in the crossing directions, away from the nominal track used to compute the MSS.

The contribution of wavelengths higher than 50 km is analyzed in figure 48 on the left. Larger differences between Jason-1 and TOPEX are observed before Jason-1 cycle 8. Then Jason-1 and T/P curves are very similar, even if TOPEX figures are slightly lower than Jason ones. Orbit errors are probably responsible for Jason-1 degraded results on early cycles. It is worth recalling that when producing the GDR dataset, improvements have been brought to the Jason-1 POE orbit calculation, in particular to manage maneuvers. Because these orbits were recomputed from cycle 9 only, higher variance is obtained for the 8 first Jason-1 cycles.

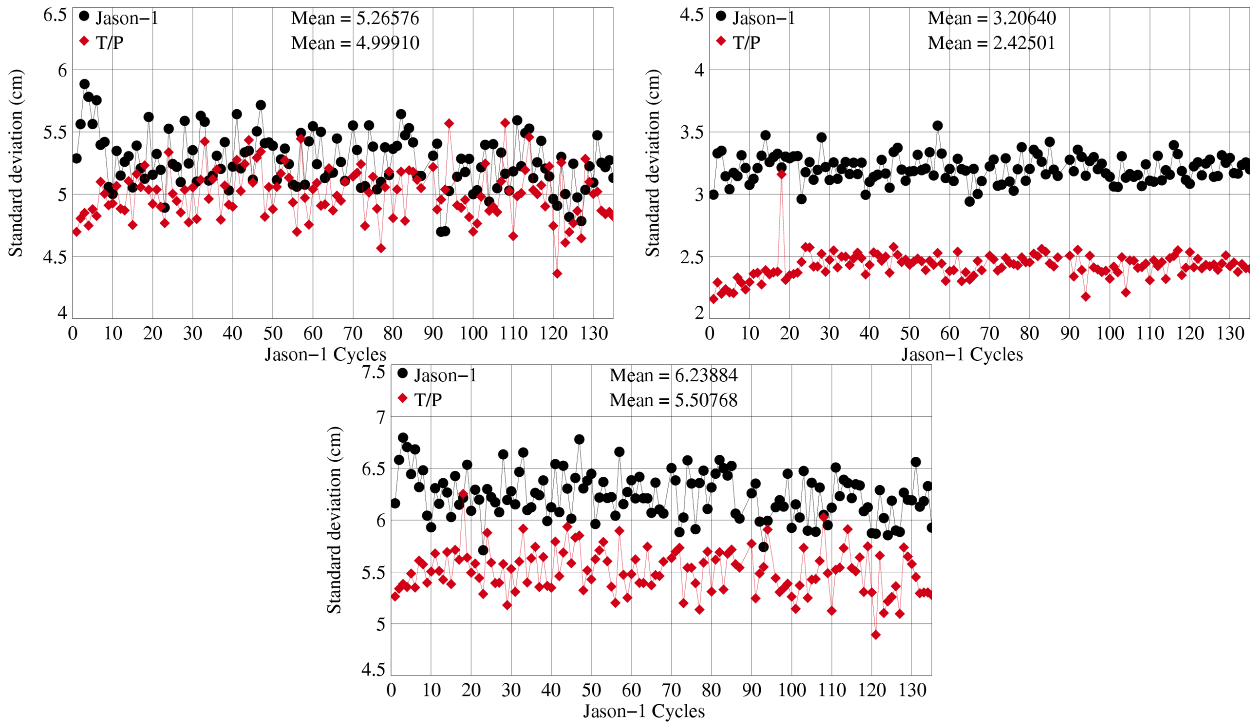

Figure 48: *Cycle per cycle standard deviation crossovers for long wave length content (left), short wave length content (right) and total content (bottom)*

6 Along-track analysis

This analysis is used to compute Sea Level Anomalies (SLA) variability and thus to estimate data quality; it is used to determine the SSH bias between Jason-1 and T/P and the trend in the Mean Sea Level (MSL).

6.1 Along-track performances

6.1.1 Along-track performances before along-track filtering

Along track analyzes are also used to assess the altimeter system performances, by computing Sea Level Anomalies (SLA). The SLA variance gives an estimate of the errors of the system, even though the ocean variability fully contributes in this case. As in the crossover analysis (see in section 5.3), the same type of comparison between Jason-1 and T/P has been performed computing the variance of SLA relative to the CLS01 MSS. This allows global and direct calculations.
The SLA standard deviation is plotted in figure 49 for Jason-1 and T/P. It exhibits similar and good performances for both satellites. However, during the verification phase, the variability is slightly higher for Jason-1 but from cycle 26 onward the performances are very similar. A significant signal is observed from cycle 25 to 35. It is due to the 2002-2003 "El Niño" (McPhaden, 2003, [46]).

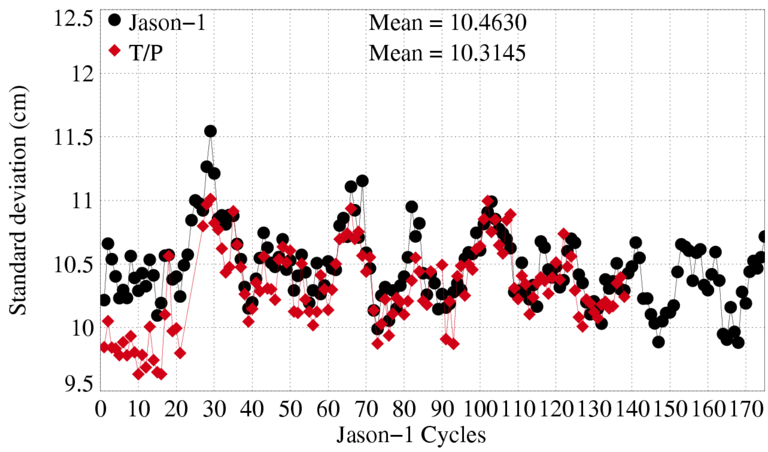

Figure 49: *Cycle per cycle SLA standard deviation*

6.1.2 Along-track performances after along-track filtering

Prior filtering of (SSH - MSS) differences has been applied to produce estimations of the variance (standard deviation) of Jason-1 and T/P SLA according to the selected wavelengths. SLA are computed relative to a global MSS model because the data can be processed in the same way before and after the T/P ground track moves. Moreover, like in the crossover analysis case, measurements are carefully extracted from common datasets and identical processing is applied to both missions.

Figure 50 shows the standard deviation of Jason-1 and T/P SLA differences after along-track filtering, in order to investigate different ranges of wavelengths: less than 50 km, between 50 and 500 km, and more than 500 km. Since geophysical corrections are the same for the two satellites, the first wavelength interval is expected to mostly represent differences in high frequency content, while the last should mainly evidence orbit error differences. Like in the crossover analysis, the Jason-1 high frequency content is higher than the TOPEX one. As already explained, the difference mainly comes from different altimeter ground processing. Poseidon cycle 361 (Jason-1 cycle 18) is evidenced on the curve, with a standard deviation estimation very close to those of Jason-1. For Wavelengths between 50 and 500 km (figure 50 on the right), the standard deviation curves obtained for Jason-1 and T/P are indistinguishable when the two satellites are flying on the same ground track. The signature of MSS errors appears in both figures 50 on the right and bottom after the T/P ground track changes. The long wavelength content showed in figure 50 on the left principally differs between the two satellites in the beginning of the Jason-1 mission. Until Jason-1 cycle 8, larger orbit errors are present on Jason-1 data because these cycles have not been reprocessed, as explained previously. However the difference seems to continue to around cycle 15, contrary to what was observed in the crossover analysis. Higher orbit errors on these Jason-1 particular cycles might be one explanation of this higher variability relative to the MSS. After the first cycles, even slightly larger, the Jason-1 results are much closer to the T/P ones.

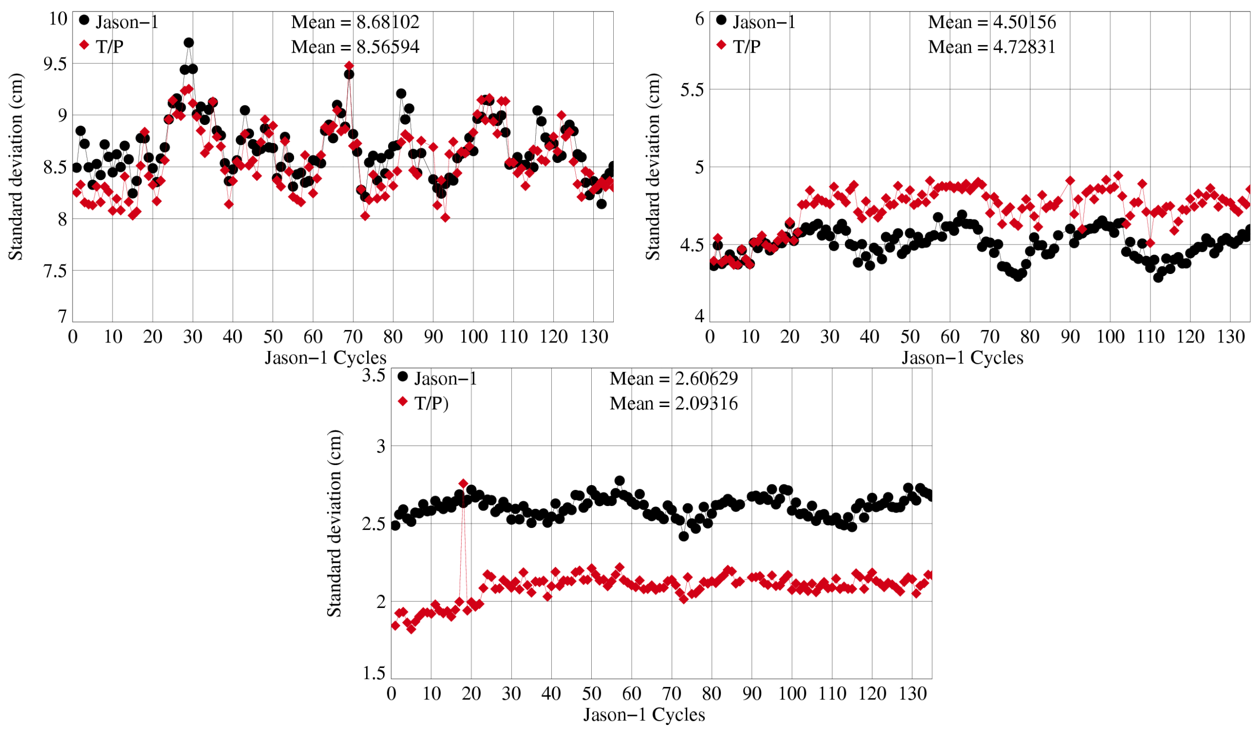

Figure 50: *Cycle per cycle SLA standard deviation for long wavelength content (left), medium wave length content (right) and short wavelength content (bottom)*

6.2 Mean sea level

6.2.1 Sea surface height estimation

The JMR wet troposphere correction experienced two major changes from the beginning of the Jason-1 mission. These changes significantly impact Jason-1 SSH estimations at the 1 cm level. Therefore, before instrumental and algorithmic investigations performed at JPL and applied in the GDRs version "b" release, the Jason-1 radiometer wet troposphere correction is not suitable for Mean Sea Level (MSL) estimations (see section 4.7.1). In order to assess the Jason-1 altimeter performances in terms of MSL estimations, the ECMWF wet troposphere correction is used, as no change in the model has impacted the data since Jason-1 cycle 1.

MSL estimations from Jason-1 and T/P are plotted in figure 51 (on the left), after reduction of the relative bias between the two measurements. The results are obtained after area weighting (Dorandeu and Le Traon 1999 [18]). The figure shows good agreement between the two missions and demonstrates that the Jason-1 mission will ensure continuous precise MSL monitoring as it was done for more than a decade by the T/P mission. On both missions, seasonal signals are observed, because the inverse barometer correction has been applied in the SSH computation (Dorandeu and Le Traon 1999 [18]). Moreover, 60-day signals are also detected on Jason-1 and T/P series, with nearly the same amplitude. This signal might be due to residual orbit errors since variations of the so-called Beta-prime angle are present at this period for both satellites. Another source of error could be from the largest tidal constituents at twice-daily periods which alias at periods near 60 days for Jason-1 and T/P (Marshall et al. 1995 [42]). Orbit errors in T/P altimeter series used to compute the tide solutions could also have contaminated these models (Luthcke et al. 2003 [41]).

On the right figure 51, annual, semi-annual, and 60-days signals have been adjusted. This allows to decrease the adjustment formal error for both satellites. The global MSL slope is higher for Jason-1 than for T/P (but for Jason-1, the shown time period is almost a year longer than for T/P).

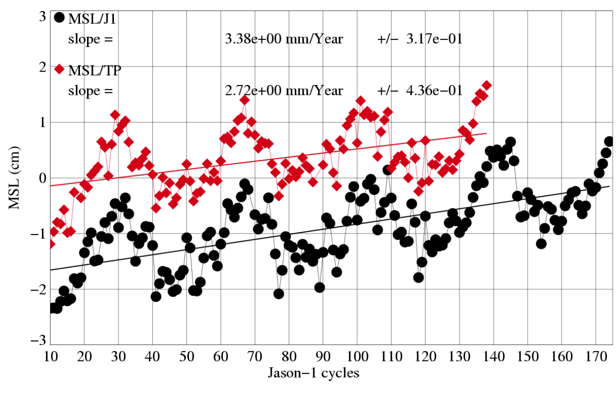

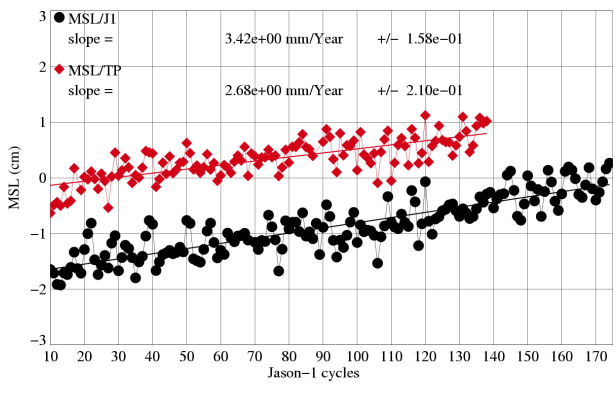

Figure 51: *Jason-1 and T/P mean sea level (on the left) with annual, semi-annual and 60-days adjustment (on the right)*

6.2.2 SSH bias between Jason-1 and T/P

The ECMWF wet troposphere correction is also used in figure 52 which represents the SSH bias between T/P and Jason-1. This prevents from errors due to radiometer biases, as the model correction is the same for the two missions. The impact of all geophysical corrections and the particular effect of the SSB correction are also investigated in the figure. Among all geophysical corrections, the greater impact on the T/P to Jason-1 SSH bias estimation is produced by the SSB correction, since results differ by more than 6 cm when applying or not this correction. Notice that present results have been obtained using a dedicated TOPEX Side B SSB estimation (S. Labroue et al. 2002), since TOPEX side A and side B SSB models are different (e.g. Chambers et al. 2003). Apart from some higher variability in the first Jason-1 cycles, probably because of orbit calculation, the T/P to Jason-1 SSH bias nearly remains constant through the Jason-1 mission period.

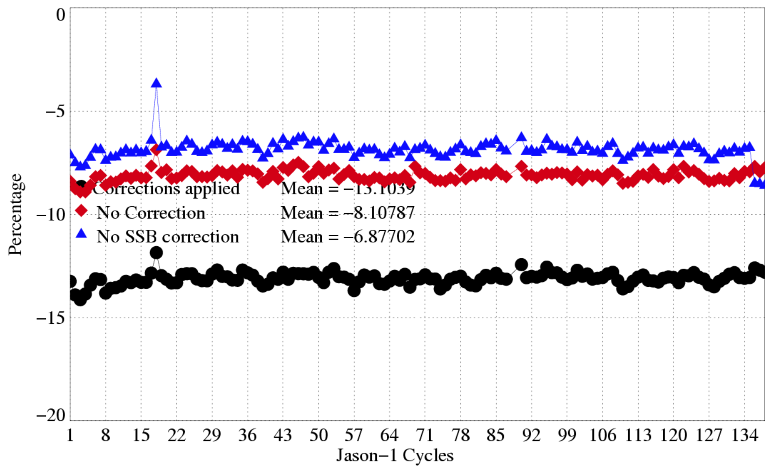

Figure 52: *Cycle per cycle mean of (T/P−Jason-1) SSH differences*

6.2.3 Hemispheric SSH bias between Jason-1 and T/P

In order to further investigate (T/P−Jason-1) SSH biases, the same calculation has been performed at global and hemispheric scales. The results are presented in figure 53. Contrary to the global estimation, large hemispheric differences appear between T/P and Jason-1. From the northern hemisphere to the southern hemisphere the (T/P−Jason-1) SSH bias estimates can thus differ by up to 2 cm. These hemispheric differences seem consistent from one cycle to another, following a long period signal: four periods can be identified on the curves, with large, low and again large hemispheric differences. These differences are mainly due to the orbit :see section 7.2.4.1 and 7.3.3 dedicated to the impact of orbit calculation. During the last couple of cycles (since cycle 136), bias between the hemispheric differences is again lower due to the use of the new orbit in the GDRs version "b".

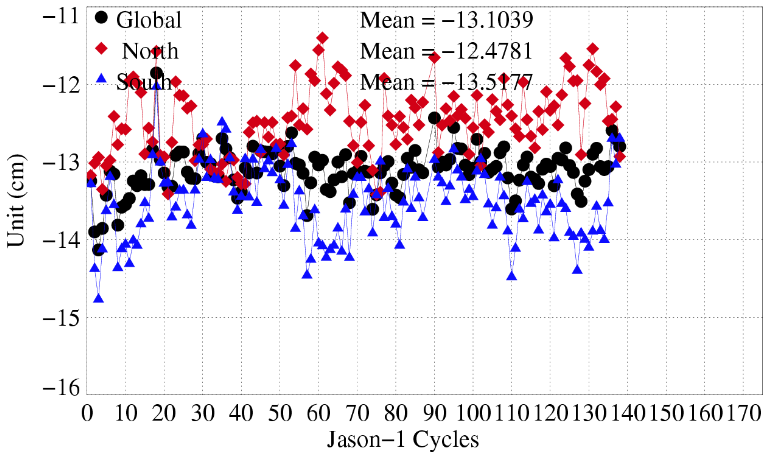

Figure 53: *Cycle per cycle mean of (T/P−Jason-1) SSH differences by hemisphere*

6.2.4 Map of SSH bias between Jason-1 and T/P

Jason-1 and T/P have not been on the same track from cycle 21 onward. Consequently, the SSH differences can not be obtained directly as a result of the ocean variability. Thus, the map of the SSH differences between Jason-1 and T/P is obtained at the Jason-T/P crossovers in figure 54. The figure was generated using Jason-1 GDR version "a" (cycle 1 to 135). As in previous figure 53, an hemispheric signal is visible. Residual orbit errors on both missions could be one candidate to explain such differences. These differences should decrease when using the new GDRs version B release. A detailed description of the SSH bias between Jason-1 and T/P using GDRs version B, can be found in section 7.3.

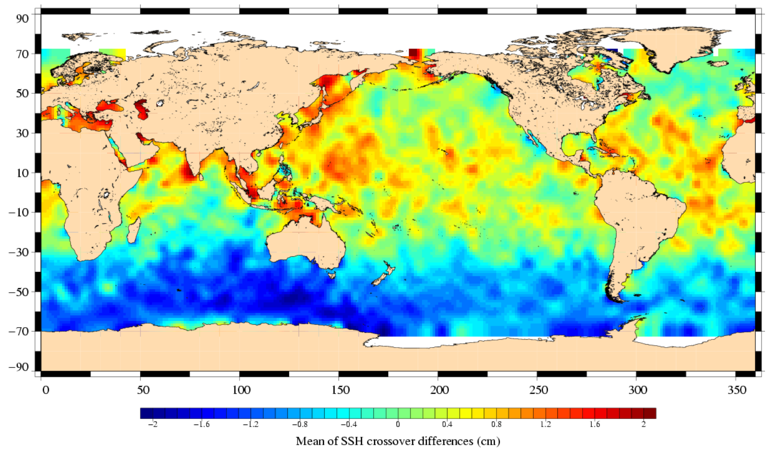

Figure 54: *Map of (T/P−Jason-1) SSH differences for Jason-1 GDR version "a" period.*

6.3 Sea level seasonal variations

From Sea Level Anomalies computed relative to the Mean Sea Surface CLS 2001 (Hernandez et al, 2001), the surface topography seasonal variations have been mapped in figure 55 for the overall Jason-1 data set. Major oceanic signals are showed clearly by these maps: it allow us to assess the data quality for oceanographic applications. The most important changes are observed in the equatorial band with the development of an El Niño in 2002-2003. The event peaked in the fourth quarter of 2002, and declined early in 2003. Conditions indicate an event of moderate intensity that is significantly weaker than the strong 1997-1998 El Niño (McPhaden,2003, [46]).

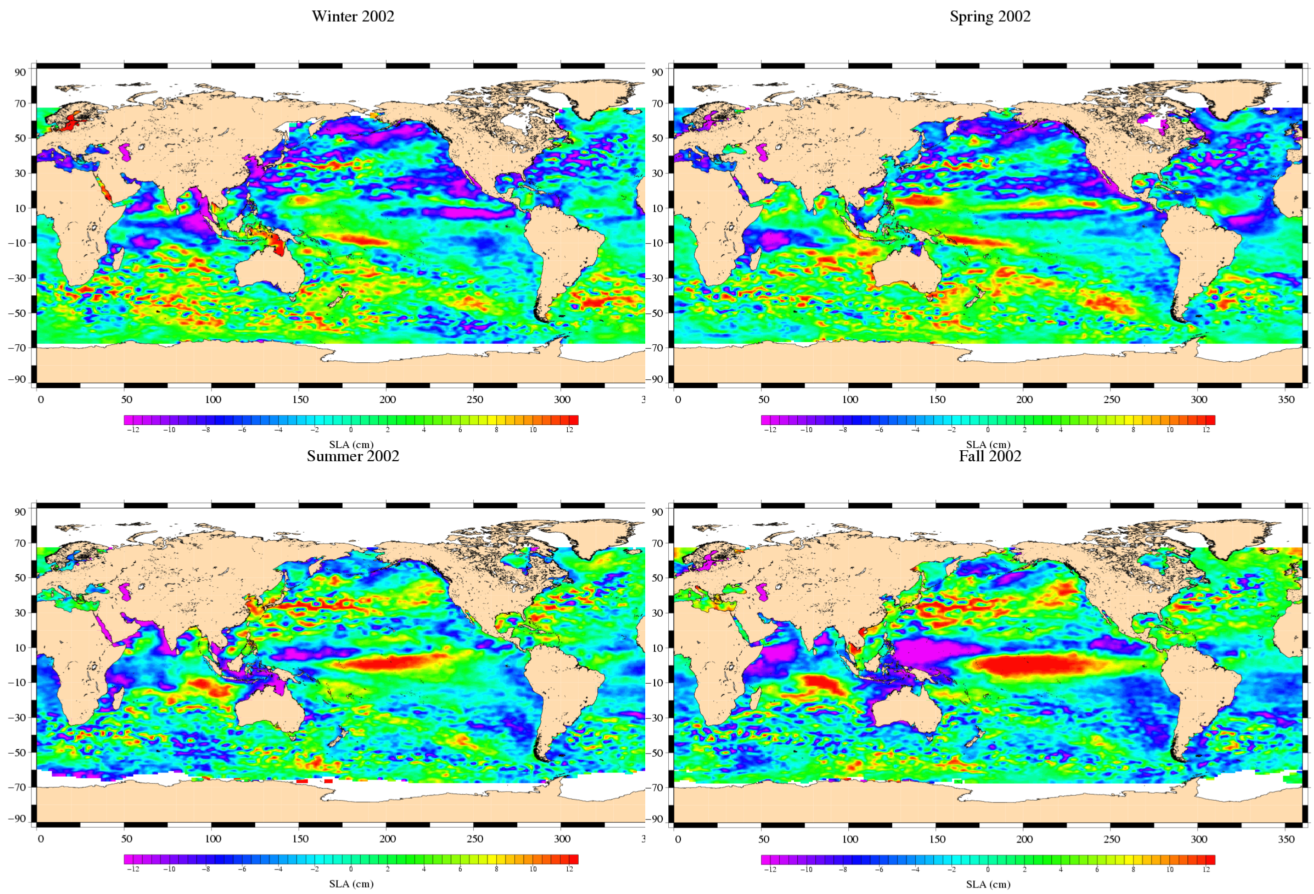

Figure 55: *Seasonal variations of Jason SLA (cm) for year 2002 relative to a MSS CLS 2001*

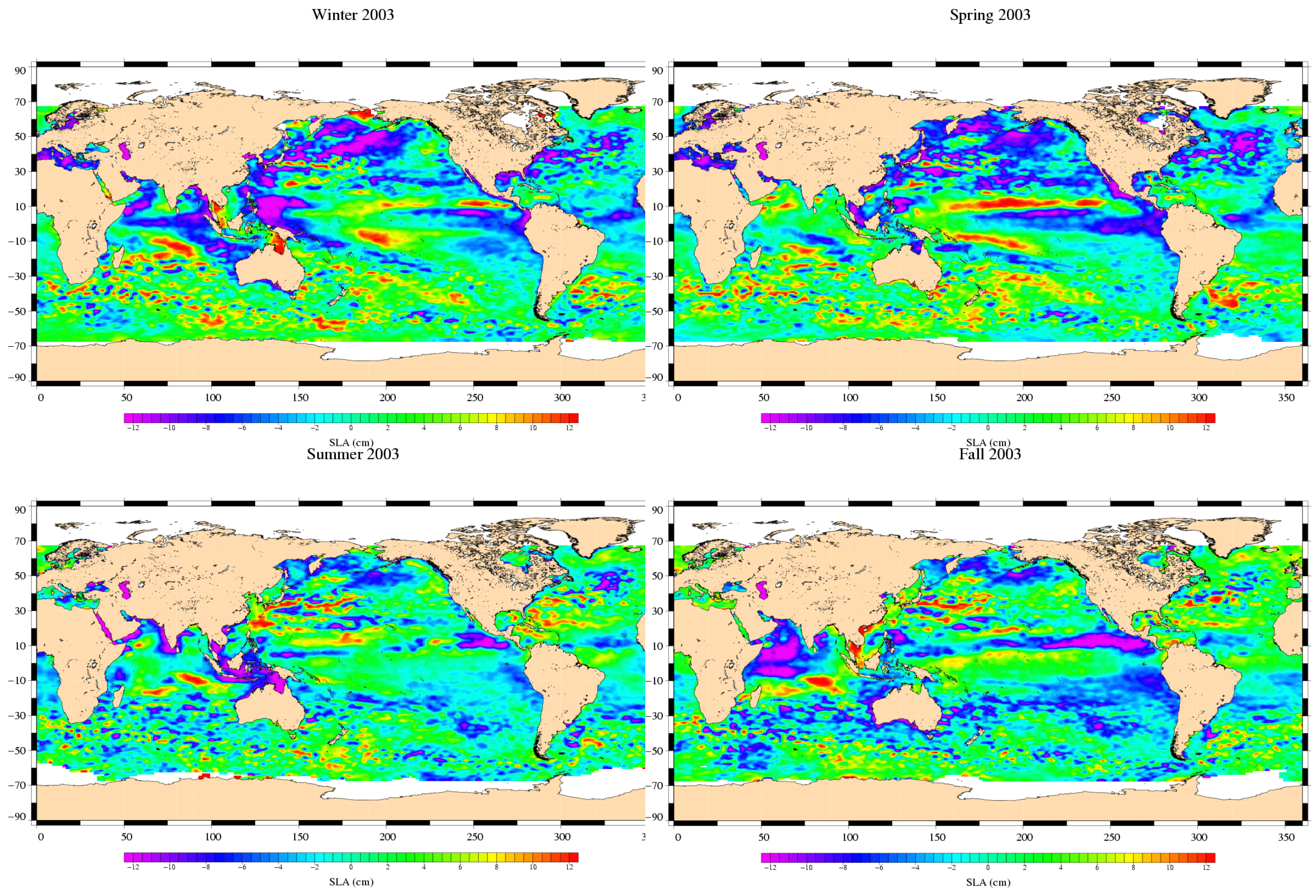

Figure 56: *Seasonal variations of Jason SLA (cm) for year 2003 relative to a MSS CLS 2001*

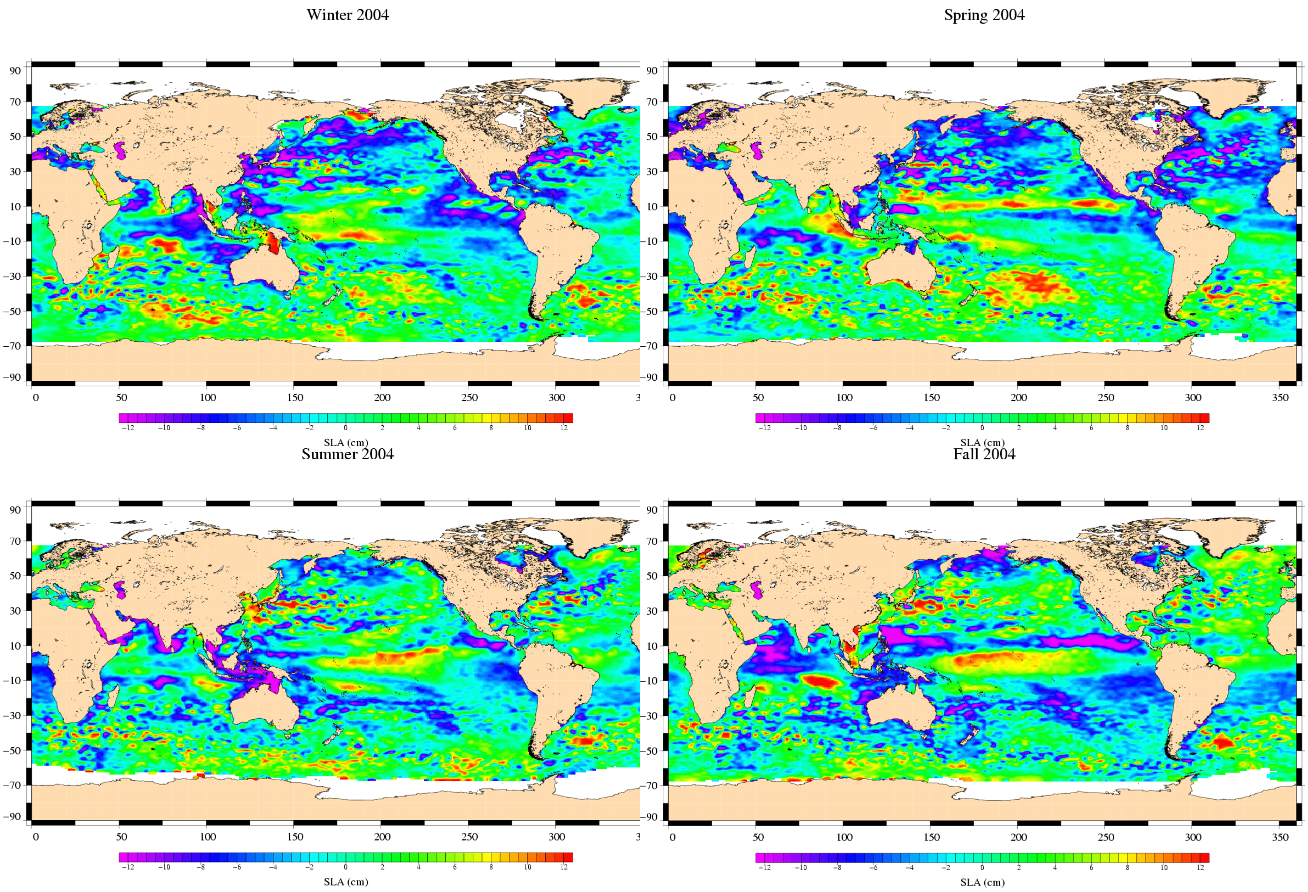

Figure 57: *Seasonal variations of Jason SLA (cm) for year 2004 relative to a MSS CLS 2001*

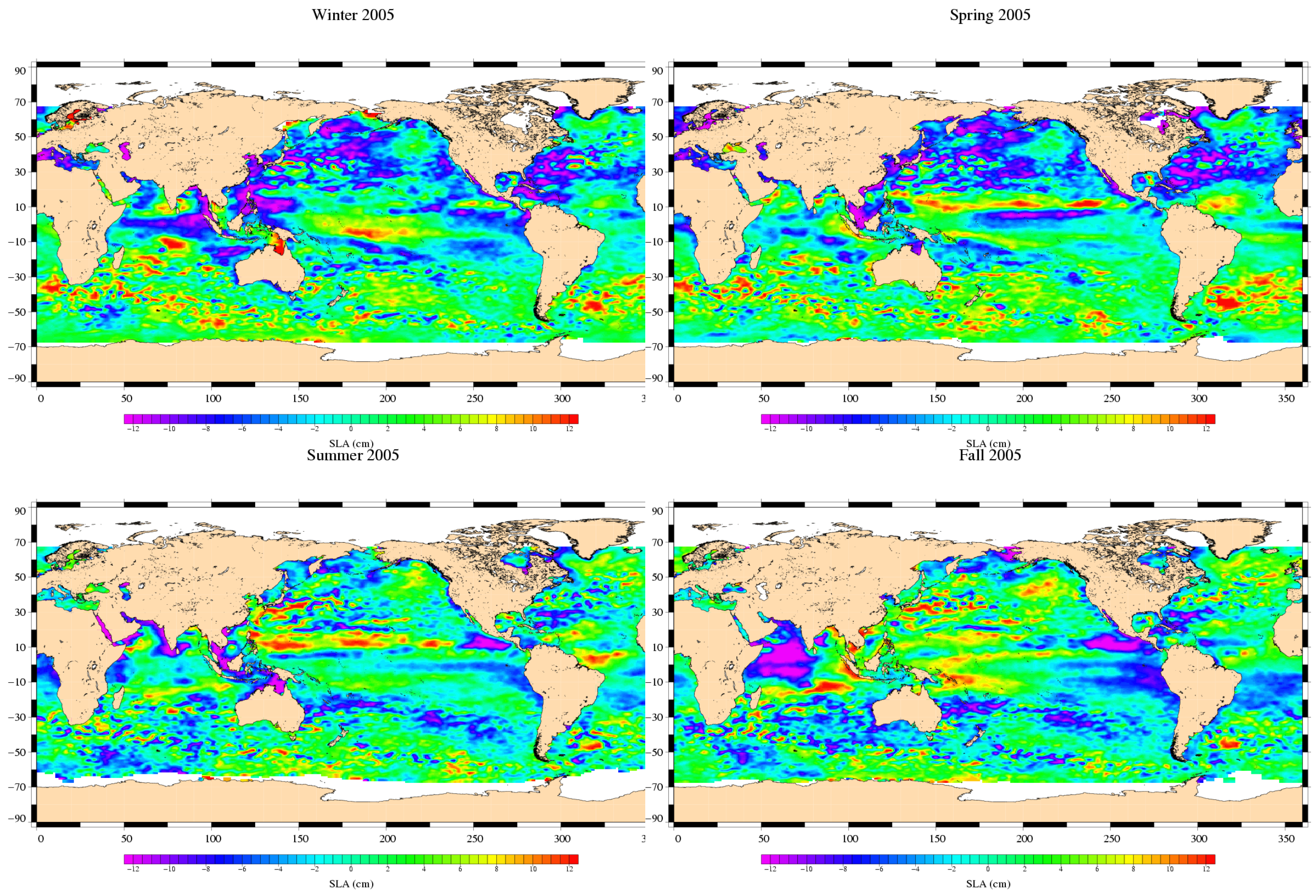

Figure 58: *Seasonal variations of Jason SLA (cm) for year 2005 relative to a MSS CLS 2001*

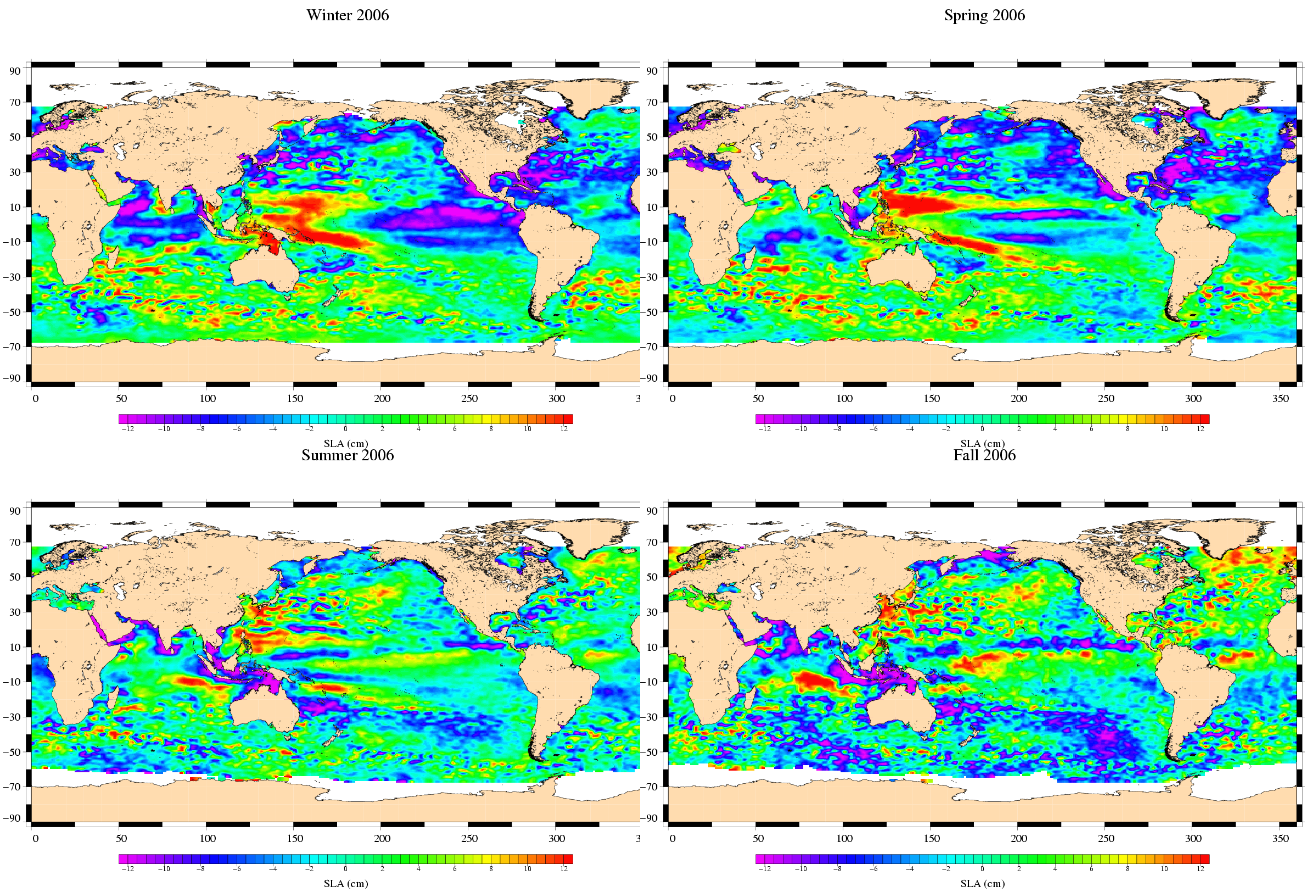

Figure 59: *Seasonal variations of Jason SLA (cm) for year 2006 relative to a MSS CLS 2001*

7 Impact of Reprocessing of Jason-1 and TOPEX data

7.1 Introduction

As described early in this report (see section 2.3), some Jason-1 GDRs have been reprocessed in version "b". A similar work has been carried out for the TOPEX data covering Jason-1 cycles 1 to 21 (TOPEX and Jason-1 were over the same track).
The objective of this chapter is to analyze the quality of the reprocessed Jason-1 data between both GDR versions and to check the consistency between the Jason-1 and TOPEX data using these new data.
Notice that these results were also presented at OSTST meeting from 16-18 March 2006 in Venice, Italy. The posters are reproduced as Figures 97 and 98.

7.2 Reprocessing of Jason-1 data

Cycles 1 to 21 were reprocessed in GDR version "b" by JPL, whereas cycles 128 to 135 were reprocessed by CNES. The data were processed by Cal/Val by a dedicated processing chain to detect missing and bad measurements (see section 3.2.1).

After validation of reprocessed data (GDR "b"), valid tables of GDR "a" and "b" were compared cycle per cycle for each altimetric parameter, as well as SLA.

7.2.1 Overview of Comparison between GDR "a" and "b"

The following principal differences between the validated data of GDR "a" and "b" were found :

- **Data presence:**
  - **23 passes in addition present in comparison to GDR "a"**
  - **2 passes less in comparison to GDR "a" (pass 7 and 161 of cycle 1)**
- **Editing:**
  - **2 passes are no longer edited by SLA out of threshold**
  - **1 pass is no longer edited by pass mean**
  - **2 (portion of) passes are no longer edited by mispointing**
- **Problems:**
  - **3 1/2 passes without radiometer correction (cycle 1, 8)**
  - **3 passes with problems of date (cycle 19)**

Table 7 gives more detail about the differences after validation.

Cycle	GDR "a"	GDR "b"
001	passes 1, 123, 250 missing	passes 1, 123, 250 missing
		.../...

Cycle	GDR "a"	GDR "b"
	passes 45-47, 121-122, 251-254 missing passes 31, 44, 48, 58 and 249 partly missing	passes 7 and 161 missing passes 8 (17.9%), 31 (17.1%), 46 (16.8%), 47 (16.8%), 58 (79.4%), 249 (44.4%) and 251 (67.5%) are partly missing small portion of pass 251, as well as complete passes 252-254 edited due to missing radiometer wet troposphere correction
002	passes 1 to 16 are missing (on board DORIS anomaly) passes 112 (Gyro Calibration) and 133 partly missing	passes 1 to 16 are missing passes 112 (92.9%) and 133 (14.8%) partly missing
003	no missing pass passes 114 and 115 partly missing (Gyro calibration) pass 1 edited by pass mean	no missing pass passes 114 (93.6%) and 115 (13.6%) partly missing pass 1 no longer edited
004	pass 235 and 236 completely missing passes 146 (gyro calibration), 184, 185, 234 and 237 partly missing (science telemetry not available)	pass 235 and 236 completely missing passes 146 (60.8%), 184 (100%), 185 (89.1%), 234 (100%) and 237 (92.7%) partly missing.
005	no missing passes 2 passes edited by SLA out of threshold	no missing passes no edited passes
006	pass 12 missing passes 11, 13, 202, 203 and 205 partly missing (no altimeter echo data available) pass 56 partly edited due to bad data quality (altimetric parameters are out of threshold)	pass 12 missing passes 11 (29.0%), 13 (85.6%), 202 (25.2%), 203 (6.0%) and 205 (14.6%) partly missing pass 56 partly edited due to bad data quality
007	no missing pass passes 99 and 148 are partly missing (due to unavailability of science telemetry)	no missing pass passes 99 (26.0%) and 148 (33.2%) are partly missing

.../...

Cycle	GDR "a"	GDR "b"
008	passes 253 and 254 missing (star tracker SEU)	passes 253 and 254 missing
	passes 81 to 83 completely and small portion of pass 084 missing (ground processing issue)	passes 82 (4.6%) , 83 (10.4%) and 84 (6.6%) partly missing
	passes 52 and 252 partly missing	passes 52 (28.2%) and 252 (52.1%) partly missing
	small portion of pass 252 edited by all altimetric parameters	small portion of pass 252 edited by all altimetric parameters
		half of pass 252 edited because of lack of wet tropospheric correction
009	passes 1-6 (Poseidon SEU) and 34-36 (ground processing issue) are completely missing	passes 1-3 completely missing, pass 4 (21.4%) partly missing, pass 4 (80%) and 5 edited by dual-frequency ionosphere criterion (data in C-band are missing)
	passes 173- 174 (gyro calibration) and 166 partly missing	passes 166 (8.4%), 173 (46.2%) and 174 (24.0%) are partly missing
010	no missing passes	No missing passes
	passes 47 and 48 partly missing	passes 47 (15.1%) and 48 (46.3%) partly missing
	pass 87 partly edited by mispointing criterion	
011	no missing passes	no missing passes
012	no missing passes	no missing passes
013	no missing passes	no missing passes
	pass 223 partly missing	pass 223 (7.3%, ca. 130 consecutive measurements) partly missing
	small portion of pass 90 edited by mispointing criterion	
014	passes 130 and 131 missing, pass 132 (38%) partly missing	no missing passes
015	passes 186 (CMA ACQ failure) and 233 missing, pass 187 missing with 100%	no missing passes, but a small portion of pass 186 is still missing
		.../...

Cycle	GDR "a"	GDR "b"
016	passes 248 and 249 missing	no missing passes
017	no missing passes	no missing passes
018	no missing passes	no missing passes
019	passes 13 and 14 missing, pass 15 partly missing	pass 13 (5.4%) partly missing datation anomaly from pass 19 to 21, The delta time between each measurement is 1 second instead of 1.019 second. The orbit values don't correspond to the range for these measurements : the SLA ranges from -5m and 5m (ground processing issue)
020	No missing passes	No missing passes
021	very small portion of pass 113 is missing near the coast of Chile (calibration over ocean) portion of pass 210 edited by several criteria due to unavailability of STR	small portion of pass 113 (2.6%) is missing portion of pass 210 edited by several criteria due to unavailability of STR
128	no missing pass	a few measurements (ca. 30) are missing on pass 90 (2005-06-30) between 23:59:28 and 23:59:59 (included)
129	no missing pass	a few measurements (ca. 30) are missing on pass 246 (2005-07-16) between 23:59:28 and 23:59:59 (included). These measurements were partially present in GDR "a".
130	no missing passes	no missing passes
131	7 passes (59 - 65) are partially missing due to TRSR2 "elephant packets" anomaly. pass 190 partially edited	7 passes (59 - 65) are partially missing due to TRSR2 "elephant packets" anomaly.
132	no missing pass pass 253 is partly missing (altimeter SEU)	no missing pass pass 253 (59.8%) is partly missing
133	no missing pass	no missing pass

.../...

Cycle	GDR "a"	GDR "b"
	passes 12 and 13 partly missing (altimeter SEU) pass 13 partly edited by dual-frequency ionospheric criterion, pass 21 partly edited by mispointing criterion	passes 12 (99.7%) and 13 (55.0%) partly missing pass 13 partly edited by dual-frequency ionospheric criterion
134	no missing passes passes 83,153,177,233 and 235 partly edited by mispointing criterion	no missing passes
135	no missing passes many passes (especially in southern hemisphere) edited by mispointing criterion	no missing passes

Table 7: *D*ifferences in absent and edited data for GDR "a" and "b".

7.2.2 Comparison of altimetric parameters

7.2.2.1 Introduction

Using the new MLE4 retracking algorithm (Amarouche et al., 2004 [6]) with 2nd order (used in GDR "b"), retrieves now 4 altimetric parameters (epoch, sigma0, SWH and apparent mispointing) instead of 3 (MLE3, used in GDR "a"). These parameters will be different from those derived with MLE3 retracking algorithm. This new retracking of Jason-1 was necessary since star tracker system behaved abnormal potentially leading to possible significant mispointing angle, which could not be resolved by MLE3 algorithm.
In this section, the altimetric parameters are compared for the two GDR versions.

7.2.2.2 Differences in Ku-band range

The range is one of the altimetric parameters, which is derived (via epoch) from the waveforms using a retracking algorithm.
The differences visible in figure 60 (left) are due to the different retracking algorithms and their corresponding instrumental correction (or look-up correction tables, Thibaut et al., 2004 [61]) of the two GDR versions (see figure 61, left).

On figure 62 the mean and standard deviation of the differences between the 2 ranges without the instrumental corrections is shown. Mean differences are especially strong near coasts and standard deviation is high in regions with strong apparent mispointing angles (rain, sigma bloom, ...). These differences are originated in the new retracking algorithm. The second plateau is no longer constrained leading to the possibility of retrieving measurements in regions with strong apparent mispointing (waveforms with disturbed second slope).

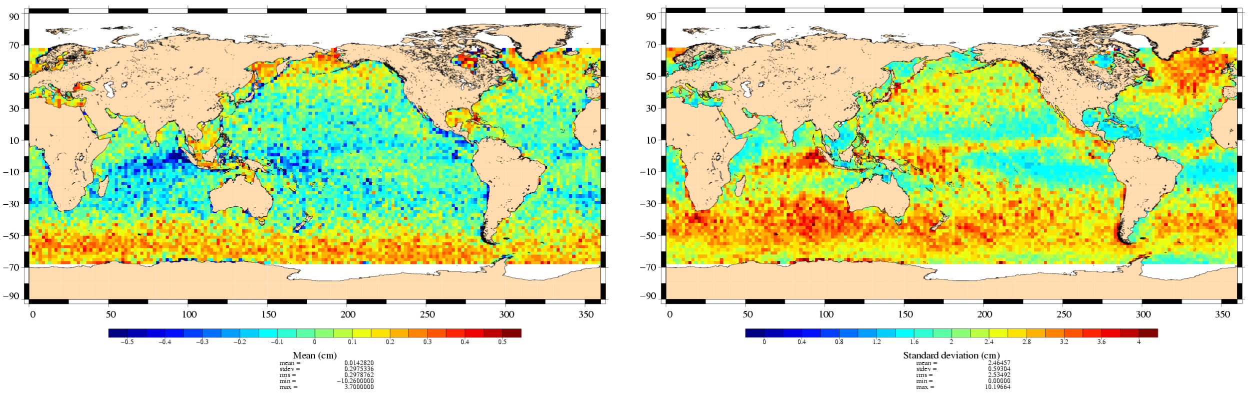

Figure 60: *Cartography of mean and standard deviation of differences between range of GDR "b" and GDR "a" over 21 cycles.*

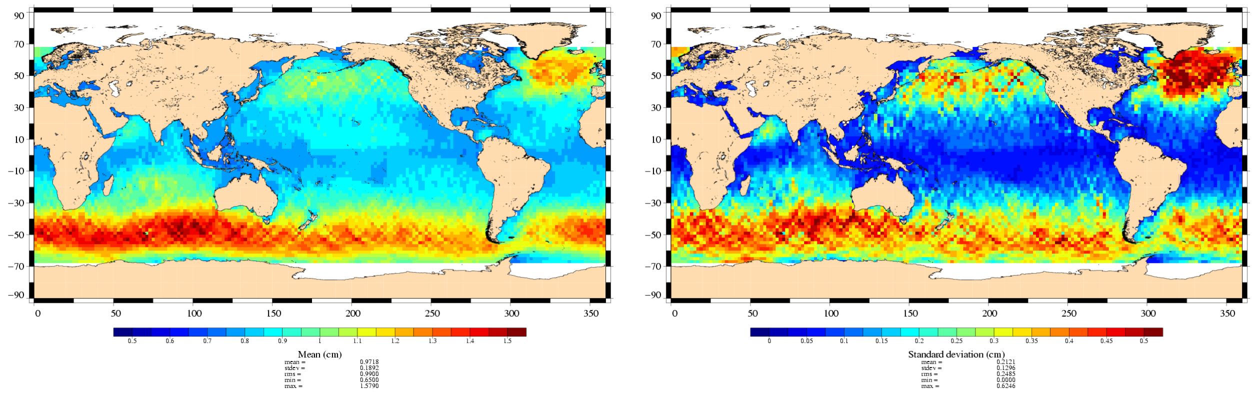

Figure 61: *Cartography of mean and standard deviation of differences between instrumental correction tables of GDR "b" and GDR "a" over 21 cycles.*

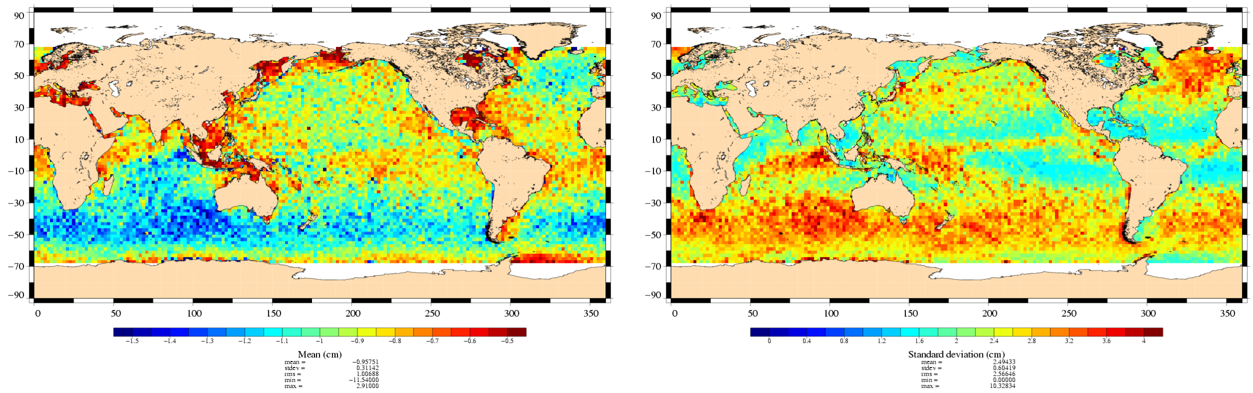

Figure 62: *Cartography of mean and standard deviation of differences between range (without instrumental correction tables) of GDR "b" and GDR "a" over 21 cycles.*

7.2.2.3 Differences in standard deviation of 20 Hz Ku-band range

Figure 63 (left) shows that the standard deviation of 20 Hz Ku-band range of GDR "b" is higher than it was in GDR "a". This is due to the use of the MLE4 retracking algorithm which retrieves 4 instead of 3 parameters therefore adding noise on the retrieved parameters.

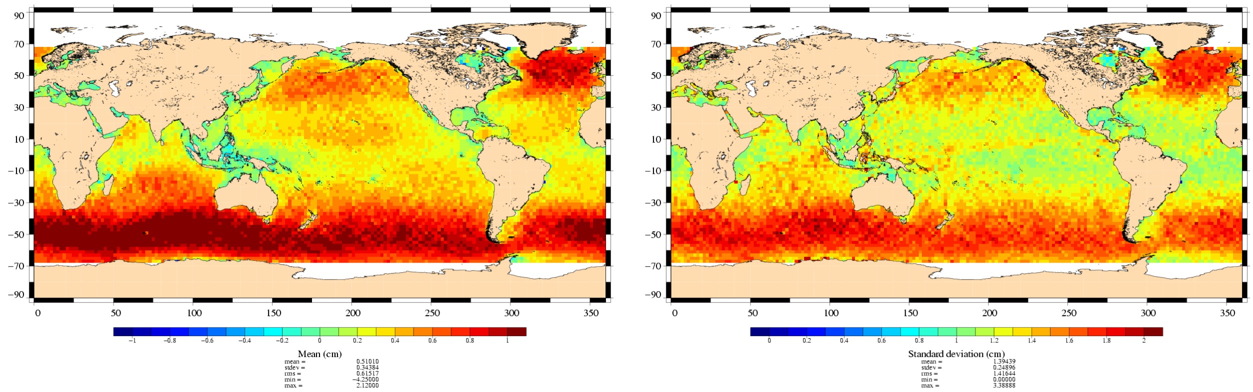

Figure 63: *Cartography of mean and standard deviation of differences between standard deviation of 20 Hz (Ku-band) range of GDR "b" and GDR "a" over 21 cycles.*

7.2.2.4 Differences of Sea Wave Height (SWH) in Ku-band

Figure 64 (left) shows the mean differences of SWH for the 2 GDR versions. There are differences of about 5 cm for strong waves and about -8 cm in regions of small waves (near coasts). Small negative differences of about -1 cm may also occur in open ocean. The right figure (standard deviation of differences) looks like the figure of standard deviation of waves itself.

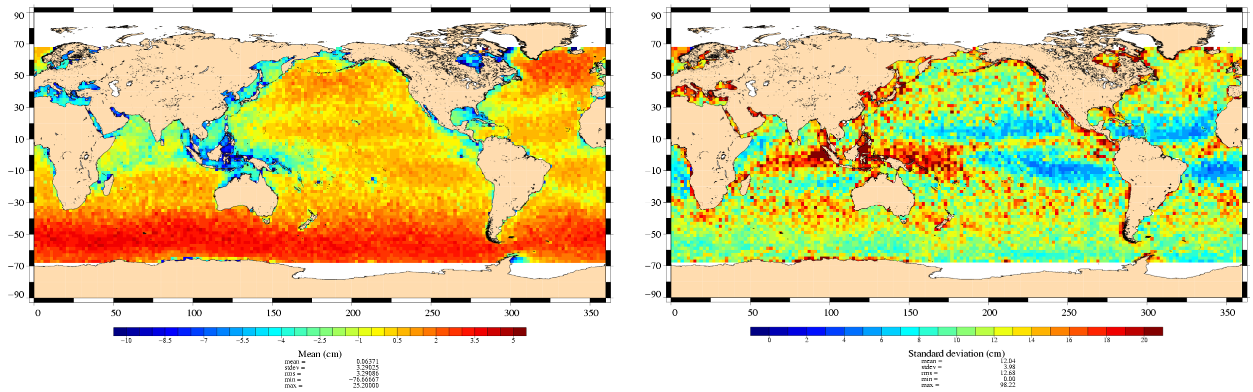

Figure 64: *Cartography of mean and standard deviation of differences between SWH of GDR "b" and GDR "a" over 21 cycles.*

7.2.2.5 Differences of Sigma0 in Ku-band

Figure 65 (left) shows that there is a mean bias of 0.1 dB of sigma0 difference between GDR "a" and "b". This difference seems to be due to MLE4 retracking, since difference of atmospheric attenuation is very small between the 2 GDR versions, and neither skewness nor instrumental correction tables do influence sigma0.

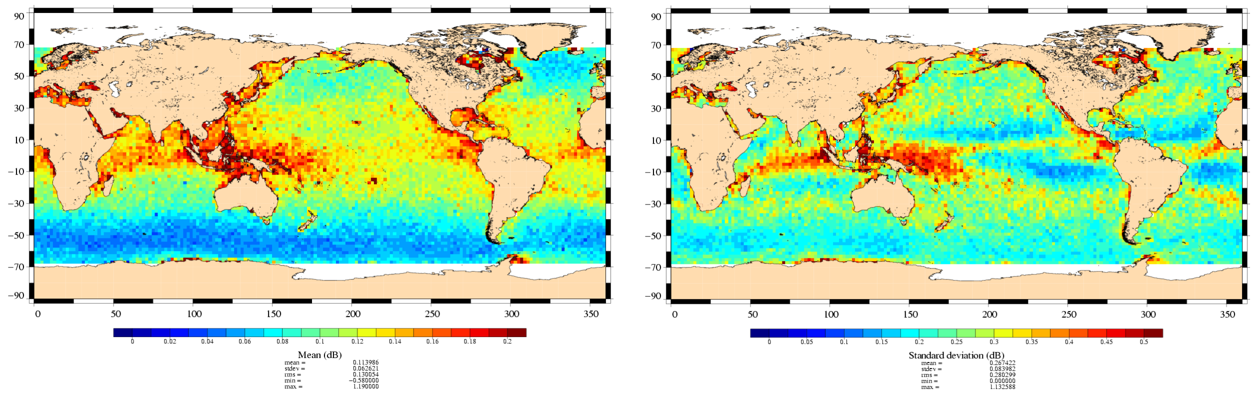

Figure 65: *Cartography of mean and standard deviation of differences between Sigma0 of GDR "b" and GDR "a" over 21 cycles.*

7.2.2.6 Differences of squared mispointing angle

The square mispointing angle is different especially in areas where the waveforms are not typical expected waveforms (rain, blooms,...) : see figure 66. For these waveforms, the estimated mispointing angle doesn't reflect a real mispointing angle but only a distortion of the waveform.

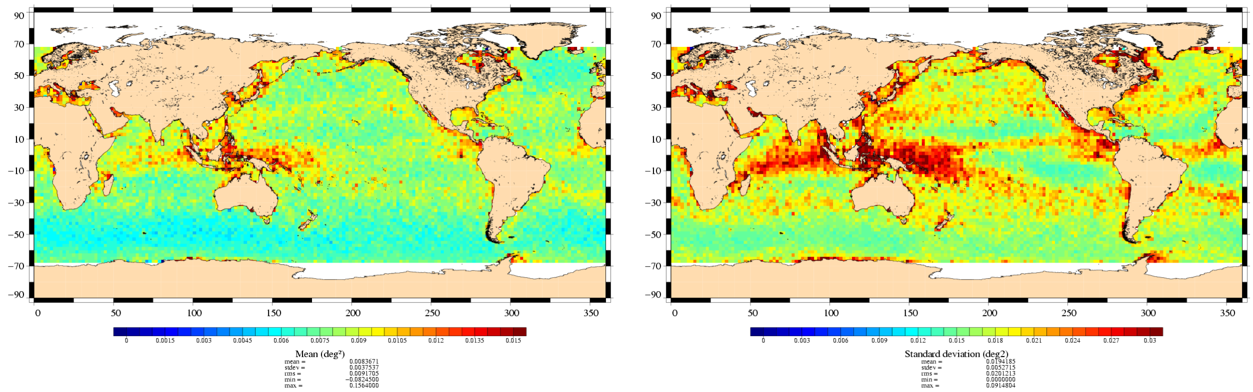

Figure 66: *Cartography of mean and standard deviation of differences between squared mispointing values of GDR "b" and GDR "a" over 21 cycles.*

7.2.2.7 Differences of JMR

Figure 67 shows that the differences between the two wet troposphere corrections are very small for this period. The impact of JMR provided in GDR "b" overall the Jason-1 mission has been described in section 4.7

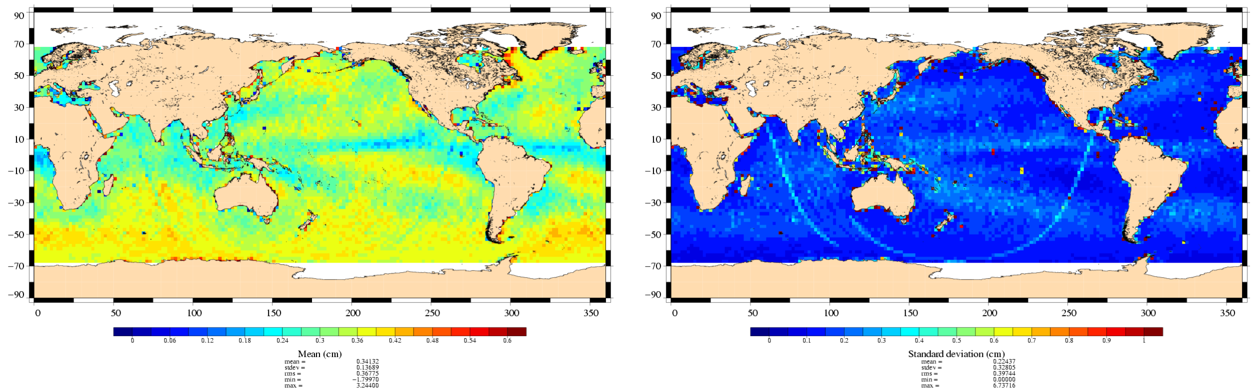

Figure 67: *Cartography of mean and standard deviation of differences between JMR of GDR "b" and GDR "a" over 21 cycles.*

7.2.3 Study of noise on 20 Hz and 1 Hz measurements for GDR "a" and "b"

Using 20 Hz data, at frequencies higher than 1 Hz, the Jason-1 signals are hidden by a plateau at $10^{-3} m^2 s$. This plateau is the signature of a 7.3 cm white noise for GDR "a" data and a 7.9 cm white noise for GDR "b" data. Estimating for GDR "b" 4 parameters instead of 3 parameters (GDR "a") with the retracking algorithm has therefore increased noise on 20 Hz data. From 1 Hz data, there is no clear plateau at high frequencies. Nevertheless noise on GDR "b" data is lower than noise on GDR "a" data. This amelioration is due to the improved estimation of apparent mispointing (using MLE4) especially for humid regions.

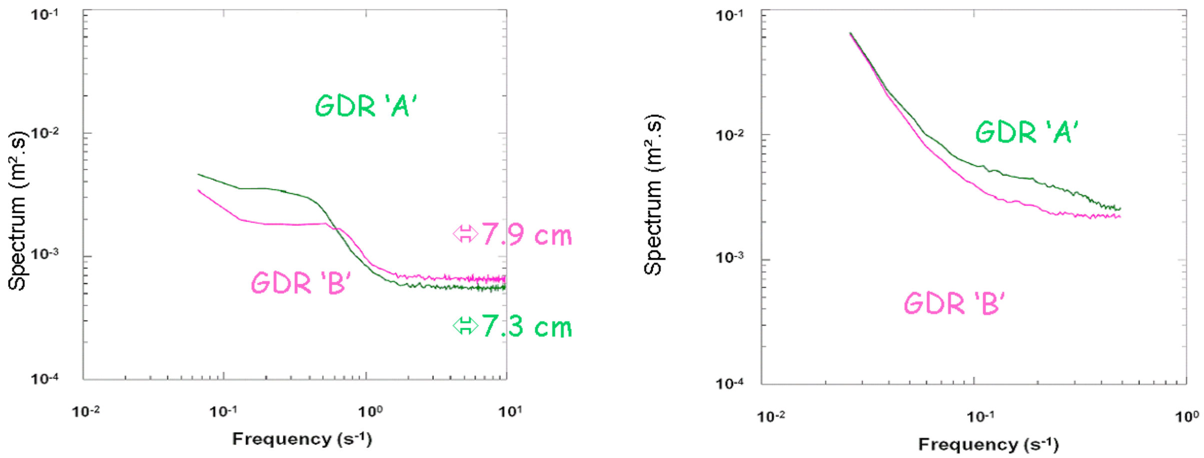

Figure 68: *Spectra of noise on SSH at 20 Hz (left) and 1 Hz (right).*

7.2.4 Comparison of performances for SSH calculation

7.2.4.1 Impact of new orbit

SSH was calculated with data from GDR "b" as described in section 5, but using either orbit of GDR "a" or of GDR "b".
GDR "b" orbit is a SLR/DORIS/GPS orbit and uses the EIGEN-CG03C gravity field (Förste et al., 2005 [27]). GDR "a" orbit is a SLR/DORIS orbit with JGM-3 gravity model (Tapley et al., 1996 [58]). Figure 69 shows mean crossover differences (ascending/ descending bias). Using GDR "a" orbit (left), large structures of high positive or negative differences can be seen, whereas the right figure using orbit of GDR "b" is much more homogeneous as it shows smaller differences at crossovers. The gain in SSH variance with the new orbit is about 1.6 cm rms.

Figure 71 shows that mean SSH differences at crossovers are very stable for cycles 15 to 21 when using the GDR "b" orbit. Figures from cycles 10 to 12 are quite negative. This effect could be partly reduced be refining the GPS data processing in orbit calculation.

Figure 73 shows that the gain in variance of SSH differences at crossovers, using orbit of GDR "b" is positive over the whole period. The gain is 1.6 cm rms for the 21 cycles, and 1.8 cm rms for the period of cycles 128-135.

With this new orbit quality, small signals can now be detected such as an hemispheric bias at crossovers (figure 69, right) using GDR "b" data. This bias is not visible when using GDR "a" altimeter data and the GDR "b" orbit (figure 70).
A time shift of 0.173 ms has been added in GDR "b" L1-B processing. A wrong sign in this time shift might explain the observed hemispheric bias.

Figure 74 (left) shows differences of SSH at crossovers when correcting for the time shift of 0.173 ms applied to the GDR "b" data. This hemispheric bias is now less important. Assuming that the time shift in GDR "b" was applied with the wrong sign, correcting the SSH with 2 times the time shift, should lead to the intended result. Figure 74 (right) shows the corresponding map. It shows again a hemispheric bias, but this time the bias is inverse to the one shown in figure 69 (right). It also seems less strong. The time shift to apply is probably less than 0.173 ms and with the opposite sign (as it was applied in GDR "b").
The difference of variance of SSH differences at crossovers using initial SSH and the one corrected for time shift is 0.195 cm^2. Difference of variance of SSH differences at crossovers using initial SSH and SSH corrected 0.346 ms is 0.177 cm^2.

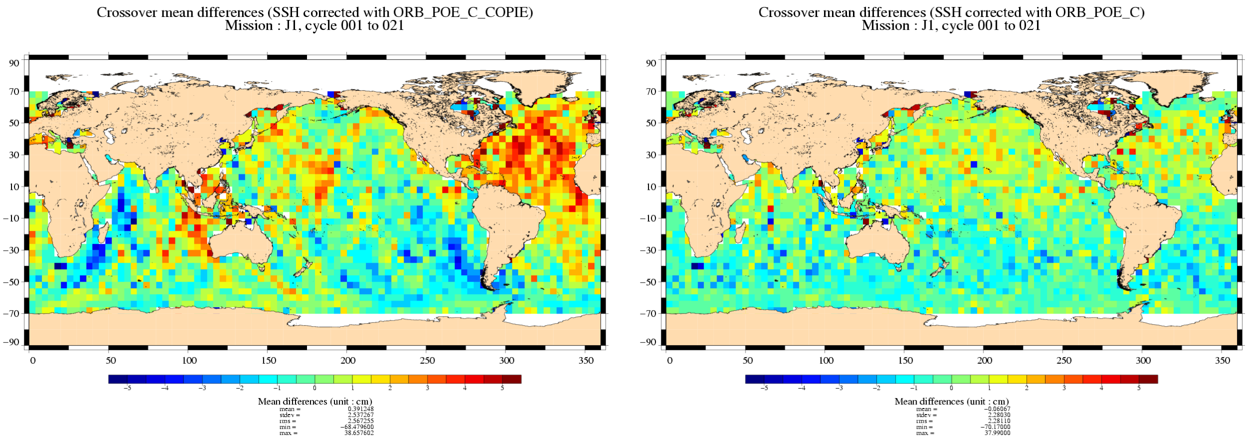

Figure 69: *Mean of SSH differences using GDR "a" orbit (left) and GDR "b" orbit (right) over 21 cycles.*

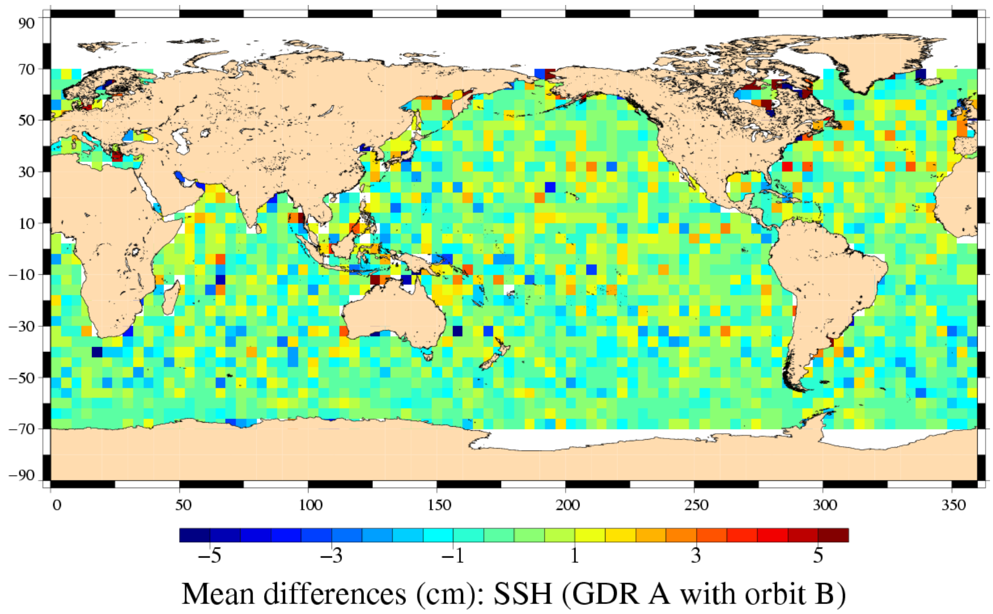

Figure 70: *Mean of SSH differences using altimeter data of GDR "a" and orbit of GDR "b" over 21 cycles.*

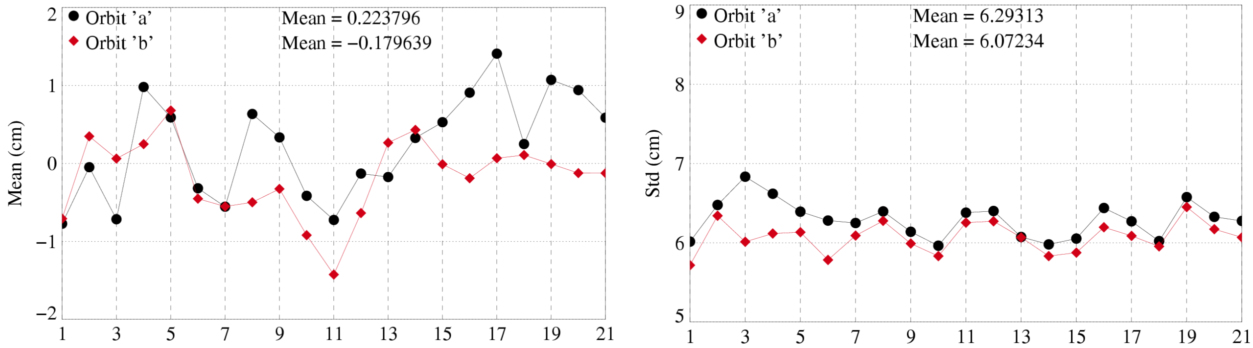

Figure 71: *Cycle per cycle monitoring of SSH differences at crossovers using orbit of GDR "a" and GDR "b" for cycles 1 to 21.*

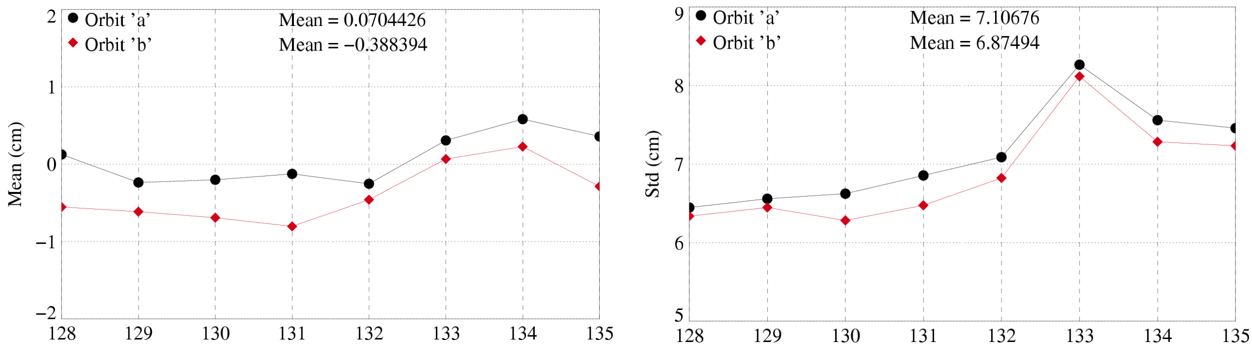

Figure 72: *Cycle per cycle monitoring of SSH differences at crossovers using orbit of GDR "a" and GDR "b" for cycles 128 to 135.*

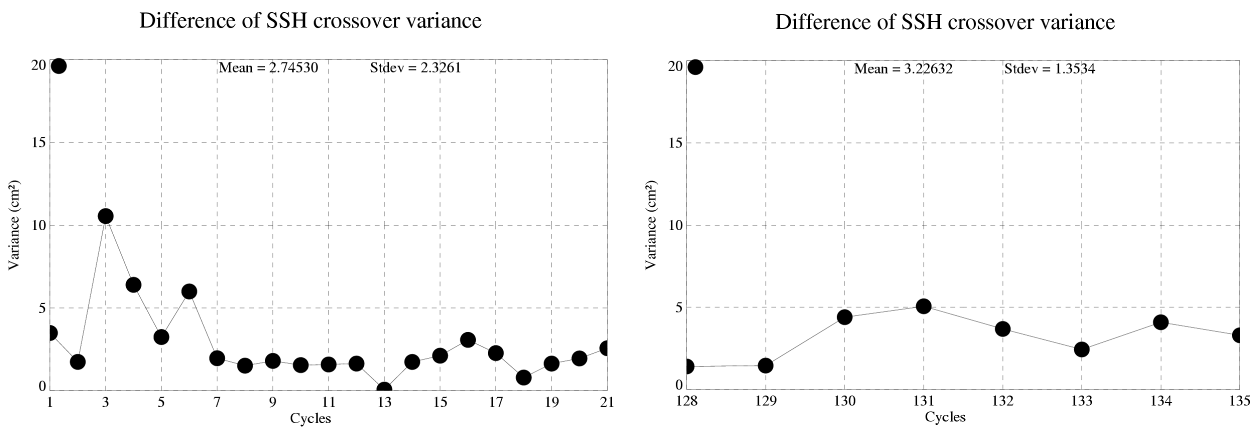

Figure 73: *Cycle per cycle monitoring of variance gain (variance of SSH differences using orbit "a" - variance of SSH differences at crossovers using orbit "b"). Left: cycles 1-21, right: cycles 128-135.*

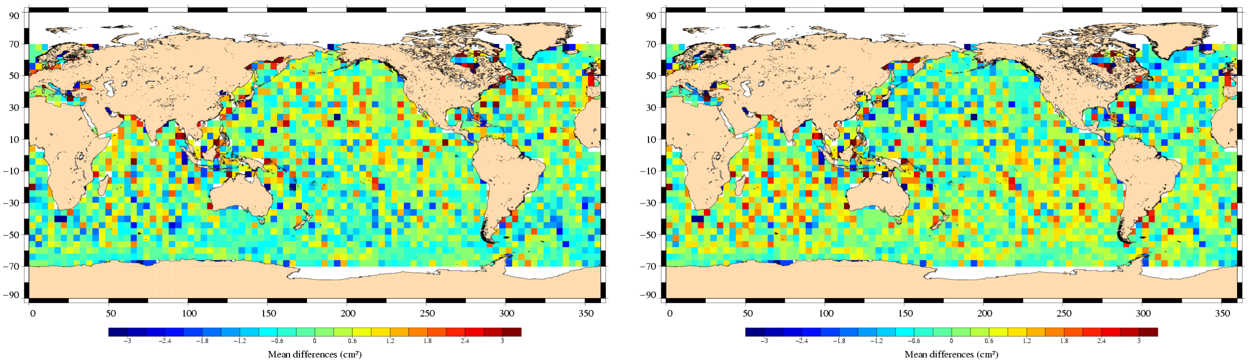

Figure 74: *Mean of SSH differences using GDR "b" corrected for time shift which was applied to GDR "b" in comparison to GDR "a" :* $SSH_{corrected} = SSH + 0.173ms * HPOINT$ *(left) and double corrected :*$SSH_{2corrected} = SSH + 2 * 0.173ms * HPOINT$ *(right).*

7.2.4.2 Impact of new range

Using data of GDR "b", impact of range on SSH differences at crossovers is studied using in figure 75 (left) range of GDR "b" corrected for the time shift, and in figure 75 (right) range of GDR "a". Thanks to the use of the range of GDR "b", SSH differences at crossovers are smaller than those using range of GDR "a".

The gain in variance using range of GDR "b" rather than GDR "a" is shown in figure 76. The gain is positive over the whole region.

The improvement of SSH performances due to use of range calculated by MLE4 algorithm is also evident on figure 77 and figure 78.

Figure 79 shows the gain in variance of along-track SLA when using range of GDR "b" instead of GDR "a". It shows improvement especially for equatorial regions.

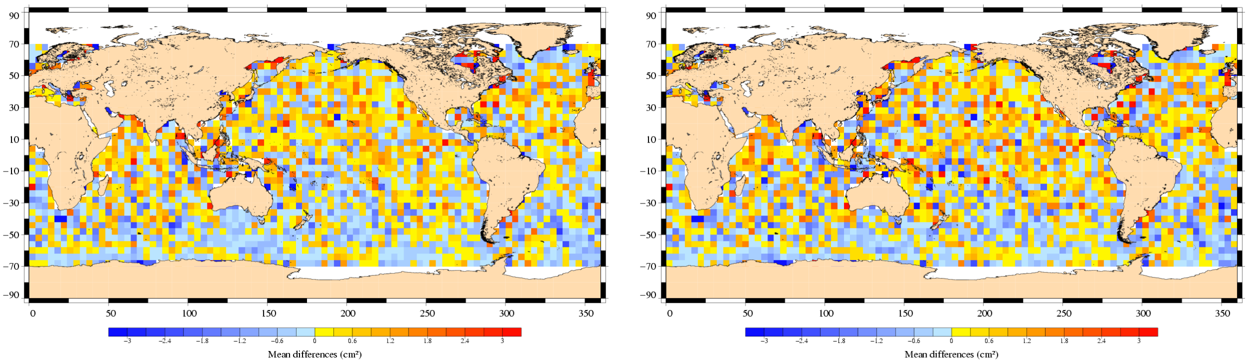

Figure 75: *Mean of SSH differences at crossovers using range of GDR "b" (corrected by 0.173 ms time shift) (lft) and range of GDR "a" (right).*

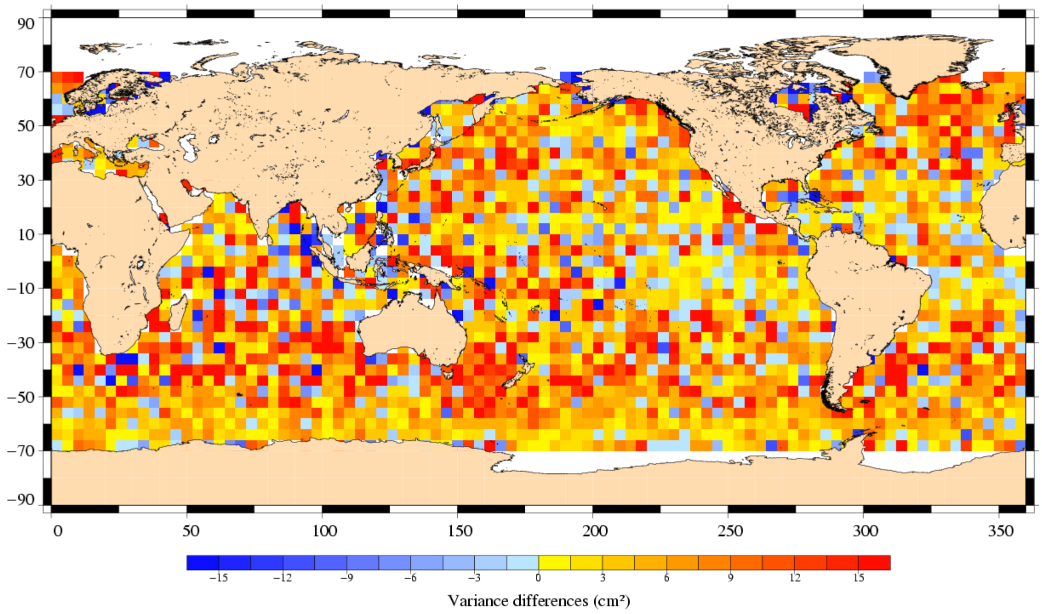

Figure 76: *Gain in variance of SSH differences at crossovers using range of GDR "b" instead of range of GDR "a".*

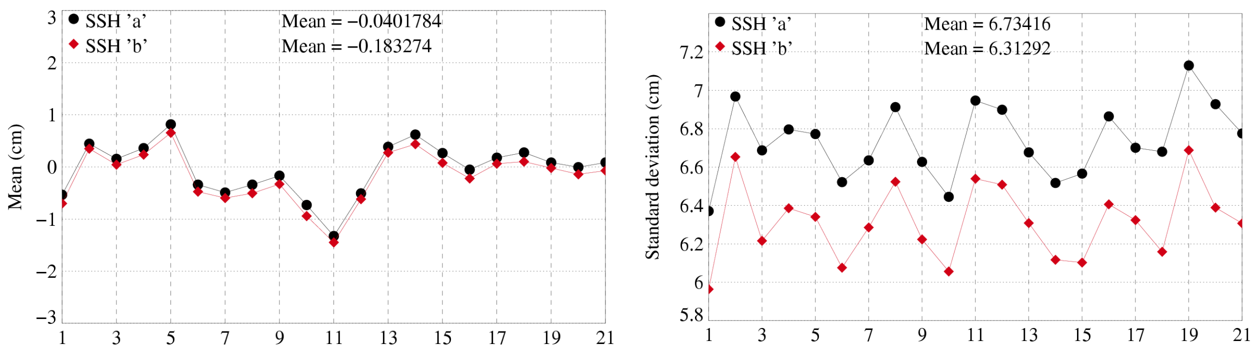

Figure 77: *Cycle per cycle monitoring of mean and standard deviation of SSH differences at crossovers.*

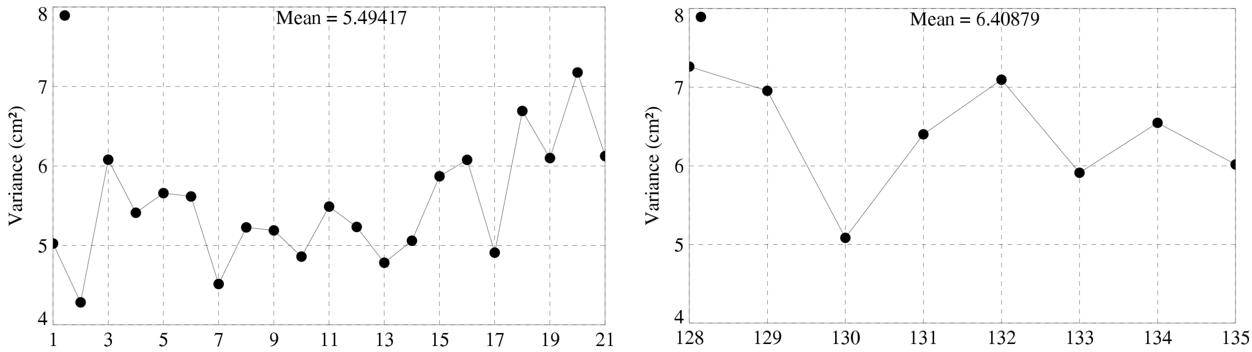

Figure 78: *Cycle per cycle variance difference (SSH variance calculated with range of GDR "a" - SSH variance calculated with range of GDR "b") at crossovers for cycles 1 to 21 (left) and cycles 128 to 135 (right).*

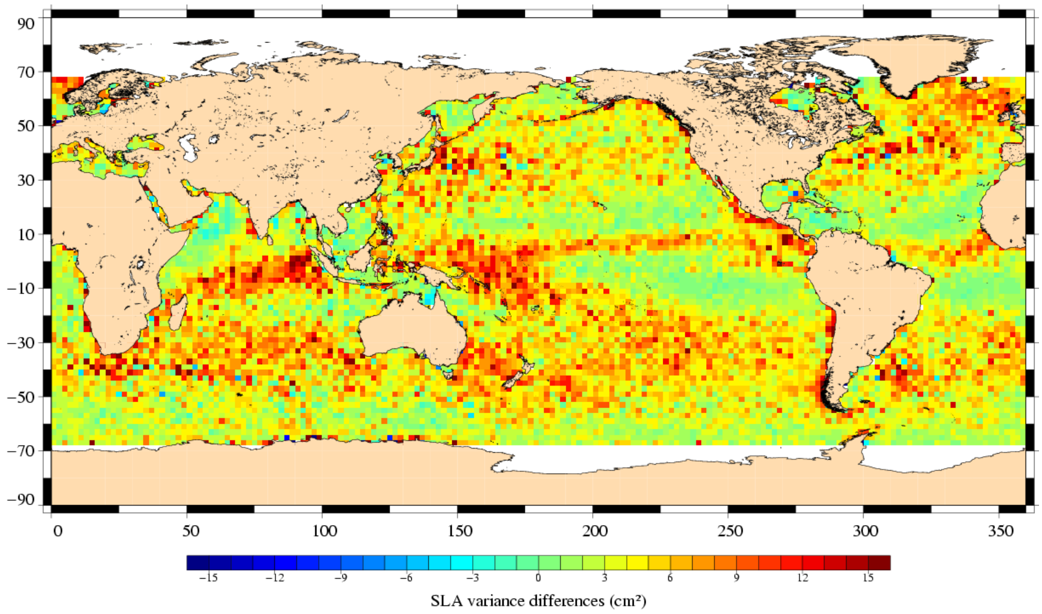

Figure 79: *Gain in variance of along-track SLA over cycles 1 to 21.*

7.2.4.3 Impact of new geophysical parameters

GDR "b" now includes new geophysical corrections: non-tidal high frequency correction from DAC (dynamic atmospheric correction), FES2004 and GOT00.2 tide models, non equilibrium long period tide, MSS CLS01 model. In addition, diurnal and semidiurnal atmospheric tides (S1/S2) are now handled according to OSTST recommendations. Using Mog2D-derived HF correction instead of inverse barometer corrections brings most of the variance reduction at crossovers (2.9 cm rms), especially in high latitudes.

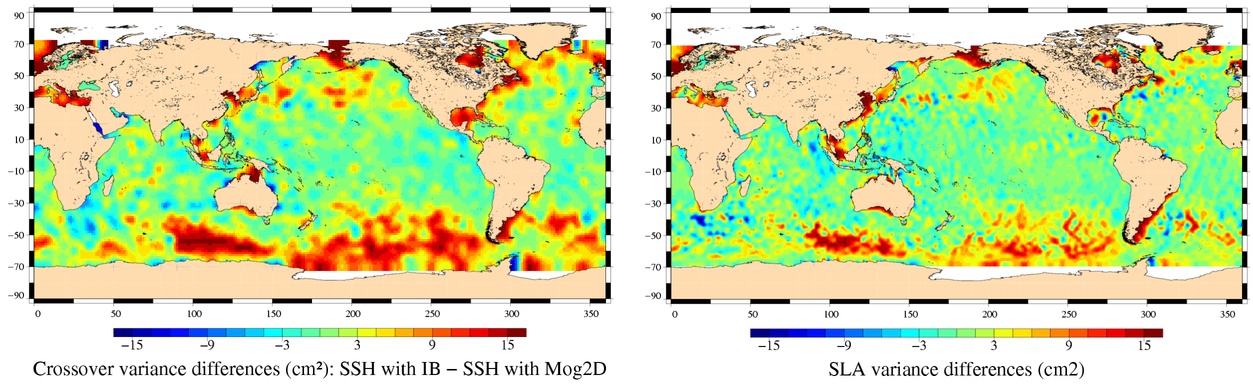

Figure 80: *Left: SSH crossover variance difference (Variance of SSH differences with inverse barometer - variance of SSH differences with DAC). Right: SLA along track variances differences when using Mog2D-derived correction rather than inverse barometer correction alone.*

7.2.4.4 Global

Figure 81 shows finally that SSH differences at crossovers are significantly lower when using GDR "b". Also variance of SSH at crossovers is considerably reduced when using GDR "b" rather than GDR "a", as can be seen on figure 82.

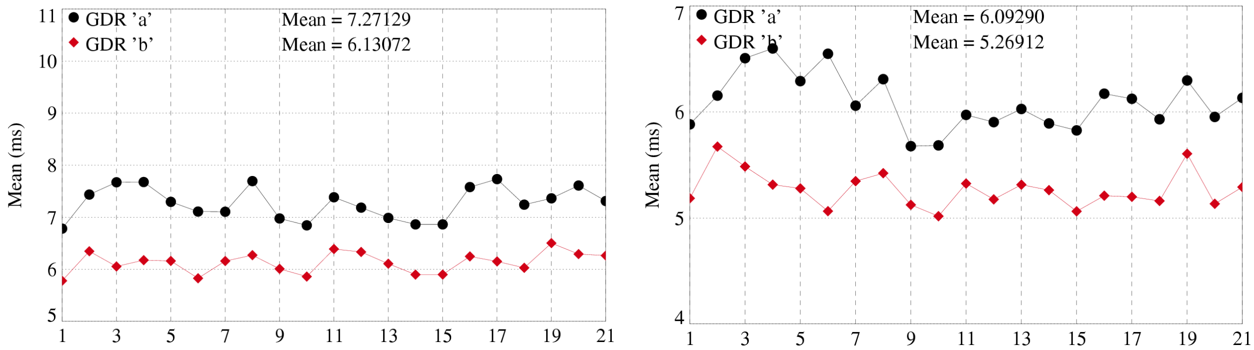

Figure 81: *Cycle per cycle monitoring of standard deviation of SSH differences at crossovers without selection (left) and with geographical selection (right)*

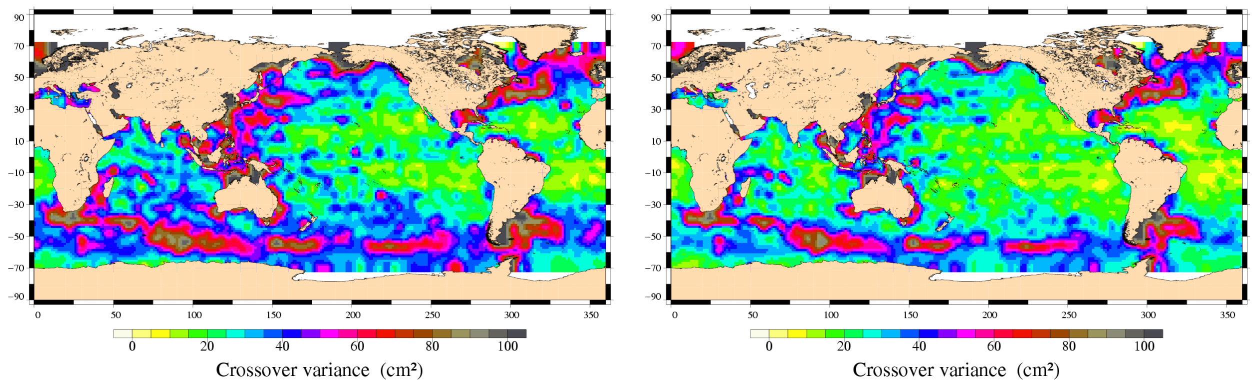

Figure 82: *SSH crossover variance when using GDR "a" data (left) and GDR "b" data (right) (cm^2)*

7.3 Consistency of Jason-1 and TOPEX reprocessing data

7.3.1 Introduction

Since TOPEX/Poseidon cycles 344 to 364 were also reprocessed by JPL - cycles where Jason-1 and TOPEX flew on the same track - it is important to check the impact of the reprocessing on the sea surface height consistency between J1 and TOPEX.
In order to get a significant data set, the following statistics are computed over the 21 cycles, excluding cycles TOPEX 361 (J1 18), which was not reprocessed and TOPEX 362, which was almost completely edited by the Cal/Val processing due to spurious altimeter parameters.
In a first time, SWH of Jason-1 and TOPEX is compared to access consistency of geophysical parameters between the 2 missions. In a second time, impact of new orbits and ranges on the SLA consistency between the 2 missions is shown. Finally, impact of new SSB correction on the SLA consistency is shown.

7.3.2 SWH consistency

Mean differences between TOPEX MGDR and J1 GDR "a" SWH estimates was about 8 cm (Figure 83 top), but this bias was higher for strong waves and smaller for small waves.

Using J1 GDR "b" SWH allows to significantly reduce theses differences even if the global bias is still about 8 cm (Figure 83 right). New instrumental correction tables in GDR "b" explain this better consistency. The impact of new TOPEX SWH (MLE5) (Figure 83 bottom) is less sensitive though the remaining discrepancies visible close to the coasts in Figure 83 (right) are removed.

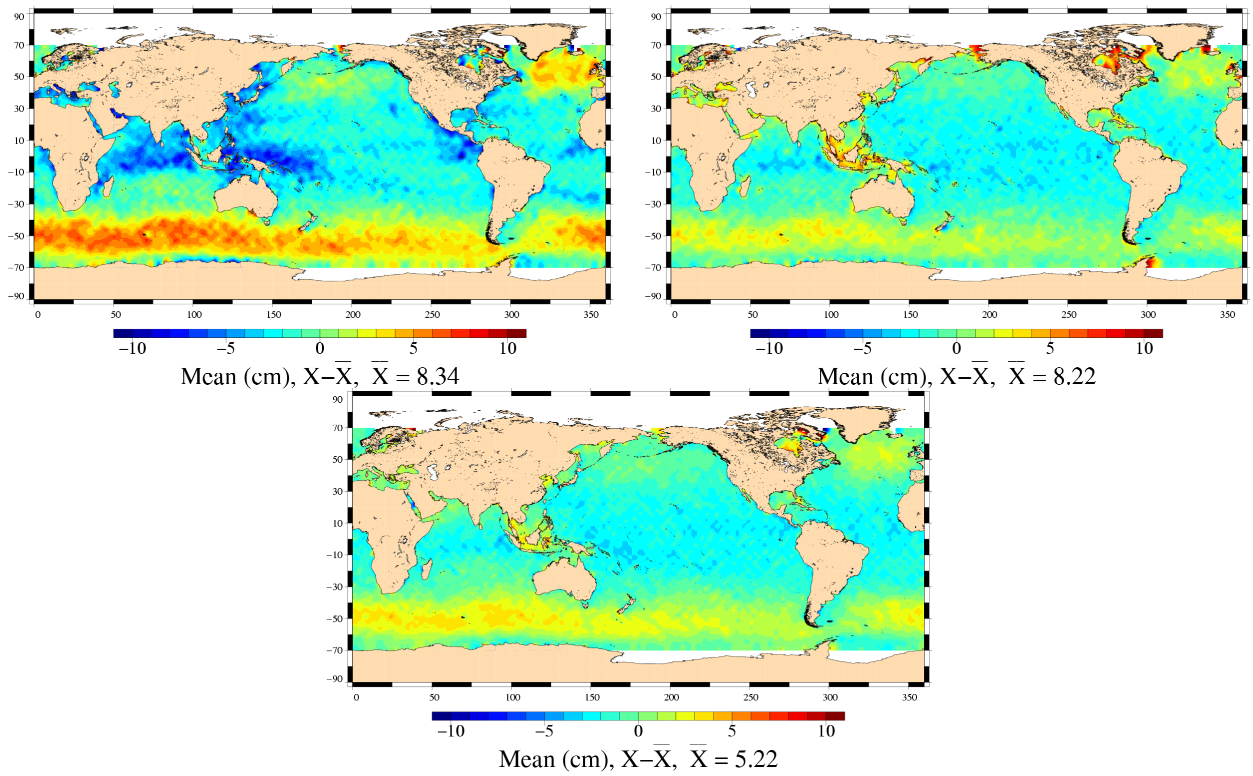

Figure 83: *SWH differences (T/P-J1) in cm for J1 GDR "a" and T/P MGDR (left), J1 GDR "b" and T/P MGDR (right) and J1 GDR "b" and T/P RGDR (bottom).*

7.3.3 Impact of new orbit for the SSH consistency

SLA differences between J1 and TOPEX are plotted (Figure 84, left) using former orbits and ranges from GDR "a" for J1 and MGDR for TOPEX. Neither geophysical corrections nor SSB correction were applied for both satellites. Large structures of negative and positive differences are visible, as well as orbit passes. Using the new orbits (GRACE family) provided by the GDR "b" for J1 and RGDR for TOPEX, removes trackiness and decreases the particular pattern in North Atlantic (Figure 84, right). Thanks to the new orbits, large structures are detected in Indian ocean and close to the shores. Some part of these discrepancies correspond to SSB differences between the two missions. Besides, a thick equatorial band is evidenced on Figure 84 (right) with negative differences. This is due to the ascending and descending SLA differences between J1 and TOPEX showing a large hemispheric signal (see Figure 86).

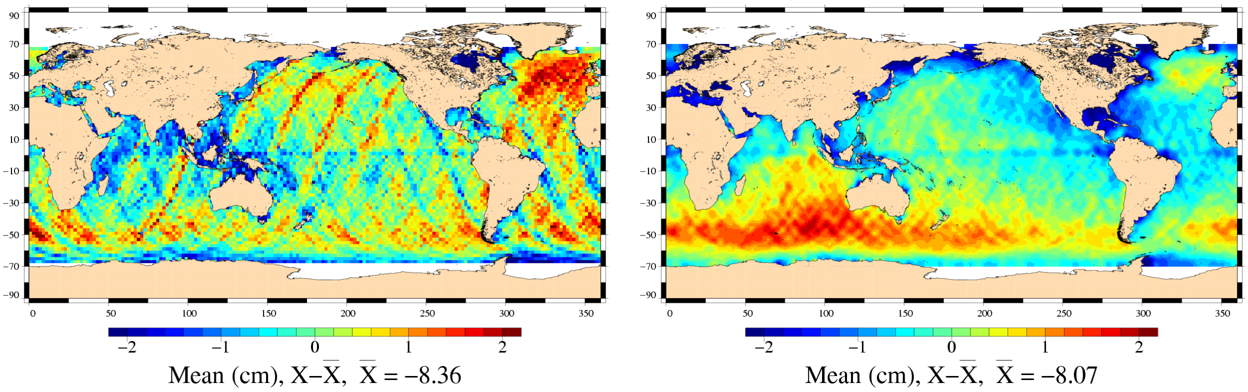

Figure 84: *SLA differences (without geophysical corrections) (T/P-J1) using old ranges. Using old orbit for T/P and J1 (left), using new orbit for T/P and J1 (right) [cm].*

7.3.4 Impact of new range for the SSH consistency

When using the new range (from MLE5 algorithm) for TOPEX, the patch in Indian ocean is strongly reduced (Figure 85). Jason-1 and TOPEX SSH are probably more homogeneous from now on ([37]). Using the new MLE4 range for Jason (Figure 85) has weak impact on the mean differences, even if the consistency is slightly better in the Indian Ocean. Nevertheless a great hemispheric bias (between -2 cm and +2 cm) is highlighted when separating the ascending and descending passes (Figure 86) :

- This bias is mainly due to TOPEX data. It was present on TOPEX M-GDR data alone (due to leakages in the waveforms, leading to errors in the on-board retracking). In the on-ground retracking of the RGDRs, the leakages seem still to be present and to have a bigger impact on the new range (MLE5 from RGDR), as shown at the TOPEX crossovers (see Figure 98). This needs more investigation.

- To a lower extent, such a signal is also visible at Jason-1 crossovers in the GDR "b" (Figure 69, right) probably due to time tag bias. But it is much weaker than for TOPEX.

Figure 86 shows SLA differences (T/P - J1, using new orbits and ranges) separated in ascending and descending passes. The ascending/descending differences are mainly due to TOPEX data.

Thanks to the MLE4 retracking for J1, the STD differences are dropped from 4.42 cm (Figure 87 left) to 4.11 cm (Figure 87 right) which is consistent with results shown in 7.2.4. Use of the T/P MLE5 range (Figure 87 bottom) slightly increases the standard deviation differences.

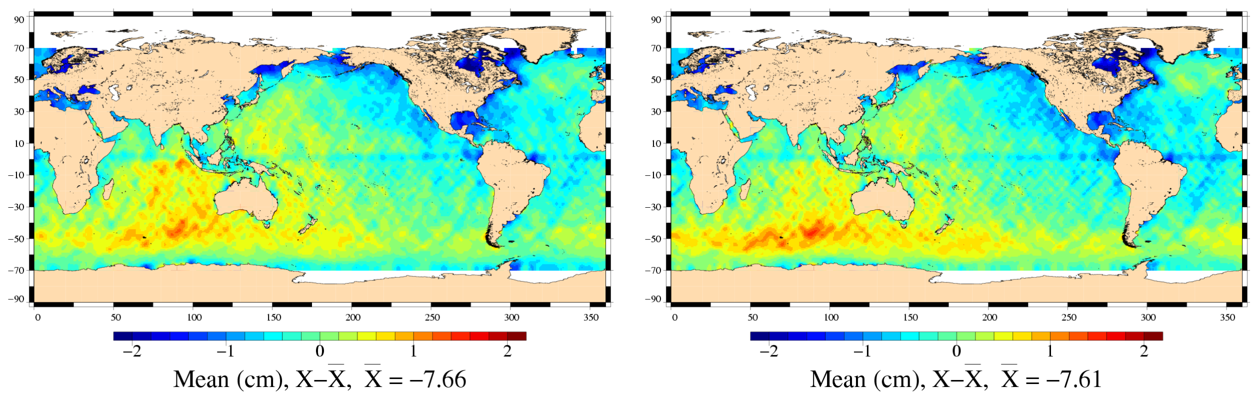

Figure 85: *SLA differences (without geophysical corrections) (T/P-J1) using new orbits. Using new TOPEX range (left), using new TOPEX ang J1 ranges (right) [cm].*

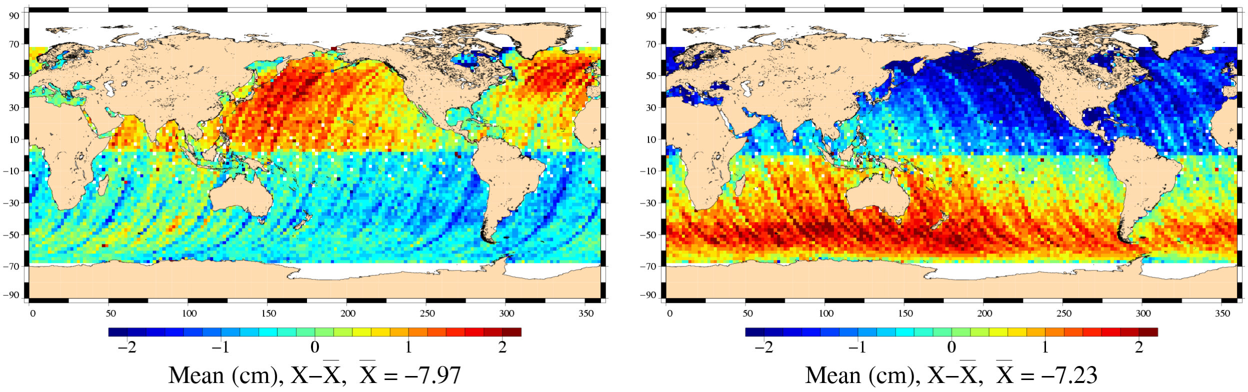

Figure 86: *SLA differences (without geophysical corrections) (T/P-J1) using new orbits and ranges [cm]. Ascending passes (left) and descending passes (right).*

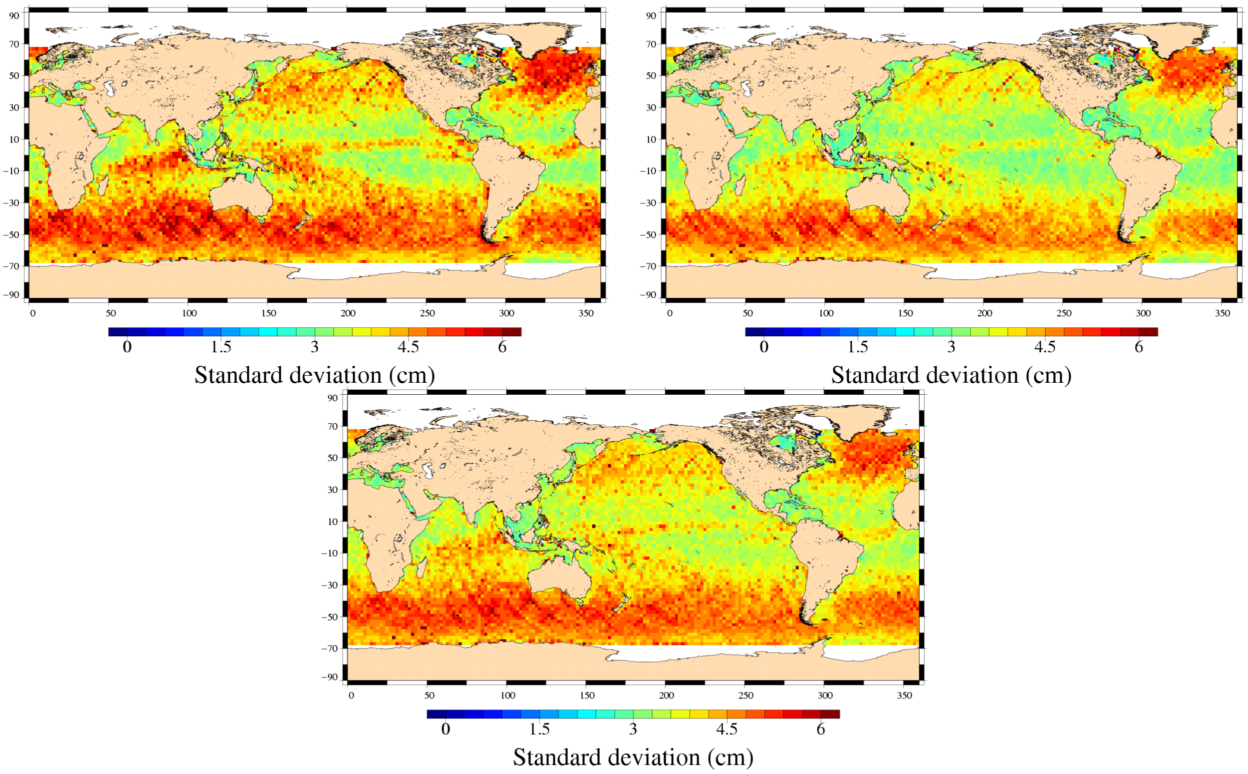

Figure 87: *Standard deviation of (T/P - J1) SLA differences [in cm] using old ranges (left), using new range for J1 (right), using new range for T/P and J1 (bottom).*

7.3.5 Impact of new sea state bias for the SSH consistency

New SSB corrections have been computed on cycles 1-21 for J1 using GDR "b" and for TOPEX using RGDR, with the collinear method ([37]). These new TOPEX and J1 SSB models are now much closer than before. When applying them in the SLA calculation in addition to the new orbits and the new ranges (Figure 88), the discrepancies between J1 and T/P are reduced. However, an East/West patch (< 1cm) remains, but it is not correlated with SWH. The origin of this signal is explained by CNES and GSFC orbit, used respectively for J1 and TOPEX. Indeed, using GSFC orbit for Jason-1 similar to those used in RGDR TOPEX data, allows to remove this East/West signal (see [5]).

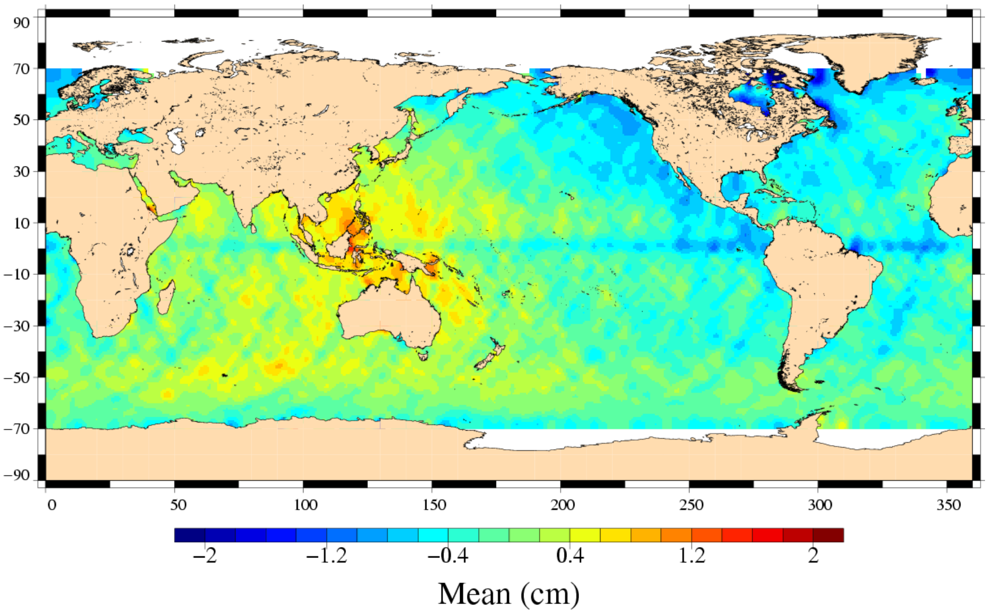

Figure 88: *SLA differences (with new SSB) using new orbits and ranges [cm].*

7.4 Conclusion

This chapter showed the impact of the reprocessing of 21 cycles of Jason-1 and TOPEX GDRs on data quality and sea surface height consistency between the two missions. It showed that quality of J1 data at crossover points were significantly increased, allowing to detect small signals, such as an hemispheric bias (possibly due to a wrong sign). The new geophysical corrections (as MOG2D-derived high frequency correction), the new orbit and MLE4-retracking are the main sources of improvement.

New TOPEX orbit reduced also SSH differences at crossover points, revealing an hemispheric bias (probably caused by leakages), which was not observed with same . Nevertheless, using the retracked TOPEX range MLE5 accentuates the hemispheric ascending/descending differences. Thanks to new orbits and retracking, reprocessed Jason-1 and TOPEX data are more homogeneous than those before, leading to a reduction of discrepancies between Jason-1 and TOPEX SLA. In addition, TOPEX and J1 SSB models, derived from these new data, are also more homogeneous.

To further improve the data, the time tag bias visible in Jason-1 orbits should be corrected, as well as the hemispheric bias in TOPEX range.

8 Mean Sea Level (MSL) and Sea Surface Temperature (SST) comparisons

This study has been carried out in order to monitor the MSL seen by all the operational altimeter missions. Long-term MSL change is a variable of considerable interest in the studies of global climate change. Then the objective here is on the one hand to survey the mean sea level trends and on the other hand to assess the consistency between all the MSL. Besides, the Reynolds SST is used to compare the MSL with an external data source. The mean SST is calculated in the same way as the MSL.
The following missions have been used : TOPEX/Poseïdon (T/P), Jason-1 (J1), Geosat Follow-On (GFO) and Envisat. Moreover the PVA products available on the aviso web site are used to calculate an homogeneous MSL since the beginning of the T/P mission until now.
The MSL and SST time series have been plotted over global ocean. This allows us to correlate the MSL trends seen by each mission and to compare them with the SST.
In addition to these analysis, the maps of regional MSL change and SST change have been plotted for each mission over the Jason-1 period and the Envisat period. The differences of these maps have been performed; this is a way to display eventual local drifts.

8.1 SSH definition for each mission

The SSH formula is defined for all the satellites as below :

$$SSH = Orbit - Altimeter\ Range - \sum_{i=1}^{n} Correction_i$$

with :

$$\begin{aligned}
\sum_{i=1}^{n} Correction_i \quad = \quad & Dry\ troposhere\ correction : new\ S1\ and S2\ atmospheric\ tides\ applied \\
+ \quad & Combined\ atmospheric\ correction :\ MOG2D\ and\ inverse\ barometer \\
+ \quad & Radiometer\ wet\ troposhere\ correction \\
+ \quad & Filtered\ dual\ frequency\ ionospheric\ correction \\
+ \quad & Non\ parametric\ sea\ state\ bias\ correction \\
+ \quad & Geocentric\ ocean\ tide\ height,\ GOT\ 2000 :\ S1\ atmospheric\ tide\ is\ applied \\
+ \quad & Solid\ earth\ tide\ height \\
+ \quad & Geocentric\ pole\ tide\ height
\end{aligned}$$

Some additional corrections have been applied :

- For Jason-1 and Envisat the wet troposphere correction has been changed by the ECMWF model in order to remove the effects of abnormal changes or trends observed on the radiometer wet troposphere correction.
- For Envisat, the USO correction has been applied (drift and anomaly : see Envisat yearly report [26]

- For T/P, the radiometer wet troposphere correction drift has been corrected with Scharroo's correction (Scharroo R., 2004 [57])
- For T/P, the relative bias between TOPEX and Poseidon and between TOPEX A and TOPEX B has been taken into account
- For T/P, the drift between the TOPEX and DORIS ionosphere corrections has been corrected for on Poseidon cycles.
- For Geosat Follow-On, the GIM model has been used for the ionospheric correction.

8.2 MSL and SST time series

8.2.1 MSL over global ocean

The MSL has been monitored for each satellite altimeter over global ocean in figure 89 since the beginning of T/P mission (left figure) and since the beginning of Jason-1 mission (right figure). The observed MSL trends have a similar shape for each satellite except for Envisat. The estimation of the Envisat MSL slope seems impacted by a unexpected behavior on the first year probably linked to a USO correction drift as explained in Faugere et al. (2005, [24]).

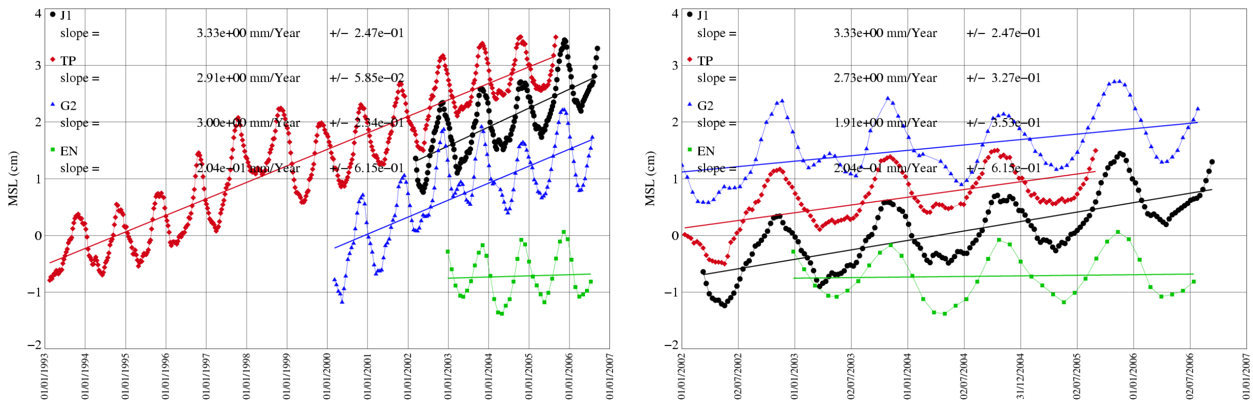

Figure 89: *MSL over global ocean since the beginning of T/P mission on the left and since the beginning of Jason-1 mission on the right.*

In the following figure 90, MSL have been plotted after removing annual signal, semi-annual signal, and signals lower than 60 days. The T/P, Jason-1 slopes since the beginning of Jason-1 period are still similar, withe respectively 2.7 mm/year and 3.3 mm/year and an adjustment formal error around 0.1 mm/year. The GFO slope is smaller than Jason-1 one by 1.4 mm/year over the Jason-1 period. But notice that the GFO MSL slope over the global period is stronger with 3.2 mm/year.
The differences between the different global MSL slope show that the real error of the MSL slope estimation is significantly greater than the formal error adjustment which is only a mathematical error, not linked with the physical errors such as the orbit errors for instance. The formal error adjustment show here the linear evolution of the MSL and the intrinsic consistency of the data.

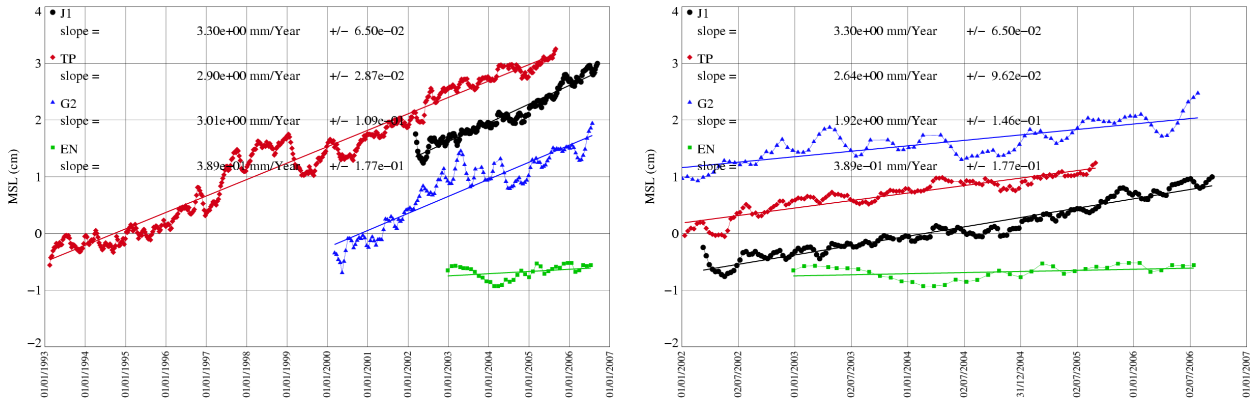

Figure 90: *MSL over global ocean since the beginning of T/P mission on the left and since the beginning Jason-1 mission on the right after removing annual, semi-annual and 60-day signals.*

8.2.2 SST over global ocean

In figure 91 on the left, the SST mean is compared to the MSL computed since the beginning of the T/P mission until now using the T/P and Jason-1 data. In the same figure on the right, annual signal, semi-annual signal, and signals lower than 60 days have been removed. The global MSL slope is 2.92 mm/year with a very small error adjustment (0.02 mm/year) which reveals a very linear evolution with a very good intrinsic consistency of the data. Besides, the SST increases by about 0.016 degree/year with a formal error close to 0.001 degree/year. The MSL and the SST don't have the same unit ("cm" and "degree"), thus to compare the 2 quantities, the SST scale is adjusted on the MSL scale so that the SST trend and the MSL trend are visually the same. This allows us to highlight that the SST dynamic is stronger than the MSL one. Inter-annual signal or climatic phenomena have a greater impact on the SST than on the MSL.

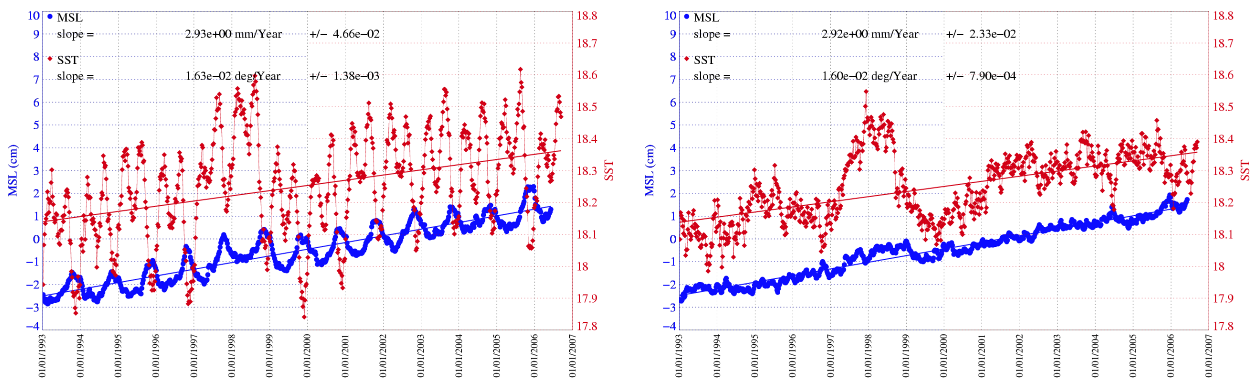

Figure 91: *MSL and SST over global ocean for the T/P period on the left, and after removing annual, semi-annual and 60-day signals on the left.*

8.3 Spatial MSL and SST slopes

8.3.1 Methodology

In order to monitor the MSL, the spatial MSL slopes have been calculated. The SLA grids (2x2 degree bins) have been computed cycle per cycle, and the slope has been computed on each grid point. As for time analysis, 60 day, semi-annual and annual signals have been removed before estimating the slopes. Then, the MSL slopes have been mapped for each mission. These maps are used to compare the MSL slopes between each altimeter mission. This allows us to detect potential local drifts.
Besides, the SST slopes have been computed the same way in order to correlate them with the MSL slopes.

8.3.2 Spatial MSL slopes over Jason-1 period

The MSL slopes have been plotted for Jason-1 (on the right) and T/P (on the left) over Jason-1/TOPEX overlapping period in figure 92. The MSL trends seen by the two satellites are similar. However, differences greater than 10 mm/year can be observed on the T/P-Jason-1 map (bottom figure).

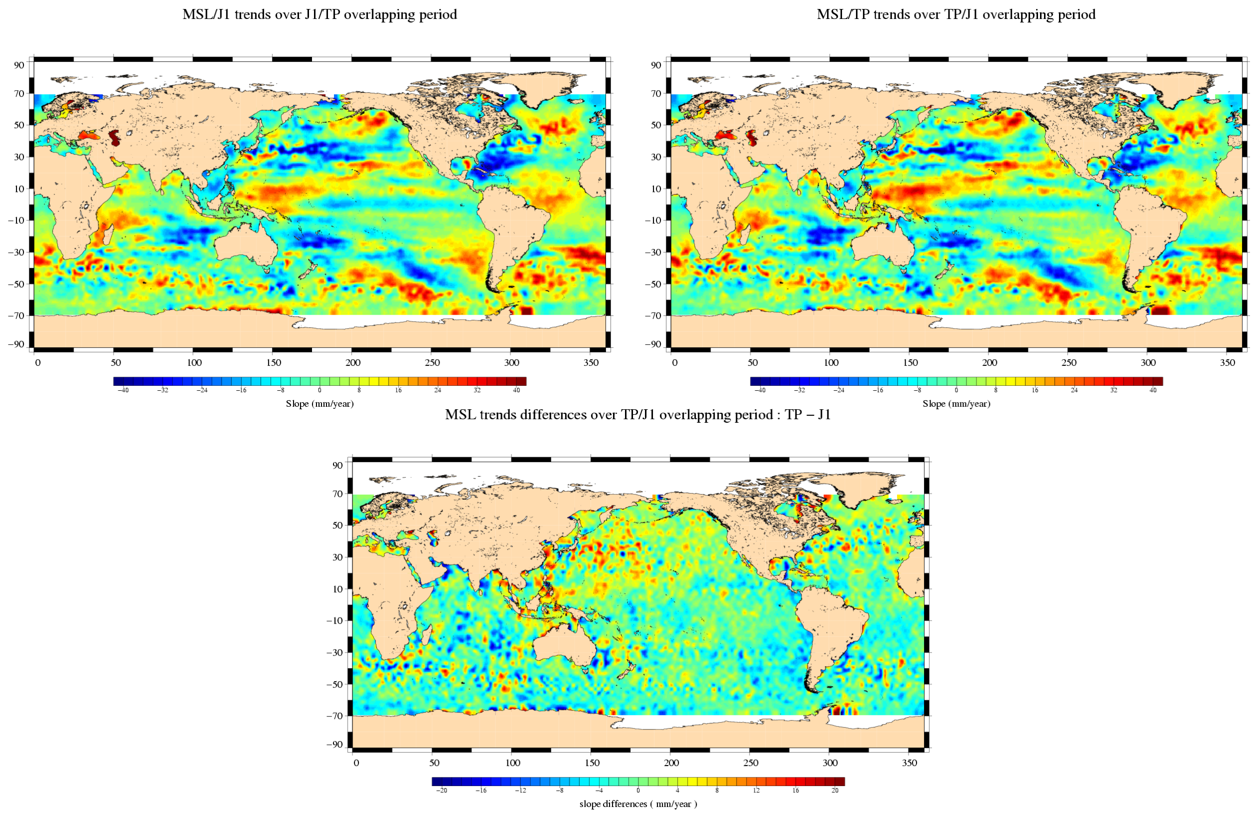

Figure 92: *MSL slopes over Jason-1/TOPEX overlapping period for T/P (left) and Jason-1 (right), MSL slope differences between Jason-1 and T/P (bottom)*

8.3.3 Spatial MSL slopes over Envisat period

The same work has been performed over Jason-1/Envisat overlapping period using Envisat data in figure 93. The 3 maps are quite similar. They allow us to observe differences in some areas between Jason-1 and Envisat.

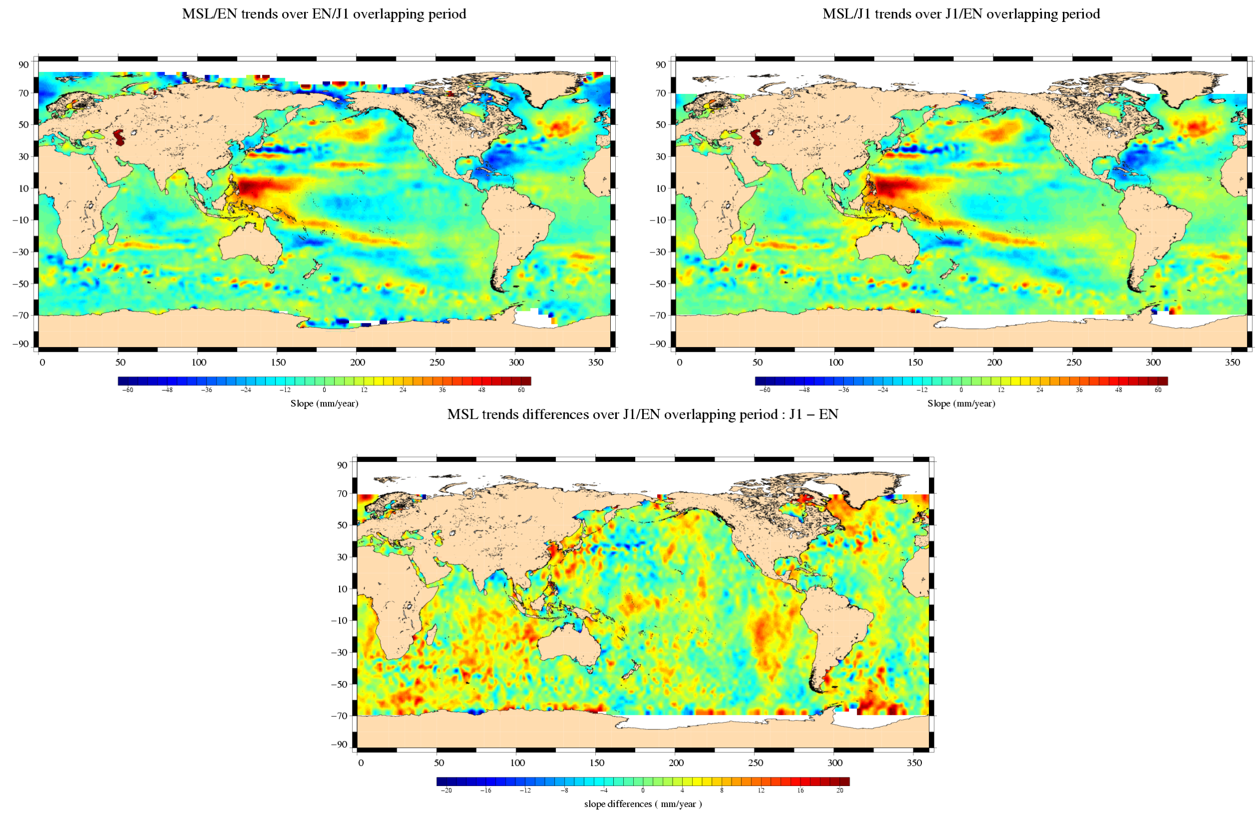

Figure 93: *MSL slopes over Envisat/Jason-1 overlapping period for Envisat (left) and Jason-1 (right), MSL slope differences between Jason-1 and Envisat (bottom)*

8.3.4 Spatial SST and MSL slopes since the beginning of T/P mission

In order to compute the local MSL slopes since the beginning of the T/P mission, the PVA products (available on aviso website) are used. These products combine different altimetric data coming from T/P, Jason-1 , ERS-2, Envisat, and GFO missions which allows us to increase the spatial resolution.
The MSL slopes are mapped in figure 94 on the left. In order to correlate the MSL and the SST, the SST slopes have been plotted in the same figure on the right.
14 years of altimetric data have been used to estimate the slopes which allows us to have a good estimation of the local MSL trends. The adjustment errors of the MSL and the SST slopes are mapped in figure 95.

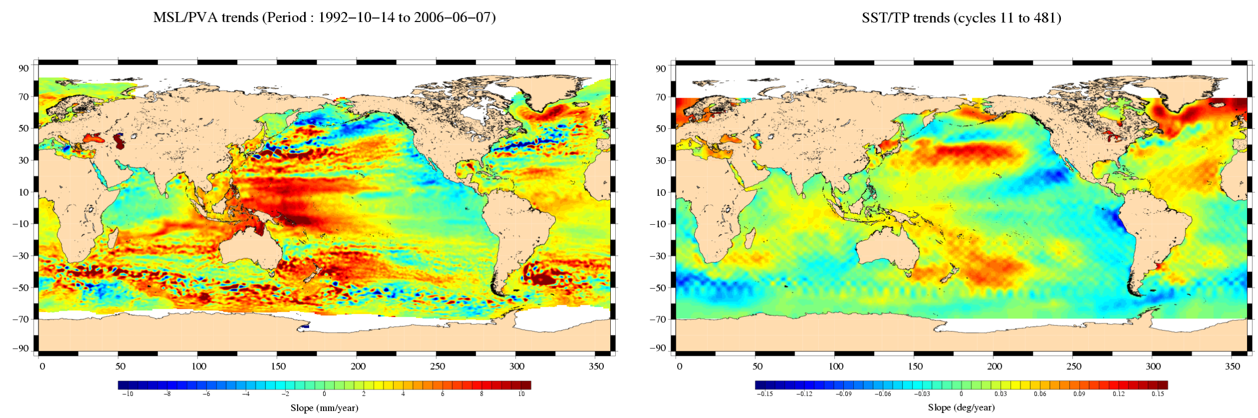

Figure 94: *T/P MSL and SST slopes over 13 years*

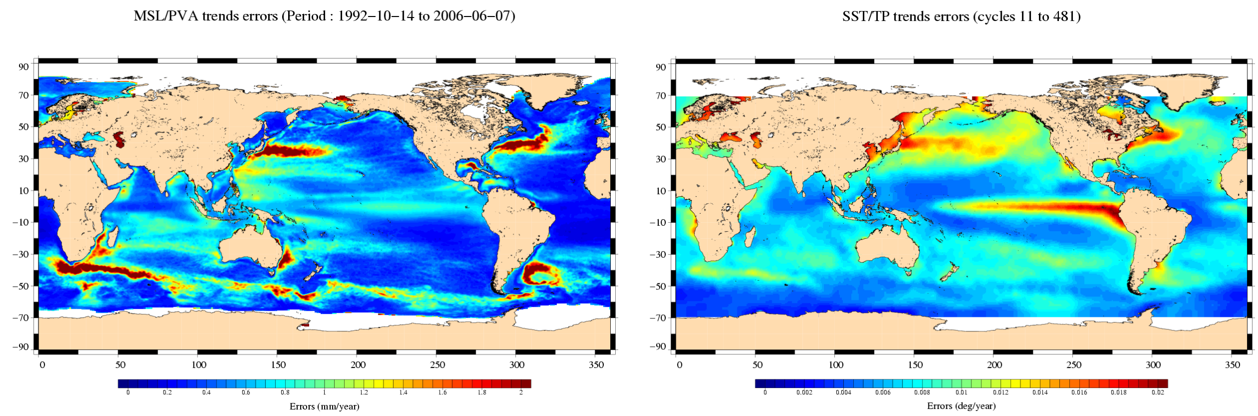

Figure 95: *Adjustment errors of T/P MSL and SST slopes over 13 years*

8.3.5 "El Niño" impact on SST and MSL slope estimations

The MSL and SST regional trends are largely impacted by inter-annual signal or oceanic phenomena such as "El Niño" for instance. The 4 maps in the figure 96 show the trend for the SST and the MSL before and after "El Niño". The first period ranges from 1992 and 1996 included, whereas the second period ranges from 1999 to 2004 included.
MSL and SST trends are stronger for each period separately than for the global period. In the Pacific ocean, the absolute values are greater than 20 mm/year for the MSL and 0.3 degree/year for the SST. SST and MSL maps show a strong correlation on the two periods of time. But for both SST and MSL, the trends on the first period are very different from the trends of the second period. This is particularly true in tropical areas. Finally, these maps highlight the importance of having long time series to evaluate the regional trends with a good accuracy.

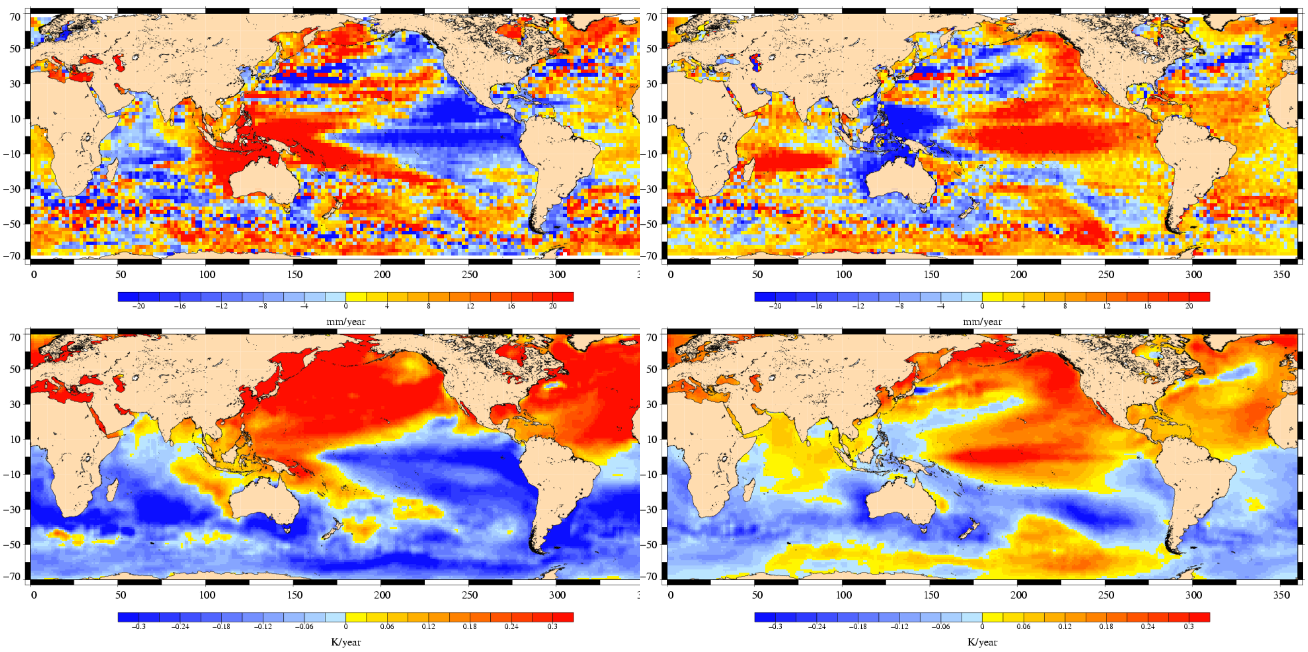

Figure 96: *Adjustment errors of T/P MSL and SST slopes over 13 years before and after "El Niño"*

9 Conclusion

Since the beginning of the Jason-1 mission and until the end of the T/P mission in October 2005, T/P and Jason-1 overflew the ocean over 2 parallel passes except the 21 first cycles, when there were on the same pass. Thanks to this long flight configuration, performances comparisons between both missions have been performed with success during 4 years, proving that the major objective of the Jason-1 mission to continue the T/P high precision has been reached. Five years of Jason-1 data are now available. The good quality of Jason-1 data has been shown in this report : the main altimeter parameters are stable and have the same behaviors as T/P ones for the 4 first years, the crossover and along-track performances remain very good.

Moreover, the new GDR release (version "b") allowed us to impove significantly the Jason-1 data in comparison with the former GDR version. The new geophysical corrections (as DAC high frequency correction), the new orbit (using Grace data) and new retracking (MLE-4) are the main sources of improvement. Thanks to these improvements, the SSH correlated geographical biases have been reduced and the SSH performances are significantly better. However some problems are remaining and will be taken into account in a future GDR release. First, the radiometer wet troposphere correction provided in the GDRs "b" allows us to correct partially the anomalies observed in the GDR "a' especially for the 60-day signal linked to the yaw maneuvers. Secondly, the orbit improvement highlighted a time tag shift of about 0.3 ms in the new GDR Jason-1. The impact of this anomaly is an SSH ascending/descending bias of about 0.5 cm.

Besides, the reprocessing of Jason-1 GDR (version b) and TOPEX data over the 21 first Jason-1 cycles allowed us to show the better agreement between both SSH proving the importance to reprocess Jason-1 and TOPEX data with the same geophysical corrections, the same orbit and an equivalent retracking over all the dataset.

The Jason-1 GDR reprocessing in version 'b' is on going from cycle 22 to 127 in order to complete the dataset in a homogeneous series. It will be finished early 2007. It is also planned to make an other GDR release probably end of 2007 . The major evolutions will be a new precise orbit based on new Grace data and new ITRF model, better ECMWF meteo fields, new geophysical corrections, new SSB correction. Besides it is planned to re-process T/P M-GDRs data with similar algorithms. Then, performances and comparisons will be carried out again using these new data in order to assess the GDRs reprocessing and to assess the consistency between Jason-1 and T/P sea surface height.

10 References

References

[1] Ablain, M., J. Dorandeu, Y. Faugère, F. Mertz, B. Soussi, F. Mercier, P. Vincent, and N. Picot. 2003a. SSALTO/CALVAL Jason-1 data quality assessment and Jason-1 / TOPEX cross-calibration using GDRs. *Paper presented at the Jason-1 and TOPEX/Poseidon Science Working Team Meeting, Arles (France), November.*

[2] Ablain, M., J. Dorandeu, Y. Faugere, F. Mertz, 2004. Jason-1 Validation and Cross-calibration activities Contract No 731/CNES/00/8435/00. Available at: http://www.jason.oceanobs.com/documents/calval/validation_report/j1/annual_report_j1_2004.pdf

[3] Ablain, M. and J. Dorandeu, 2005. TOPEX/Poseidon validation activities, 13 years of T/P data (GDR-Ms), Available at: http://www.jason.oceanobs.com/documents/calval/validation_report/tp/annual_report_tp_2005.pdf

[4] Ablain, M., S. Philipps, P. Thibaut, J. Dorandeu, and N. Picot 2005. Jason-1 GDR Quality Assessment Report. Cycle 135. SALP-RP-P2-EX-21072-CLS135, May. http://www.jason.oceanobs.com/html/calval/validation_report/j1/j1_calval_bulletin_135_fr.html

[5] Ablain, M., S. Philipps, S. Labroue, J. Dorandeu, and N. Picot, 2007. SSALTO CALVAL Consistency assessment between Jason-1 and TOPEX. poster presented at OSTST meeting, Hobart, Australia, 12-15 march 2007. Available at: http://www.jason.oceanobs.com/documents/swt/posters2007/ablain_J1TP.pdf

[6] Amarouche, L., P. Thibaut, O.Z. Zanife, P. Vincent, and N. Steunou. 2004. Improving the Jason-1 Ground Retracking to Better Account or Attitude Effects. *Mar. Geod.***27 (1-2): 171-197.**

[7] Arnault, S., N. Chouaib, D. Diverres, S. Jaquin, and O. Coze, 2004. Comparison of TOPEX/Poseidon and JASON Altimetry with ARAMIS In Situ Observations in the Tropical Atlantic Ocean. *Mar. Geod.***27 (1-2): 15-30.**

[8] Brown G.S., "The average impulse response of a rough surface and its application", IEEE Transactions on Antenna and Propagation, Vol. AP 25, N1, pp. 67-74, Jan. 1977.

[9] Callahan, Phil. electronic communication (retrk-gdr-data-rec-r10.062.pdf) send to OSTST on 13 February 2006.

[10] Carayon, G., N. Steunou, J. L. Courrière, and P. Thibaut. 2003. Poseidon 2 radar altimeter design and results of in flight performances. *Mar. Geod.***26(3-4): 159-165.**

[11] Carrère, L., and F. Lyard, Modeling the barotropic response of the global ocean to atmospheric wind and pressure forcing - comparisons with observations. 2003. Geophys. Res. Lett., 30(6), 1275, doi:10.1029/2002GL016473.

[12] Chambers, D. P., S. A. Hayes, J. C. Ries, and T. J. Urban. 2003. New TOPEX sea state bias models and their effect on global mean sea level. J. Geophys. Res. 108(C10): 3305.

[13] Chambers, D., P., J. Ries, T. Urban, and S. Hayes. 2002. Results of global intercomparison between TOPEX and Jason measurements and models. Paper presented at the Jason-1 and TOPEX/Poseidon Science Working Team Meeting, Biarritz (France), 10-12 June.

[14] Chambers, D. P. and B. D. Tapley, 1998: Reduction of Geoid Gradient Error in Ocean Variability from Satellite Altimetry. *Mar. Geod.*, **21, 25-39.**

[15] Choy, K, J. C. Ries, and B. D Tapley, 2004. Jason-1 Precision Orbit Determination by Combining SLR and DORIS with GPS Tracking Data. *Mar. Geod.***27(1-2): 319-331.**

[16] Desai, S. D., and B. J. Haines, 2004. Monitoring Measurements from the Jason-1 Microwave Radiometer and Independent Validation with GPS. *Mar. Geod.***27(1-2): 221-240.**

[17] Dorandeu, J., M. H. De Launay, F. Mertz and J. Stum, 2001. AVISO/CALVAL yearly report. 8 years of TOPEX/Poseidon data (M-GDRs).

[18] Dorandeu, J. and P.Y. Le Traon, 1999: Effects of Global Atmospheric Pressure Variations on Mean Sea Level Changes from TOPEX/Poseidon. *J. Atmos. Technol.,***16, 1279-1283.**

[19] Dorandeu, J, M. Ablain, Y . Faugere, B. Soussi, and J . Stum. 2002a. Global statistical assessment of Jason-1 data and Jason-1/TOPEX/Poseiodn Cross-calibration. Paper presented at the Jason-1 and TOPEX/Poseidon Science Working Team Meeting, Biarritz (France), **10-12 June.**

[20] Dorandeu, J., P. Thibaut, O. Z. Zanife, Y. Faugère, G. Dibarboure, N. Steunou, and P. Vincent. 2002b. Poseidon-1, Poseidon-2 and TOPEX noise analysis. Paper presented at the Jason-1 and TOPEX/Poseidon Science Working Team Meeting, New-Orleans (USA), **October.**

[21] Dorandeu., J., M. Ablain, P. Y. Le Traon, 2003a. Reducing Cross-track Geoid Gradient Errors around TOPEX/Poseidon and Jason-1 Nominal Tracks. Application to Calculation of Sea Level Anomalies. *J. Atmos. Oceanic Technol.,***20, 1826-1838.**

[22] Dorandeu, J., Y. Faugère, and F. Mertz. 2003b. ENVISAT data quality: Particular investigations. Proposal for ENVISAT GDR evolutions. Paper presented at the ENVISAT Ra-2 & MWR Quality Working Group meeting. **October.**

[23] Dorandeu.,J., M. Ablain, Y. Faugère, F. Mertz, 2004 : Jason-1 global statistical evaluation and performance assessment. Calibration and cross-calibration results. *Mar. Geod.***This issue.**

[24] Y.Faugere, J.Dorandeu, F.Lefevre, N.Picot and P.Femenias, 2005: Envisat ocean altimetry performance assessment and cross-calibration. Submitted in the special issue of SENSOR 'Satellite Altimetry: New Sensors and New Applications'

[25] Y.Faugere and J.Dorandeu, 2004: Nouvel algorithme de détection des glaces de mer pour Jason-1. SALP-PR-MA-EA-21235-CLS.

[26] Y.Faugere and J.Dorandeu, 2006: Envisat validation activities. 2006 yearly report, Available at: http://www.jason.oceanobs.com/documents/calval/validation_report/en/annual_report_en_2006.pdf

[27] Förste, C., F. Flechtner, R. Schmidt, U. Meyer, R. Stubenvoll, F. Barthelmes, R. König, K.-H. Neumayer, M. Rothacher, C. Reigber, R. Biancale, S. Bruinsma, J.-M. Lemoine, and J.C. Raimondo. A New Heigh Resolution Global Gravity Field Model Derived From Combination of GRACE and CHAMP Mission and Altimetry/ Gravimetry Surface Gravity Data. *Poster presented at EGU General Assembly 2005, Vienna, Austria, 24-29 April 2005.*

[28] Fu, L. L., 2002. Minutes of the Joint Jason-1 and TOPEX/Poseidon Science Working Team Meeting, Oct. 21-23, JPL Tech. Report. JPL D-25506, edited by L. Fu, USA.

[29] Gaspar, P., S. Labroue, F. Ogor, G. Lafitte, L. Marchal and M. Rafanel, 2002: Improving non parametric estimates of the sea state bias in radar altimeter measurements of sea level. *J. Atmos. Oceanic Technol.,***19, 1690-1707.**

[30] Haines, B., Y. Bar-Sever, W. Bertiger, S. Desai, P. Willis, 2004: One-Centimeter Orbit Determination for Jason-1: New GPS-Based Strategies. *Mar. Geod.***27(1-2): 299-318.**

[31] Hamming, R. W., 1977. Digital Filter. Prentice-Hall Signal Processing Series, edited by A. V. Oppenheim Prentice-Hall, Englewood Cliffs, N. J.

[32] Hernandez, F. and P. Schaeffer, 2000: Altimetric Mean Sea Surfaces and Gravity Anomaly maps intercomparisons AVI-NT-011-5242-CLS, 48 pp. CLS Ramonville St Agne.

[33] Hirose N., Fukumori I., Zlotnicki V., Ponte R. M. 2001: High-frequency barotropic response to atmospheric disturbances : sensitivity to forcing, topography, and friction, J. Geophys. Res. 106(C12), 30987-30996.

[34] Keihm, S. J., V. Zlotnicki, and C. S. Ruf. 2000. TOPEX Microwave Radiometer performance evaluation, 1992-1998, *IEEE Trans. Geosci. Rem. Sens.,***38(3): 1379-1386.**

[35] Labroue, S. and P. Gaspar, 2002: Comparison of non parametric estimates of the TOPEX A, TOPEX B and JASON 1 sea state bias. Paper presented at the Jason 1 and TOPEX/Poseidon SWT meeting, New-Orleans, 21-12 October.

[36] Labroue, S. P. Gaspar, J. Dorandeu, O.Z. Zanifé, P. Vincent, and D. Choquet. 2004. Non Parametric Estimates of the Sea State Bias for Jason 1 Radar Altimeter. *Mar. Geod.***This issue.**

[37] Labroue, S., Ph. Gaspar, J. Dorandeu, O.Z. Zanife. Latest Results on Jason-1 Sea State Bias with the Non-Parametric Technique. *Talk presented at OSTST meeting, Venice, Italy, 16-18 March 2006.*

[38] Lemoine, F. G., S. B. Luthcke, N. P. Zelinsky, D. S. Chinn, T. A. Williams, C. M. Cox, and B. D. Beckley. 2003. An Evaluation of Recent gravity Models Wrt to Altimeter Satellite Missions.*Paper presented at the Jason-1 and TOPEX/Poseidon Science Working Team Meeting,***Arles (France), November.**

[39] Le Traon, P.-Y., J. Stum, J. Dorandeu, P. Gaspar, and P. Vincent, 1994: Global statistical analysis of TOPEX and POSEIDON data. *J. Geophys. Res.,***99, 24619-24631.**

[40] Le Traon, P. Y., and G. Dibarboure, 2004. An Illustration of the Contribution of the TOPEX/Poseidon-Jason-1 Tandem Mission to Mesoscale Variability Studies. *Mar. Geod.***27(1-2) 3-13.**

[41] Luthcke. S. B., N. P. Zelinsky, D. D. Rowlands, F. G. Lemoine, and T. A. Williams. 2003. The 1-Centimeter Orbit: jason-1 Precision Orbit Determination Using GPS, SLR, DORIS, and Altimeter Data. *Mar. Geod.***26(3-4): 399-421.**

[42] Marshall, J. A., N. P. Zelinsky, S. B. Luthcke, K. E., Rachlin, and R. G. Williamson. 1995. The temporal and spatial characterustics of TOPEX/Poseidon radial orbit error. *J. Geophys. Res.* **100(C2):25331-25352.**

[43] Martini A., 2003: Envisat RA-2 Range instrumental correction : USO clock period variation and associated auxiliary file, Technical Note ENVI-GSEG-EOPG-TN-03-0009 Available at http://earth.esa.int/pcs/envisat/ra2/articles/USO_clock_corr_aux_file.pdfhttp://earth.esa.int/pcs/envisat/ra2/auxdata/

[44] Ménard, Y. 2003. Minutes of the Joint TOPEX/Poseidon and Jason-1 Science Working Team Meeting. CNES-SALP-CR-MA-EA-15190-CN.

[45] Obligis, E, N. Tran, and L. Eymard, 2004. An assessment of Jason-1 microwave radiometer measurements and products. *Mar. Geod.***27(1-2) 255-277.**

[46] Phaden Mc.J., April2003 : Evolution of the 2002-03 El Niño, *UCLA Tropical Meteorology and Climate Newsletter,***No57**.

[47] Picot, N., K. Case, S. Desai and P. Vincent, 2003. AVISO and PODAAC User Handbook. IGDR and GDR Jason Products, SMM-MU-M5-OP-13184-CN (AVISO), JPL D-21352 (PODAAC).

[48] Provost., C. Arnault, N. Chouaib, A. Kartavtseff, L. Bunge, and E. Sultan, 2004. TOPEX/Poseidon and Jason Equatorial Sea Surface Slope Anomaly in the Atlantic in 2002: Comparison with Wind and Current Measurements at 23W. *Mar. Geod.***27(1-2) 31-45.**

[49] Quartly, G. D., 2004. Sea State and Rain: A Second Take on Dual-Frequency Altimetry. Mar. Geod. 27(1-2) 133-152

[50] Queffeulou, P. 2004. Long Term Validation of Wave Height Measurements from Altimeters. *Mar. Geod.***This issue.**

[51] Ray, R. (1999). A Global Ocean Tide Model From TOPEX/Poseidon Altimetry/ GOT99.2 - NASA/TM-1999-209478. Greenbelt, MD, Goddard Space Flight Center/NASA: 58

[52] Ray, R. D., and B. D. Beckley, 2003. Simultaneaous Ocean Wave Measurements by the Jason and Topex Satellites, with Buoy and Model Comparisons *Mar. Geod.***26(3-4): 367-382.**

[53] Ray, R. D. 2003. Benefits of the joint T/P−Jason mission for improving knowledge of coastal tides. Paper presented at the Jason-1 and TOPEX/Poseidon Science Working Team Meeting, Arles (France), November.

[54] Ray, R.D. and R.M. Ponte, Barometric tides from ECMWF operational analyses. *Annales G*, **99, 24995-25008**, 1994.

[55] Ruf C., S. Brown, S. Keihm and A. Kitiyakara, 2002a. JASON Microwave Radiometer : On Orbit Calibration, Validation and Performance, *Paper presented at the Jason-1 and TOPEX/Poseidon Science Working Team Meeting, New-Orleans (USA),***21-23 October.**

[56] Ruf. C. S., 2002b. TMR Drift - Correction to 18 GHz Brightness Temperatures, Revisited. Report to TOPEX Project, June.

[57] Scharroo R., J. L. Lillibridge, and W. H. F. Smith, Cross-Calibration and Long-term Monitoring of the Microwave Radiometers of ERS, TOPEX, GFO, Jason-1, and Envisat, **Marine Geodesy, 27:279-297**, 2004.

[58] Tapley, B.D., M.M. Watkins, J.C. Ries, G.W. Davis, R.J. Eanes, S.R. Poole, H.J. Rim, B.E. Schultz, C.K. Shum, R.S. Nerem, F.J. Lerch, J.A. Marshall, S.M. Klosko, N.K. Pavlis, and R.G. Williamson, 1996. The Joint Gravity Model 3. *J. Geophys. Res.***101(B12): 28029-28049.**

[59] Tierney, C., J. Wahr, et al. 2000. Short-period oceanic circulation: implications for satellite altimetry. Geophysical Research Letters 27(9): 1255-1258

[60] Thibaut, P. O.Z. Zanifé, J.P. Dumont, J. Dorandeu, N. Picot, and P. Vincent, 2002. Data editing : The MQE criterion. Paper presented at the Jason-1 and TOPEX/Poseidon Science Working Team Meeting, New-Orleans (USA), 21-23 October.

[61] Thibaut, P. L. Amarouche, O.Z. Zanife, N. Steunou, P. Vincent, and P. Raizonville. 2004. Jason-1 altimeter ground processing look-up tables. *Mar. Geod.***This issue.**

[62] Tournadre, J. 2002. Validation of the rain flag. Paper presented at the Jason-1 and TOPEX/Poseidon Science Working Team Meeting, Biarritz (France), 10-12 June.

[63] Tran, N., D. W. Hancock III, G.S. Hayne. 2002. "Assessment of the cycle-per-cycle noise level of the GEOSAT Follow-On, TOPEX and POSEIDON." *J. Atmos. Oceanic Technol.,***19(12): 2095-2117.**

[64] Vincent, P., S. D. Desai, J. Dorandeu, M. Ablain, B. Soussi, P. S. Callahan, and B. J. Haines 2003a. Jason-1 Geophysical Performance Evaluation. *Mar. Geod.***26(3-4): 167-186.**

[65] Vincent, P., S. Desai, J. Dorandeu, M. Ablain, B. Soussi, Y. Faugère, B. Haines, N. Picot, K. Case, A. Badea, 2003b. Summary about Data Production and Quality. Paper presented at the Jason-1 and TOPEX/Poseidon Science Working Team Meeting, Arles (France), November

[66] Vincent, P., J.P. Dumont, N. Steunou, O.Z. Zanife, P. Thibaut, and J. Dorandeu. 2003c. Jason-1 I/GDR science processing: ground retracking improvements. Paper presented at the European Geophysical Society meeting, Nice, April.

[67] Zanife, O. Z., P. Vincent, L. Amarouche, J. P. Dumont, P. Thibaut, and S. Labroue, 2003. Comparison of the Ku-band range noise level and the relative sea-state bias of the Jason-1, TOPEX and Poseidon-1 radar altimeters. *Mar. Geod.***26(3-4): 201-238.**

11 Annex

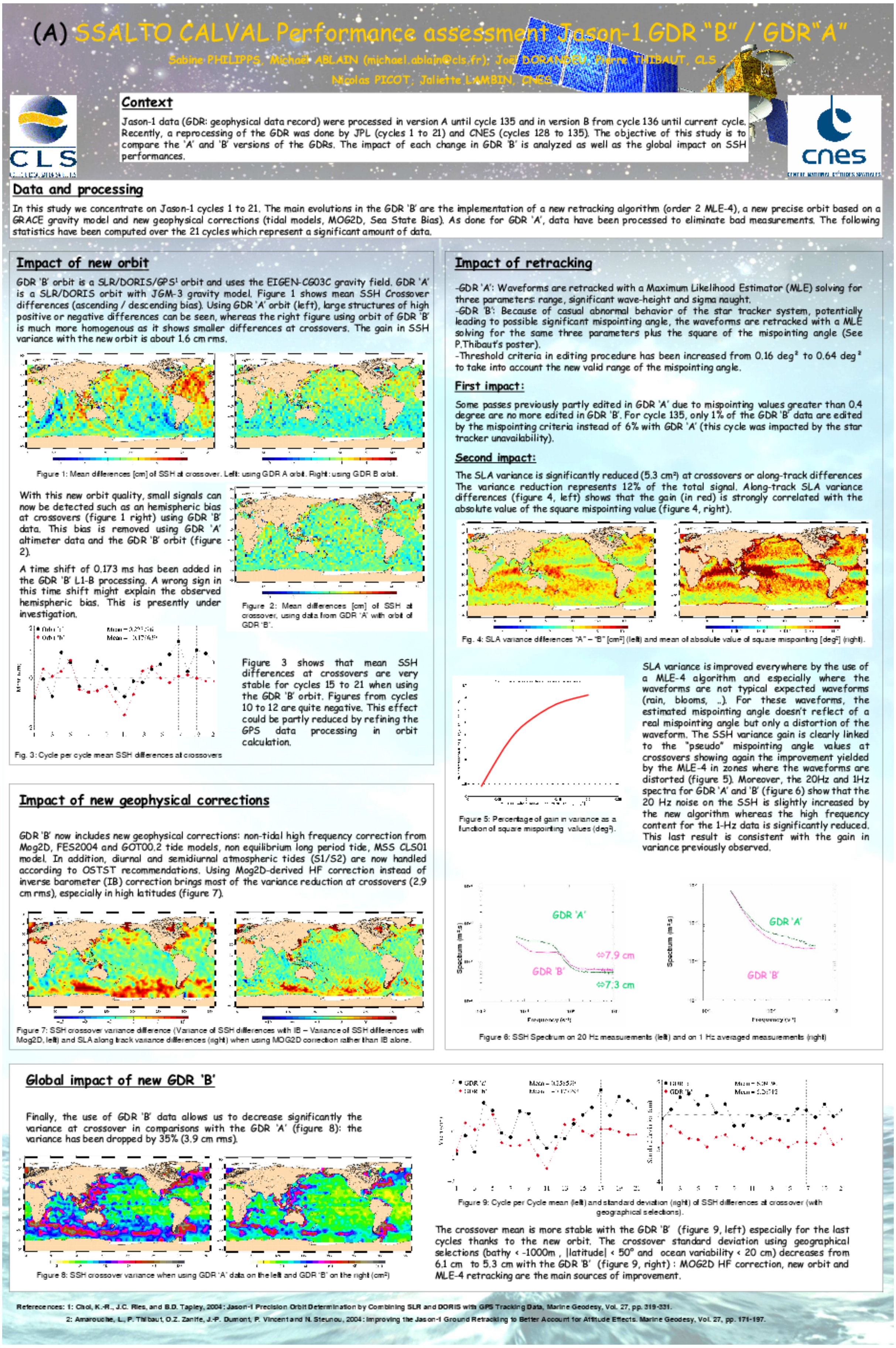

Figure 97: *Poster presented at OSTST meeting, Venice 2006*

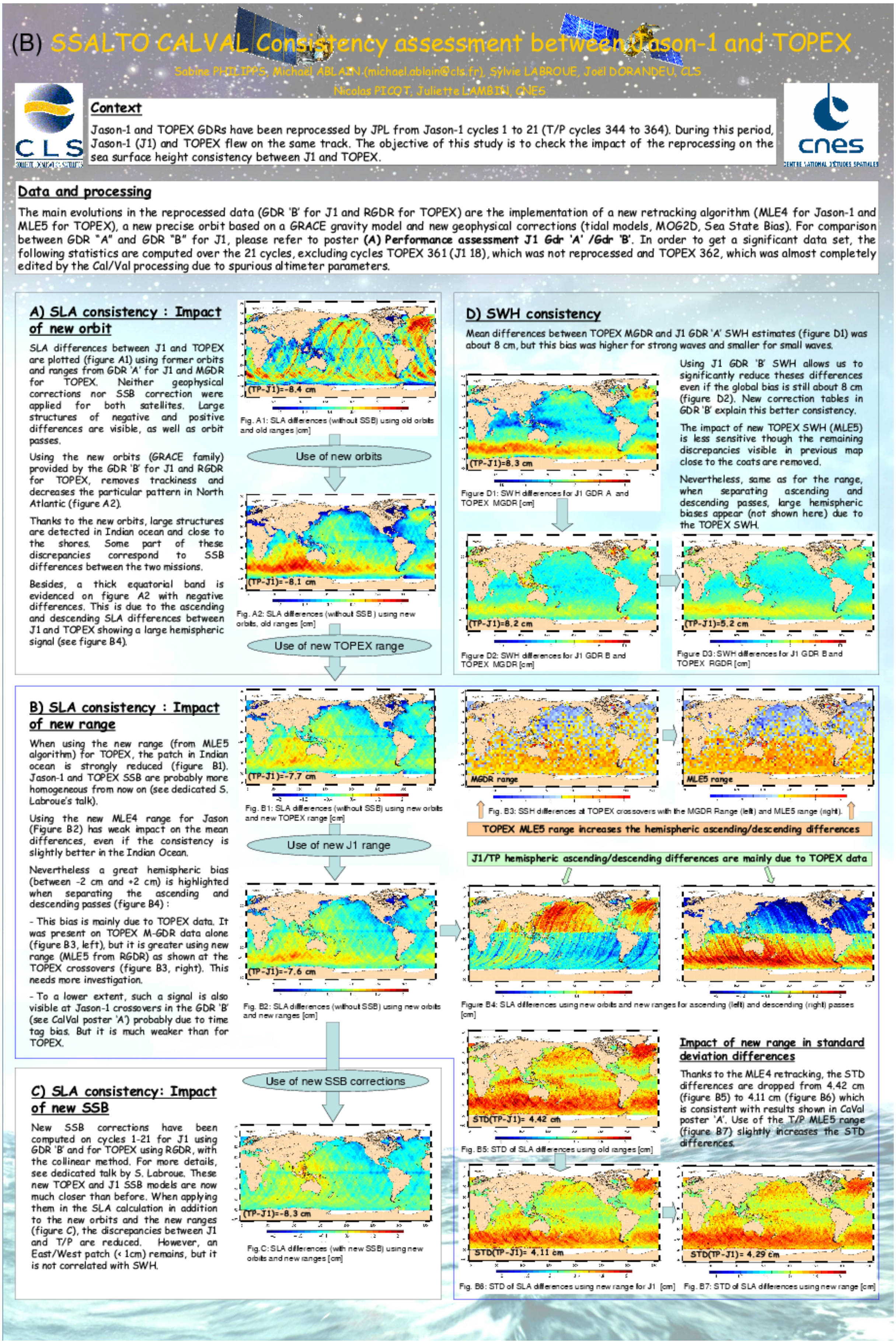

Figure 98: *Poster presented at OSTST meeting, Venice 2006*